VOLUME 33 SEPTEMBER 1955 NUMBER 5

UNIVERSITY
OF MICHIGAN
SEP 9 1955
ENGINEERING
LIBRARY

Canadian Journal of Technology

Editor: G. A. LEDINGHAM

Published by THE NATIONAL RESEARCH COUNCIL
OTTAWA CANADA

CANADIAN JOURNAL OF TECHNOLOGY

Notes to Contributors

Manuscripts

(i) ***General.*** Manuscripts, in English or French, should be typewritten, double spaced, on paper 8½×11 in. **The original and one copy are to be submitted.** Tables and captions for the figures should be placed at the end of the manuscript. Every sheet of the manuscript should be numbered.

Style, arrangement, spelling, and abbreviations should conform to the usage of this journal. Names of all simple compounds, rather than their formulas, should be used in the text. Greek letters or unusual signs should be written plainly or explained by marginal notes. Superscripts and subscripts must be legible and carefully placed.

Manuscripts and illustrations should be carefully checked before they are submitted. Authors will be charged for unnecessary deviations from the usual format and for changes made in the proof that are considered excessive or unnecessary.

(ii) ***Abstract.*** An abstract of not more than about 200 words, indicating the scope of the work and the principal findings, is required, except in Notes.

(iii) ***References.*** References should be listed **alphabetically by authors' names,** numbered, and typed after the text. The form of the citations should be that used in this journal; in references to papers in periodicals, inclusive page numbers should be given but titles should not. All citations should be checked with the original articles and each one referred to in the text by the key number.

(iv) ***Tables.*** Tables should be numbered in roman numerals and each table referred to in the text. Titles should always be given but should be brief; column headings should be brief and descriptive matter in the tables confined to a minimum. Vertical rules should be used only when they are essential. Numerous small tables should be avoided.

Illustrations

(i) ***General.*** All figures (including each figure of the plates) should be numbered consecutively from 1 up, in arabic numerals, and each figure referred to in the text. The author's name, title of the paper, and figure number should be written in the lower left corner of the sheets on which the illustrations appear. Captions should not be written on the illustrations (see Manuscripts (i)).

(ii) ***Line Drawings.*** Drawings should be carefully made with India ink on white drawing paper, blue tracing linen, or co-ordinate paper ruled in blue only; any co-ordinate lines that are to appear in the reproduction should be ruled in black ink. Paper ruled in green, yellow, or red should not be used unless it is desired to have all the co-ordinate lines show. All lines should be of sufficient thickness to reproduce well. Decimal points, periods, and stippled dots should be solid black circles large enough to be reduced if necessary. Letters and numerals should be neatly made, preferably with a stencil (**do NOT use typewriting**) and be of such size that the smallest lettering will be not less than 1 mm. high when reproduced in a cut 3 in. wide.

Many drawings are made too large; originals should not be more than 2 or 3 times the size of the desired reproduction. In large drawings or groups of drawings the ratio of height to width should conform to that of a journal page but the height should be adjusted to make allowance for the caption.

The original drawings and one set of clear copies (e.g. small photographs) are to be submitted.

(iii) ***Photographs.*** Prints should be made on glossy paper, with strong contrasts. They should be trimmed so that essential features only are shown and mounted carefully, with rubber cement, on white cardboard with no space or only a very small space (less than 1 mm.) between them. In mounting, full use of the space available should be made (to reduce the number of cuts required) and the ratio of height to width should correspond to that of a Journal page (4½×7½ in.); however, allowance must be made for the captions. Photographs or groups of photographs should not be more than 2 or 3 times the size of the desired reproduction.

Photographs are to be submitted in duplicate; if they are to be reproduced in groups one set should be mounted, the duplicate set unmounted.

Reprints

A total of 50 reprints of each paper, without covers, are supplied free. Additional reprints, with or without covers, may be purchased.

Charges for reprints are based on the number of printed pages, which may be calculated approximately by multiplying by 0.6 the number of manuscript pages (double-spaced typewritten sheets, 8½×11 in.) and including the space occupied by illustrations. An additional charge is made for illustrations that appear as coated inserts. The cost per page is given on the reprint requisition which accompanies the galley.

Any reprints required in addition to those requested on the author's reprint requisition form must be ordered officially as soon as the paper has been accepted for publication.

Canadian Journal of Technology

Issued by THE NATIONAL RESEARCH COUNCIL OF CANADA

VOLUME 33 SEPTEMBER 1955 NUMBER 5

AUTOMATIC PLOTTING OF THE POSITION OF A MOVING RADIOACTIVELY TAGGED OBJECT[1]

BY B. C. GREEN AND J. W. T. SPINKS

ABSTRACT

A machine has been developed which is able to record automatically the movement, in three spatial dimensions and in time, of a radioactively tagged object. The present machine was designed specifically for recording the movements of a radioactively tagged soil burrowing wireworm.

INTRODUCTION

During the last few years, studies of the movements of soil burrowing insects have been made using radioactively tagged insects (1). The method involved finding the position of maximum response of a manually operated portable Geiger tube and ratemeter, and it was suggested that an automatic device for continuously following and recording the position of a suitably tagged insect would be of some value.

Two possible principles immediately suggest themselves—scanning and tracking. The scanning approach has already been utilized in devices such as the scintiscanner, and could be applied, after suitable modification, to the present problem. It would seem, however, to be best applied to problems involving movements of the insect in question within a relatively small restricted area and will not be further discussed here.

DISCUSSION OF FUNDAMENTAL PRINCIPLES

Tracking Over a Restricted Area

Tracking or following continuously requires, first of all, a sensitive head and recorder which will follow the insect's movements. The sensitive head must be such that when it is not directly over the insect, a definite type of error signal is produced. The error signal is amplified and the amplified signal applied to a servomechanism which causes the head to move in such a way that the error is minimized by the restoration of the head to a position directly over the insect. The movable parts must be carried on a suitable movable framework, the type of framework depending on whether the movement is to

[1]*Manuscript received April 7, 1955.*
Contribution from the Department of Chemistry, University of Saskatchewan, Saskatoon, Sask.

be within a relatively restricted area or not. In the former case various possibilities exist; for example, the device might be mounted on an arm, along which it could position itself, the arm being capable of angular motion about a fixed axis (this would require two motors, each capable of motion in a forward and a reverse direction).

Tracking Over an Indefinite Area

If the surface over which the follower operates is reasonably smooth and solid, the movable framework can consist of a cart or trolley mounted on wheels. Here again, considerable mechanical variation is possible. One of the simplest schemes is to have two main traction wheels capable of independent rotation in both forward and reverse directions, the third point of support for the framework being merely a castor. The area covered by such a free follower would be limited by power considerations; it could be a battery operated mechanism and completely free, or it could receive power through a cable, in which case movement would be limited only by the length and flexibility of the cable. The path taken by the insect could be marked directly on the surface traversed or recorded remotely, using a suitable remote recording device.

Error Signal

All these continuous following devices must contain a head which will sense the direction of the error and its magnitude. In principle, only two parameters need be known, angle (or bearing) and distance, and presumably a device patterned after the wartime radar would be possible. However, it appears to be mechanically simpler to work on a system based on Cartesian rather than polar co-ordinates. One simple scheme would be to have four sensitive elements situated at the corners of a square and arranged in pairs. When the tagged insect is under the center of the square, the responses from each sensitive element would be equal and could be made to cancel one another. Any movement of the insect would upset this balance. The difference in response of the members of a pair can constitute an error signal. For example, using four Geiger tubes the difference in response can appear as a difference in voltages across the integrating circuits of ratemeters attached to each member of the pair. The voltage difference can be amplified and used to drive a servomotor in such a way as to reposition the pair of sensing elements symmetrically with respect to the insect. Having two pairs of sensing elements would serve to keep the head directly over the insect. In principle, the number of sensing elements could be reduced to three, positioned at the corners of an equilateral triangle.

A considerable saving in equipment can be achieved by using only one sensing element instead of four. The error signal might then be obtained by using a rotating shield which exposes the sensing element in sequence to radiations from the four quadrants. A commutating device would permit storage of error signals collected from each direction and these could be used to correct the error, as above. A variation of this method is to revolve the sensing element about an axis, thereby allowing collection of information from

each of the four direction quadrants in sequence. This method has been used in the present equipment.

Control Systems

With the sensing method suggested, the error signal appears as a voltage difference between the integrating condensers of a pair of ratemeters. This voltage must be amplified and may then be used to control the operation of the servomechanism in either a continuous or a discontinuous manner. While both types of control are possible, the discontinuous or on–off type, in which the servomotors are controlled by relays, is reasonably well suited to following the sluggish movement of a wireworm. A number of problems are involved, including the time lag of the equipment, the relative speeds of the follower and the insect, and the control of continuous hunting or oscillation because of overshooting the insect.

Servomotor

Various types of servomotors are available, the electrical type seeming best adapted to this problem. Series-wound motors were used in the present equipment.

Sensitive Element

Geiger tubes are the most likely sensitive elements in these devices although both scintillation counters and ionization chambers could be used as alternatives. For gamma rays the scintillation counter would have some obvious advantages, but there might be some added technical difficulties when rotating a scintillometer head as compared to those experienced when rotating a Geiger tube.

Ratemeter Operation and Statistics

The use of a Geiger tube in a sensing element would very probably involve using a ratemeter type of circuit in which the pulses from the Geiger serve to build up the voltage of a condenser. Statistical error is related to the time constant of the ratemeter, and this will, therefore, be of importance in determining the accuracy with which a moving insect can be tracked. Unfortunately, high statistical accuracy is not compatible with a short time lag, and it is, therefore, necessary in practice to adopt a compromise in order to get optimum results.

Directional Effect

Directional effects may often be improved by shielding (2). The optimum design of shielding is a much more complex problem than appears at first sight. It involves compromise since effective shielding usually cuts down the signal very considerably and thereby tends to decrease the over-all sensitivity of the system. Interest in medical applications has resulted in the development of some directional probes, but care has to be taken in applying these ideas since they do not usually involve the time lag problem inherent in insect-following devices.

DESCRIPTION OF APPARATUS

As has already been mentioned, there are two basic units in the device. One is a sensing element to determine the errors of position of a reference axis or point on the machine with respect to the radioactive source. The other is a carriage mechanism which can move the sensing element so as to effectively eliminate the measured position errors.

In the present apparatus the sensing element is a thyrode tube (Victoreen Co. 1B85) which is rotated about a vertical axis at the end of a fixed arm. The longitudinal axis of the tube lies in a plane parallel to the operating surface (soil). This axis is tangential to the circumference of a circle lying in this plane and about whose center the arm supporting the Geiger rotates (Fig. 1).

If a radioactive source lies on the axis of revolution, the distance between the source and Geiger tube will not vary during a revolution, and the counting rate of the Geiger tube per unit of revolution will be "constant" except for variations arising from the usual statistical fluctuations associated with radioactive disintegration and background.

If, however, the source does not lie on the axis of revolution, the distance between the tube and source will vary during a revolution. The count rate generated per unit angle of revolution will not then be "constant" during a revolution and will tend to be higher in those arcs of revolution where the Geiger tube is nearest the radioactive source. This variation, which is superimposed on the usual background, can be used to cause the carriage to reposition the sensing unit so as to bring the axis of revolution closer to the radioactive source. Shielding may be used to intensify these variations.

In the present model of the following unit, the Geiger pulses for each quadrant of revolution are separated by mechanical commutation. These pulses are effectively temporarily *stored* in order to develop voltages which are a function of the *average* count rate for each quadrant. The voltages resulting from collections from opposite quadrants are balanced against each other. These two different voltages are used to control the carriage movements (Fig. 2).

The carriage chosen for the present tests involves a "free" unit which is capable of a crab-like motion. This machine is free to move over a horizontal area limited only by the boundaries of a suitable operating surface and the length of the presently associated electrical cable.

There appear to be at least two possible "crab" carriage mechanisms which can utilize the error information provided by the sensing element for explicit position correction. In the one chosen, the axis of revolution of the Geiger tube passes through the vertex of a triangle which is isosceles and approximately right-angled, the axis of revolution being at right angles to the plane of the triangle.

This triangle lies in a plane approximately parallel to the plane of revolution of the Geiger and in or near the operating surface. Tractive effort produced by reversible electric motors is applied at each end of the base of this triangle. The direction of application of this effort is approximately at right angles to the base of this triangle. Most of the weight of the unit is distributed equally

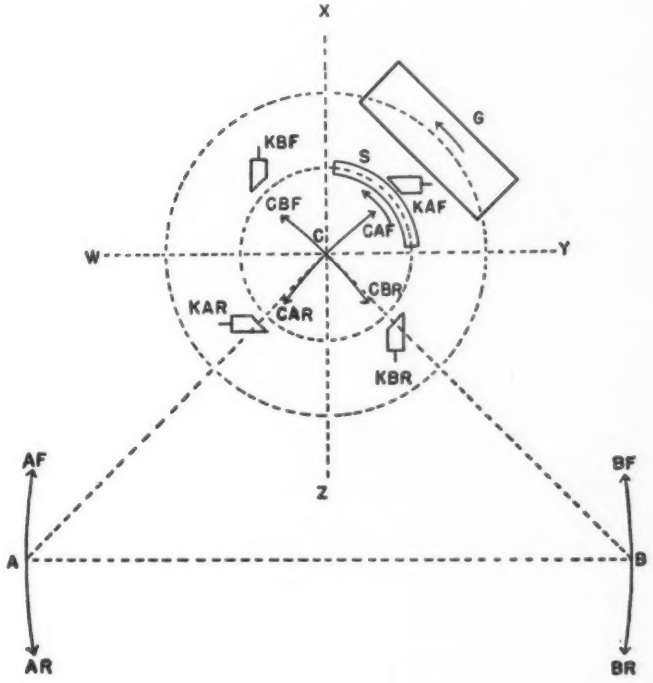

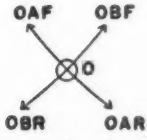

FIG. 1. Schematic diagram for interaction of sensing element and carriage unit.

ABC	Operating triangle, approximately right-angled and isosceles
A	Left traction point
B	Right traction point
C	Axis of revolution of Geiger tube and its supporting arm
AF–AR	Path of A when B is stationary
BF–BR	Path of B when A is stationary
CAF–CAR	Path of C corresponding to AF–AR
CBF–CBR	Path of C corresponding to BF–BR
O	Coaster
OAF–OAR	Path of O corresponding to AF–AR
OBF–OBR	Path of O corresponding to BF–BR
G	Geiger tube
S	Commutator segment
KAF, KAR	Collecting brushes for quadrants, XCY and WCZ, which are involved in the control of movements of A
KBF, KBR	Collecting brushes for quadrants, WCX and YCZ, which are involved in the control of movements of B

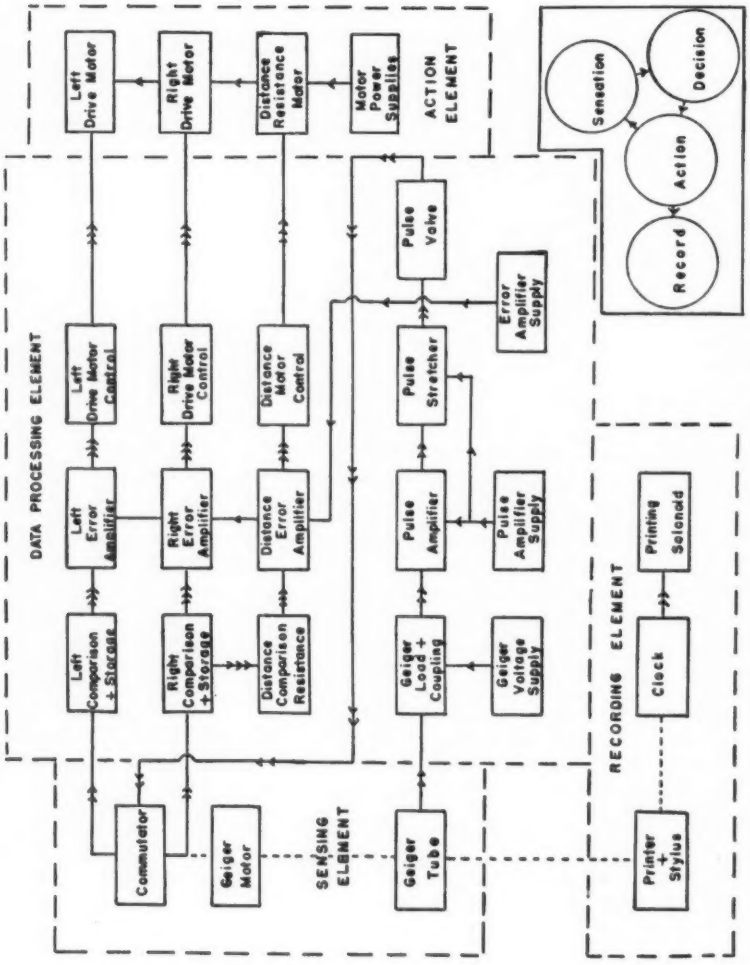

FIG. 2. Block diagram for automatic following device.

on the traction members. The remaining weight is carried by a small polished surface (coaster) which can glide freely to any position.

Small movements by either tractor result in the machine pivoting about the opposite stationary traction point. The vertex of the triangle describes a small arc of a circle for movements of either traction unit. The arcs meet approximately at right angles. The quadrants of collection for pulses from the moving Geiger tube are approximately bisected by these arcs (Fig. 1).

The motors which produce the tractive effort may operate in either direction and may operate singly or simultaneously. If the source position does not lie on or close to the axis of Geiger revolution, error signals develop and the appropriate corrective action by one or both motors is initiated. This method of steering has proved "dodge" free.

There are many general methods of converting the measured error signals into corrective tractive efforts, and for each of these general methods there are many possible variations in the arrangement of electronic and electrical components. The electrical circuits were selected mainly on the basis of availability of components. The model in its present form is not the ultimate in performance or simplicity, but it does demonstrate that a simple, economical, and practical unit is possible, and its present performance is equal to expectations.

Control in the model is of the on–off type and traction is supplied by relay-controlled series-wound electric motors. The relays are driven from the error signal voltages by d-c. amplifiers using hard vacuum tubes (Fig. 3). The error signal voltages are obtained by amplifying, lengthening, storing, and balancing the Geiger pulses. Control of hunting was obtained by limiting the speed of correction. One method used was to limit position correction to small "parcels." These "parcels" were approximately half the size of the error which could be detected. The application of these "parcels" was followed by a forced inoperative interval. This interval allowed the storage and balancing circuits to readjust and accumulate reliable error data as a basis for each succeeding parcel of correction. (It was also possible to achieve control of hunting by using relay-controlled, continuous correction at a constant slow speed of about 45 in. per hr. which is, of course, much greater than the speed at which wireworms normally move.)

All translatory movements of the axis of Geiger revolution are recorded on the operating surface by a stylus which is almost coincident with this axis.

A record of the time at which the machine and active source were in a given position is obtained from a clock-driven printing wheel carrying suitable marking symbols representing the time on its periphery. At chosen intervals this wheel is inked and momentarily pressed against the operating surface. The printer is presently activated by a solenoid controlled by the clock through a switch, a sensitive relay, and a slowly charged condenser.

A record of the distance of the radioactive source from the operating surface is also available. This is obtained by measuring the mean of one pair of the voltages collected for position error determination. The magnitude of these mean voltages depends on the distance of the radioactive source from the operating surface. It is measured with a self-balancing bridge. The collected

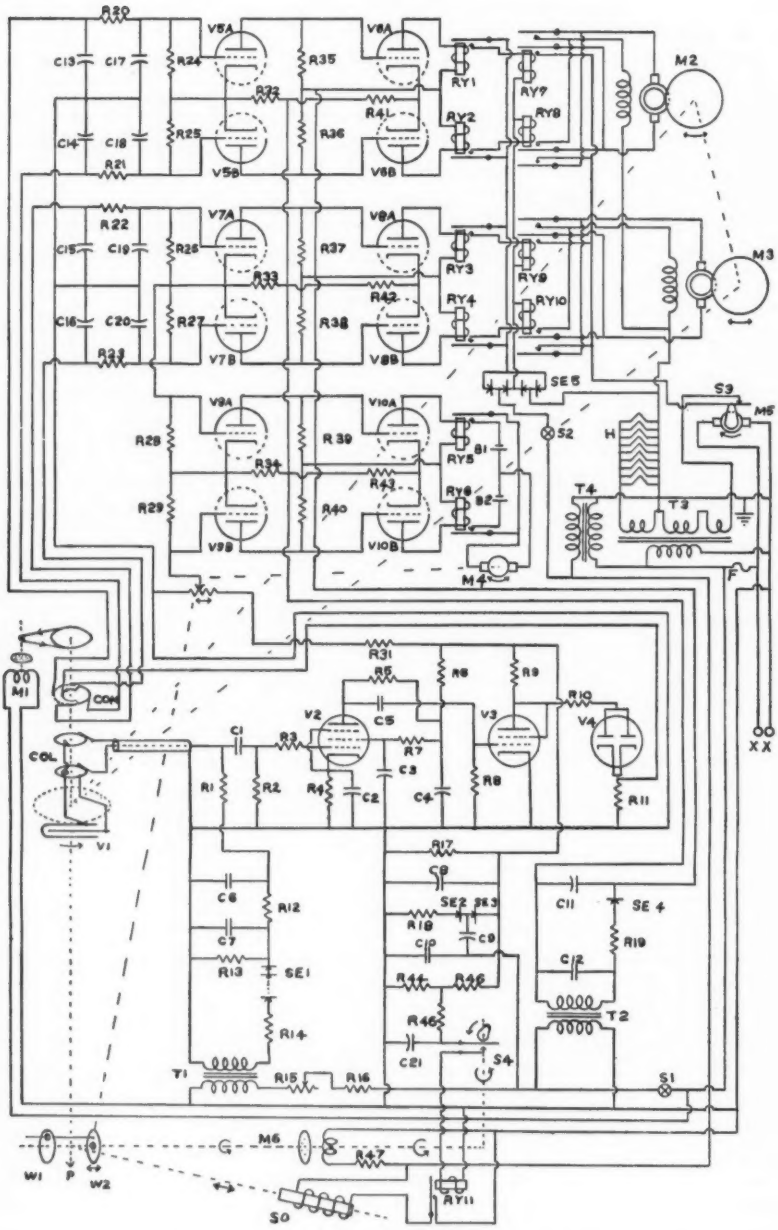

FIG. 3. Circuit diagram for automatic following device.

PARTS LIST FOR AUTOMATIC FOLLOWING MECHANISM (Fig. 3)

Condensers

C 1— 50 μμf., 2500 v., mica
C 2— 25 μf., 25 v., electrolytic
C 3— 8 μf., 450 v., electrolytic
C 4— 8 μf., 450 v., electrolytic
C 5—0.02 μf., 600 v., paper
C 6— 0.5 μf., 2000 v., oil filled
C 7— 0.5 μf., 2000 v., oil filled
C 8— 8 μf., 450 v., electrolytic
C 9— 40 μf., 150 v., electrolytic
C10— 0.1 μf., 600 v., paper
C11— 80 μf., (2 × 40), 150 v., electrolytic
C12— 0.1 μf., 600 v., paper
C13— 30 μf., 150 v., electrolytic
C14— 30 μf., 150 v., electrolytic
C15— 30 μf., 150 v., electrolytic
C16— 30 μf., 150 v., electrolytic
C17— 100 μf., 50 v., electrolytic
C18— 100 μf., 50 v., electrolytic
C19— 100 μf., 50 v., electrolytic
C20— 100 μf., 50 v., electrolytic
C21— 100 μf., 50 v., electrolytic

Resistances

R 1—10 megohms, 1 w.
R 2—100,000 ohms, 2 w.
R 3—100,000 ohms, 2 w.
R 4—300 ohms, 2 w.
R 5—50,000 ohms, 10 w.
R 6—5000 ohms, 10 w.
R 7—100,000 ohms, 2 w.
R 8—1 megohm, 2 w.
R 9—20,000 ohms, 10 w.
R10—30,000 ohms, 2 w.
R11—5000 ohms, 2 w.
R12—2 megohms, 2 w.
R13—4 megohms (2 × 2), 2 w.
R14—10,000 ohms, 2 w.
R15—500 ohms, variable
R16—500 ohms, 10 w.
R17—20,000 ohms, 10 w.
R18—50 ohms, 10 w.
R19—50 ohms, 10 w.
R20—5000 ohms, 2 w.
R21—5000 ohms, 2 w.
R22—5000 ohms, 2 w.
R23—5000 ohms, 2 w.
R24—47,000 ohms, ½ w.
R25—47,000 ohms, ½ w.
R26—47,000 ohms, ½ w.
R27—47,000 ohms, ½ w.
R28—47,000 ohms, ½ w.
R29—47,000 ohms, ½ w.
R30—10,000 ohms, potentiometer, wire-wound, linear taper
R31—50,000 ohms, 10 w.
R32—50,000 ohms, 2 w.
R33—50,000 ohms, 2w.
R34—50,000 ohms, 2 w.
R35—100,000 ohms, 2 w.
R36—100,000 ohms, 2 w.
R37—100,000 ohms, 2 w.
R38—100,000 ohms, 2 w.
R39—100,000 ohms, 2 w.
R40—100,000 ohms, 2 w.
R41—20,000 ohms, 2 w.
R42—20,000 ohms, 2 w.
R43—20,000 ohms, 2 w.
R44—10,000 ohms, 2 w.
R45—20,000 ohms, 2 w.
R46—500,000 ohms, 2 w.
R47—50 ohms, 10 w.

Tubes

V 1—1B85 (Victoreen)
V 2—6AC7
V 3—6V6
V 4—6H6
V 5—6SL7GT
V 6—6SN7GT
V 7—6SL7GT
V 8—6SN7GT
V 9—6SL7GT
V10—6SN7GT

Relays

RY 1—Plate circuit relay, 5000 ohms, SPDT
RY 2—Plate circuit relay, 5000 ohms, SPDT
RY 3—Plate circuit relay, 5000 ohms, SPDT
RY 4—Plate circuit relay, 5000 ohms, SPDT
RY 5—Plate circuit relay, 5000 ohms, SPDT
RY 6—Plate circuit relay, 5000 ohms, SPDT
RY 7—Medium power relay, 24 v., DPST
RY 8—Medium power relay, 24 v., DPST
RY 9—Medium power relay, 24 v., DPST
RY10—Medium power relay, 24 v., DPST
RY11—Plate circuit relay, 5000 ohms, SPDT

Rectifiers

Se1—Selenium rectifier, 1000 v.
Se2—Selenium rectifier, 150 v., 100 ma.
Se3—Selenium rectifier, 150 v., 100 ma.
Se4—Selenium rectifier, 150 v., 100 ma.
Se5—Selenium bridge rectifier, 30 v., 1 amp.

Transformers (all have 110 v., 60 cycle primaries)

T1—1100 v., 1.5 ma.
T2—110 v., 15 ma.
T3—6.3, 5, and 2.5 v. filament
T4—30 v., 3.5 amp.

Motors

M1—110 v., 60 cycle gramophone type
M2— 12 v., series with gear train
M3— 12 v., series with gear train
M4— 1.5 v., with gear train
M5—110 v., stirring motor
M6— 24 v., 60 cycle, synchronous clock motor with gear train

Switches

S1—Toggle, SPST
S2—Toggle, SPST
S3—Micro switch, SPST
S4—Micro switch, SPST

Miscellaneous

H—Tube heaters
B1—Size D flashlight cell
B2—Size D flashlight cell
So—Solenoid, 12 v.
W1—Time printing wheel
W2—Depth printing wheel
P—Tracing stylus
Com—Commutator
Col—Collector rings
F—Fuse
XX—Power input terminals (to 115 v. constant voltage transformer)

voltage is compared with the voltage across the slider and ground end of a potentiometer by a third d-c. amplifier. If these voltages are not in close agreement, a relay-controlled motor repositions the potentiometer slider so as to obtain agreement. Rotation of this potentiometer shaft moves a crank which changes the distance between the time printing wheel and a similar and angularly synchronized distance printing wheel. The printing operation therefore produces two identical characters whose character indicates time, and whose separation is a measure of the distance of the radioactive source from the operating surface.

GENERAL COMMENTS

The apparatus described has been built. It is able to home on to a wireworm tagged with 20 μc. of Co^{60} from a distance of about 15 in. It is quite able to follow such a tagged wireworm through 4 in. of soil, with an average position error of about $\frac{1}{4}$ in. It is capable of continuous operation at the usual speed for wireworms, a few inches per hour. It can, if necessary, travel much faster than this (up to 45 in. per hr.).

The principle of a rotating Geiger would seem to be capable of numerous other applications. Some of these will be described in subsequent publications.

ACKNOWLEDGMENT

We are grateful to the Dominion Department of Agriculture, Division of Entomology, for generous financial assistance.

REFERENCES

1. Arnason, A. P., Fuller, R. A., and Spinks, J. W. T. Science, 111: 5. 1950.
2. Corbett, B. D. and Honour, A. J. Nucleonics, 9 (No. 5): 43. 1951.

AMINOMETHIONATE SALTS

II. OPTIMUM CONDITIONS FOR FORMATION OF MONOPOTASSIUM AMINOMETHIONATE BY THE VON PECHMANN AND MANCK PROCESS[1]

By R. A. B. Bannard[2] and J. H. Ross

ABSTRACT

Maximum recovery of monopotassium aminomethionate from aqueous solution results by acidification to pH 3.0 or lower. When the reaction between potassium cyanide and potassium bisulphite is initiated at 25°C. and a closely controlled heating cycle is used, the yield of monopotassium aminomethionate varies with pH and reaches a maximum of 60% at pH 7.85. The relationship between pH and yield is unaffected by changing the temperature of initiation of the reaction to 10°C. or 40°C. The rate of heating does not affect the relationship between pH and yield provided it exceeds approximately 1°C. per minute. The yield reaches a maximum where the molar ratio SO_2/CN is 2.3.

INTRODUCTION

In 1895 von Pechmann and Manck (2) described a process for the preparation of monopotassium aminomethionate (I). In this process potassium cyanide was added to a potassium bisulphite solution and the resultant solution was heated on a water bath with addition of hydrochloric acid to neutralize the alkaline reaction which occurred. Acidification of the cooled solution furnished the monopotassium salt I in 58–72% yield.

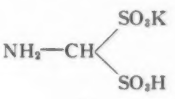

I

Repetition of the procedure given by von Pechmann and Manck (2) gave only a 40% yield of the desired substance and a study was begun to determine the limits within which the yield is influenced by solubility of monopotassium aminomethionate, pH, temperature of initiation, rate of heating, and the molar ratio SO_2/CN.

RESULTS AND DISCUSSION

Dipotassium aminomethionate (II) was considered by von Pechmann and Manck (2) to be the primary reaction product, formed by addition of two molecules of potassium bisulphite across the carbon—nitrogen triple bond in the hydrogen cyanide molecule. Monopotassium aminomethionate (I) was,

[1]*Manuscript received April 29, 1955.*
Contribution from McGill University and the Pulp and Paper Research Institute of Canada, Montreal, Quebec, with financial assistance from the National Research Council of Canada and the Defence Research Board of Canada.
[2]*Holder of Studentships under the National Research Council of Canada, 1947–49. Present address: Defence Research Chemical Laboratories, Ottawa, Ontario.*

then, a secondary product resulting from acidification of the solution of the dipotassium salt II. If the hypothesis advanced by von Pechmann and

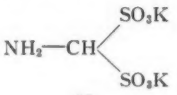

II

Manck is correct, the formation of aminomethionate salts is analogous to the well-known formation of α-hydroxysulphonates by interaction of bisuphites with carbonyl compounds. It was not the purpose of this investigation to reach a conclusion regarding the mechanism of the reaction. However, some observations made during the present study tend to emphasize the similarity of the bisulphite–cyanide reaction to bisulphite – carbonyl addition reactions and are noted here because they would be of importance should a detailed mechanistic study be undertaken.

It was desirable to determine the influence of pH on recovery of monopotassium aminomethionate from aqueous solution since this substance contains an acidic group and a potentially basic group. From Fig. 1 it is clear

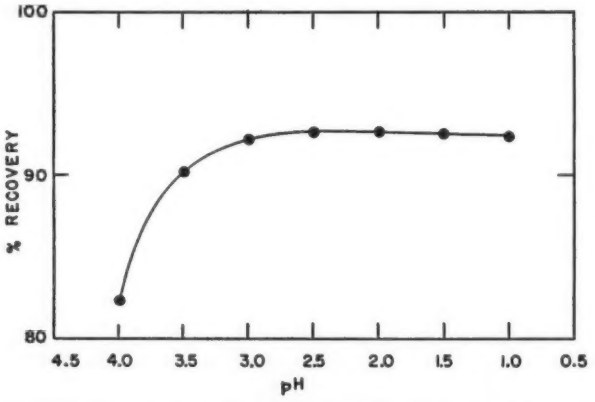

FIG. 1. Percentage recovery of monopotassium aminomethionate from aqueous dipotassium aminomethionate solutions at 25°C.

that maximum recovery of 92% is realized at 25°C. at a pH below 3. Since the solubility of the monopotassium salt I is 1 gm./100 ml. at 25°C., losses caused by this factor will be negligible in this pH range.

It was evident from von Pechmann and Manck's (2) description of the process that they had operated in solutions approximately 3.5 molar (*M*) in potassium bisulphite. Preliminary experiments established that addition of potassium cyanide to such solutions caused an almost instantaneous increase in pH and temperature and suggested that the original workers had probably conducted their process at a pH level within the range 7 to 9 and at temperatures within the range 20° to 80°C.

Fig. 2 shows the critical influence which pH exerts on the yield of monopotassium aminomethionate within the range 6.60 to 9.00 when heating schedule A in Table I is used. A maximum yield of approximately 60% is obtained at pH 7.85, above or below which pH the yield decreases rapidly. The reason for maximum yields at pH 7.85 is not known with certainty. However, it appears probable that this pH level corresponds to maximum

TABLE I

HEATING SCHEDULES FOR PREPARATION OF MONOPOTASSIUM AMINOMETHIONATE

Time, min.	Temperature, °C.,* for heating schedule:				
	A	A+15	A−15	2A	½A
0	25	40	10	25	25
1	33	48	20	33	33
5	42	58	27	51	38
10	50	66	35	68	42
15	56	71	41	79	45
20	62	77	47	80	48
25	70	80	55	80	52
30	75	80	60	80	55
35	79	80	65	80	58
40	80	80	70	80	61
45	76	76	75	77	64
50	73	73	80	73	67
55	70	70	80	70	70
60			77		73
65					76
70					79
75					80
80					80

*±2°C.

stability of dipotassium aminomethionate (II). This is an attractive explanation because it has been found that monopotassium aminomethionate (I) decomposes in aqueous solution with evolution of sulphur dioxide; that dipotassium aminomethionate (II) in alkaline solution decomposes with regeneration of sulphite and cyanide; and that the equivalence point in potentiometric titration of 0.01 *M* monopotassium aminomethionate with 0.01 *M* potassium hydroxide is at pH 8 (1).

The influence of pH in this reaction seems to be analogous to the effect of pH on the formation of α-hydroxysulphonates. Shriner and Land (4) have pointed out that the reaction which leads to formation of α-hydroxysulphonates is an equilibrium process which is readily shifted in favor of the addition product or original reactants, depending on the pH of the reaction medium. It has been shown (5, 6) that the pH of maximum stability may be expected to shift with different members of the α-hydroxysulphonate series. Stewart and Donnally (5) found sodium benzaldehyde-bisulphite to possess maximum stability at pH 1.8, whereas Tomoda (6) found sodium acetaldehyde-bisulphite to be stable at pH 6–8.

It does not appear that a preponderance of either sulphite or bisulphite ions favors the formation of aminomethionate salts since extrapolation of the

curve in Fig. 2 suggests that no aminomethionate salt would be obtained by operating at a pH at which one or other of these ions is exclusively present (viz. pH 4.40 for bisulphite or pH 10.65 for sulphite). This inference from Fig. 2 was verified in the case of sulphite solutions. If a 3.5 *M* potassium

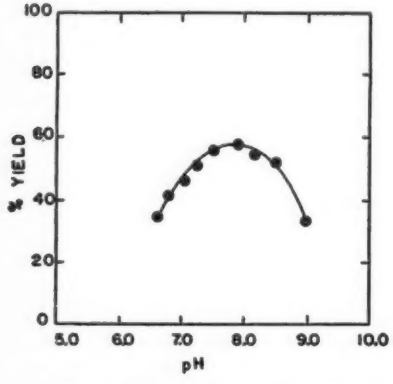

FIG. 2. Relation between pH and yield of monopotassium aminomethionate for heating schedule A.

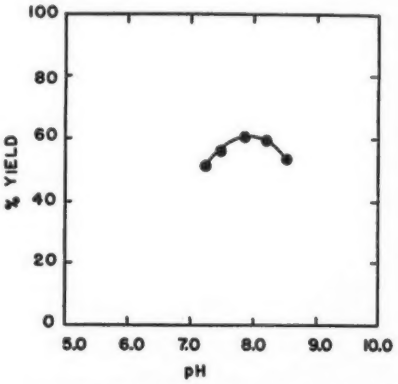

FIG. 3. Relation between pH and yield of monopotassium aminomethionate for heating schedule A+15.

sulphite solution is treated with potassium cyanide and the resultant solution (pH 11.50) heated according to schedule A without pH control, cooled rapidly to room temperature, and acidified to pH 2.5, no monopotassium aminomethionate is obtained. If, however, the pH of a solution such as described above is adjusted rapidly, after 25 min. of heating, to a pH level known from Fig. 2 to favor aminomethionate formation and the reaction continued at the favorable pH by addition of acid, a good yield of monopotassium aminomethionate is obtained. This result suggests that there is no interaction between sulphite and cyanide in solutions of high pH.

It was expected that the relationship between pH and yield established for heating schedule A would be displaced by the use of a different heating schedule. It was hoped that judicious alteration of the heating schedule would produce higher yields by upward displacement of the curve in Fig. 2.

The effect of changing the temperature of initiation of the reaction from 25°C. to 40°C. or 10°C. was studied by substituting heating schedules A+15 and A−15 for schedule A (Table I). Results are summarized in Fig. 3 and experiments 12 and 13 in Table II. It is clear that yields are the same as those obtained under otherwise identical conditions by the use of schedule A. It must, therefore, be concluded that displacement of the temperature of initiation within reasonable limits does not affect the yield.

The effect of changing the rate of heating was studied by substituting heating schedules 2A and ½A in Table I for schedule A. The results given in Table II indicate by comparison with Fig. 2 that doubling the rate of heating

TABLE II

pH–YIELD RELATIONSHIPS FOR HEATING SCHEDULES 2A, ½A, AND A–15

Experiment number	pH	% yield*	Heating schedule
1	7.85	57.6	2A
2	7.85	57.3	2A
3	7.20	51.4	2A
4	7.20	50.7	2A
5	7.85	50.7	½A
6	7.85	48.9	½A
7	7.85	48.0	½A
8	7.85	51.0	½A
9	7.85	55.0	½A
10	7.10	46.5	½A
11	7.20	44.0	½A
12	7.85	58.4	A–15
13	7.85	59.1	A–15

**Based on cyanide.*

used in schedule A has no effect on the yield (experiments 1 to 4) but that halving the rate of heating used in schedule A causes a general downward displacement in yield and poorer reproducibility (experiments 5 to 11). It is, therefore, evident that the yield of monopotassium aminomethionate at any given pH is unaffected by the rate of heating provided it exceeds a limiting value of approximately 1°C. per minute. However, when the work is done in an open system care must be exercised in the choice of initial acidity and temperature of initiation since considerable hydrogen cyanide may be lost by volatilization from a solution which contains a high percentage of free hydrogen cyanide.

If the ratio SO_2/CN is varied over a relatively wide range, the yield based on cyanide reaches a maximum where $SO_2/CN = 2.3$. Above this ratio there is no advantage in increasing the quantity of combined sulphur dioxide relative to cyanide, as shown in Fig. 4.

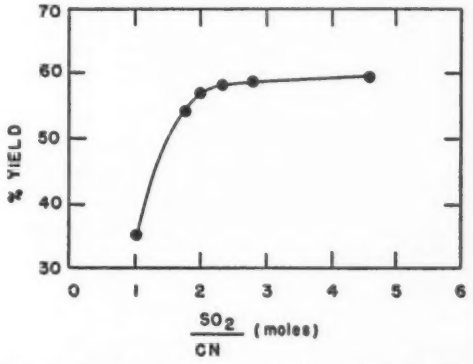

FIG. 4. Relation between sulphur dioxide – cyanide ratio and yield of monopotassium aminomethionate.

EXPERIMENTAL

The experiments were performed in a beaker of appropriate size equipped with a thermometer, high temperature glass and calomel electrodes, mechanical stirrer, and burette. A Beckman Model H2 pH meter was used to obtain pH readings. When necessary, the temperature of the system was controlled within ±2°C. by use of a water bath of 2 liters' capacity.

Potassium bisulphite solutions were prepared either by interaction of sulphur dioxide and potassium hydroxide in aqueous solution or by dissolving potassium metabisulphite and potassium sulphite in water. All chemicals were reagent grade and their purities were redetermined by standard methods before use. The sulphur dioxide content of potassium bisulphite solutions prepared from sulphur dioxide and aqueous alkali was established by a standard iodometric procedure (3).

The purity of air-dried monopotassium aminomethionate from the process was determined by routine analysis for nitrogen by the Kjeldahl method (7). Anal. Calc. for $CH_4O_6NS_2K$: N, 6.11%. Found: N, 5.91 to 6.00%.

Influence of pH on Recovery of Monopotassium Aminomethionate from Solution

The solubility of monopotassium aminomethionate in water was determined at 25°C. and found to be 1 gm. per 100 ml. Monopotassium aminomethionate (100 gm.) was dissolved in water (400 ml.) by treatment with an equimolar quantity of 20% potassium hydroxide solution (105 ml.). The solution was adjusted to pH 7 by addition of concentrated hydrochloric acid, transferred quantitatively to a 1-liter volumetric flask, and diluted to volume. In each experiment which followed, 100 ml. of the solution was transferred by means of a burette to a beaker equipped with a mechanical stirrer and electrodes for pH determination. The solution was adjusted to pH 5.50 by addition of concentrated hydrochloric acid, after which 2 *N* hydrochloric acid was added to precipitate the monopotassium aminomethionate at 25°C. The solution, became turbid at pH 4.75 and precipitation began immediately thereafter. The pH remained constant at 4.30 while considerable acid was added and precipitation continued. In successive experiments addition of acid was stopped at different pH levels within the region 4.0 to 1.0. The precipitated salt was collected, dried in a vacuum desiccator in the presence of phosphorus pentoxide, and weighed.

Influence of pH on the Yield of Monopotassium Aminomethionate

Experiments were performed according to the following method:

A potassium bisulphite–sulphite solution containing 0.702 M. of combined sulphur dioxide (3.51 *M*) was treated at 25°C. with 0.301 M. of potassium cyanide (ratio $SO_2/CN = 2.33$) in one portion. Heating was conducted according to schedule A in Table I and the pH of the solution adjusted, if necessary, to a preselected level within the pH range 6.60 to 9.00, where it was held constant (±0.05 pH units) for the remainder of the heating cycle. Concentrated hydrochloric acid was used to maintain the desired pH level. The solution was cooled to 20°C. over a period of 10 min. and the mono-

potassium aminomethionate precipitated at 20–25°C. by further addition of concentrated hydrochloric acid over a period of 11 min. to adjust the mixture finally to pH 2.5 at 20°C. After the mixture had been allowed to stand for 30 min. in a water bath at 12°C. the monopotassium aminomethionate was collected by filtration, washed with 50 ml. of water, air-dried, and weighed.

Influence of Heating Schedule on pH–Yield Relationship

The procedure was the same as described above except that heating schedule A+15, A−15, 2A, or ½A (Table I) was substituted for schedule A.

Influence of Molar Ratio SO_2/CN on the Yield of Monopotassium Aminomethionate

A series of experiments were performed according to the general method given above with control of pH at 7.85 using heating schedule A, while the molar ratio SO_2/CN was varied within the limits 1.01 to 4.56.

ACKNOWLEDGMENTS

Thanks are extended to the National Research Council of Canada for the award of two Studentships to one of us (R.A.B.B.), and to the Defence Research Board of Canada for a grant-in-aid for the purchase of equipment and summer maintenance.

REFERENCES

1. BANNARD, R. A. B. Ph.D. Thesis, McGill University, Montreal, Que. 1949. p. 145.
2. VON PECHMANN, H. and MANCK, P. Ber. 28: 2374-2383. 1895.
3. SCOTT, W. W. Standard methods of chemical analysis. Vol. I. 4th ed. D. Van Nostrand Company, Inc., New York. 1927. p. 512.
4. SHRINER, R. L. and LAND, A. H. J. Org. Chem. 6: 888–894. 1941.
5. STEWART, T. D. and DONNALLY, L. H. J. Am. Chem. Soc. 54: 2333–2340. 1932.
6. TOMODA, Y. J. Soc. Chem. Ind. Japan, 30: 747–759. 1927.
7. VOGEL, A. I. A text-book of quantitative inorganic analysis. Longmans, Green and Co., London. 1939. p. 307.

TRANSMISSION OF STRESS THROUGH A THICK SLAB SUPPORTED BY A YIELDING FOUNDATION[1]

By J. E. Campbell and H. S. Heaps

ABSTRACT

Closed formulae are obtained for the stresses and displacements in a finitely thick elastic slab of infinite lateral extent supported by a perfectly discontinuous elastic medium and subject to a load which varies in one direction only. A table is provided to facilitate the calculation of the vertical stress transmitted through the lower surface of the slab to the underlying material. The table may also be used in the case of an axially symmetric load. For a surface load distributed uniformly over a line or over a half plane the transmitted stresses are shown graphically. The results are dependent upon the foundation modulus k. The range of values chosen for k is sufficient to enable application of the results to foundations that are extremely yielding as well as to those which are effectively rigid and to intermediate cases.

1. INTRODUCTION

A problem which arises in connection with foundation design is the estimation of the stress transmitted through a thick slab to a supporting medium when a static load is applied to the upper surface of the slab. In many instances it is justifiable to suppose that the slab behaves throughout as a perfectly elastic material, the applied loads being insufficient to cause plastic flow or fracture. Also if the slab extends to a sufficient horizontal distance in all directions from the loaded area the stress transmitted through its lower surface is as for a slab of infinite lateral extent, and for purposes of calculation it may be regarded as such. The weight of the slab is then borne uniformly by the underlying material to whose consequent state of stress must be added that due to the surface load.

The state of stress of the material of the slab, and hence the stress transmitted to the underlying medium, depends upon the known elastic constants of the slab and also upon the behavior of the interface between the slab and the supporting medium with regard to both deformation and transmission of stress. The behavior of the interface depends upon the properties of the bond between the slab and the bed as well as upon the elastic or plastic properties of the material comprising the bed. In many problems such properties are unknown or may be deduced only to within a considerable degree of possible error. Accordingly any theory of stress transmission should include an estimation of the effects of inaccuracies in the assumptions upon the validity of the results.

If the underlying material is assumed to have the elastic properties of the slab and to exhibit a perfect bond with the lower surface of the slab the stress transmitted through the base is as calculated by the Boussinesq theory for a

[1]*Manuscript received March 14, 1955.*
Contribution from the Department of Civil Engineering, Nova Scotia Technical College, Halifax, Nova Scotia.

semi-infinite medium (4). While the assumptions are seldom realistic in foundation problems the Boussinesq theory is useful in providing a standard with which to compare the stresses predicted by the alternative theories.

If the underlying foundation behaves elastically but has different elastic constants from the material comprising the slab, then the stress transmitted to it depends upon the type of bond at the lower surface of the slab. The consequent analysis when the slab behaves as a thin plate and carries an axially symmetric load has been presented by Hogg (15) in terms of Terazawa's general solution (24) of Boussinesq's problem. The type of bond considered by Hogg is either one which transmits no shear forces or one at which no lateral displacement occurs. Fox (11) has dealt with the similar problem when the slab has finite thickness and when there is perfect adhesion or lack of adhesion at the bond, while Acum and Fox (1) and Burmister (5) have considered the effect of a composite slab consisting of two distinct layers.

An alternative hypothesis concerning the underlying material is that it behaves as a perfectly discontinuous elastic material in that the vertical deflection of the upper surface at any place is proportional only to the vertical stress transmitted across it at that place and is independent of the stress at neighboring points. The boundary between the slab and the supporting medium is assumed to be perfectly frictionless. Hetényi (14) has made a detailed analysis of the deflection of a thin elastic beam resting upon a perfectly discontinuous foundation, while treatments of the deflection of a circular or rectangular thin elastic plate supported by discontinuous material have been made by Timoshenko (25) and others (6, 10, 20). A discussion of the deflection of a thin elastic plate of infinite extent has been made by Livesley (18). Hetényi has also considered a foundation in which partial continuity is achieved by imbedding a continuous beam in an otherwise perfectly discontinuous medium.

Although the stresses in finitely thick slabs subject to various systems of specified forces at the upper and lower boundaries have been obtained by Filon (8), Dougall (7), and Sneddon (22, 23), relatively little attention has been paid to the consideration of a loaded thick plate supported by forces resulting from the deformation of a perfectly discontinuous medium. Jeffreys (16) has used an approximate method to determine the state of stress in the thick elastic crust of the earth below a sinusoidal mountain range of infinite extent when the crust is supported by a perfectly discontinous medium which yields according to isostatic compensation. In a previous paper (12) formulae were derived for the stresses in a thick plate of infinite extent resting upon a perfectly discontinuous elastic medium and supporting an axially symmetric load. For one particular, but somewhat arbitrary, choice of dimensions and elastic constants the stresses in the plate and the radial displacements at the upper and lower surfaces (13) were computed numerically. Calculation of the stresses for a given set of dimensions is extremely tedious and the formulae do not indicate readily the variation of the results with change of the occurring parameters.

In the present paper closed formulae are obtained for the stresses in a finitely thick elastic slab of infinite lateral extent supported by a perfectly discontinuous elastic medium and carrying a load which varies in one direction only. It is assumed that the interface between the slab and the supporting medium is able to withstand either tension or compression. The results depend upon the thickness $2b$, the modulus of elasticity E, and the Poisson's ratio σ, of the material of the slab, and also upon the foundation modulus k. The foundation modulus at the surface of a discontinuous medium is defined to be the vertical stress at any place necessary to produce unit displacement there. The slab thickness and the elastic constants affect the resulting equations through a single dimensionless parameter $c = 2kb(1-\sigma^2)/E$.

The value of the foundation modulus varies between zero in the case of a medium incapable of bearing any load and infinity in the case of a perfectly rigid base. In the problems which illustrate Hetényi's analysis (14) it is assumed that k lies in the neighborhood of 200 lb./in.^{3}; Murphy (20) uses a value of 100 lb./in.^{3}, while Livesley (18) quotes a value of 750 lb./in.^{3} Merritt and Housner (19) assume a modulus of 5.2×10^5 lb./ft.^{3} = 300 lb./in.^{3} for a foundation of medium soft clay. Field tests made by Shockley (21) in connection with a soil whose upper 10 ft. consists of a soft clay shale containing some clay suggest that k values of between 695 and 2200 lb./in.^{3} should be considered. In the latter tests it is found that the modulus is independent of the load as it varies between 300 and 10,000 lb./in.^{3}; the wide variation in k is due to the fact that the loads were applied over different rigid plane areas and thus under conditions of constant indentation rather than constant reaction. The Kansas State Highway Commission (17) reports various k values between 250 and 640 lb /in.^{3} for a subgrade of clay loam and clay while the addition of sand gravel produced a subbase for which k varied between 880 and 910 lb./in.^{3}

For a perfectly rigid foundation the modulus k is equal to infinity and the resulting analysis involves simpler mathematical expressions. Biot (3) has treated this case under the assumption of either perfect adhesion or perfect lack of friction at the lower surface of the slab. Either assumption leads to the prediction of similar vertical stresses transmitted to the underlying material but there is considerable difference from the stresses of the Boussinesq theory. Since in practice no foundation is perfectly rigid, it is of interest to consider the effect upon the stresses of a reduction of the foundation modulus from infinity to a large, but finite, value. According to Benscoter (2) the value of k to be assumed for a nearly rigid foundation is $E/100$ where E, in lb./in.^{2}, is the modulus of elasticity of the material concerned.

For a reinforced concrete slab of thickness $2b$ = 6.75 in., with $E = 6\times10^6$ lb./in.^{2} and $\sigma = 1/3$, as the foundation modulus k ranges between 100 and 1000 lb./in.^{3} the parameter c ranges between 0.0001 and 0.001. A further illustration is provided by the case of a sandstone slab of thickness $2b$ with $E = 2.8\times10^6$ lb./in.^{2} and $\sigma = 0.20$ supported upon a coal seam of the same thickness and with $E = 6\times10^5$ lb./in.^{2} If the coal behaves as a perfectly discontinuous medium, and if its lower surface may be supposed at rest,

then a deflection of 1 in. at its upper surface involves a reaction of magnitude $k = (1/2b)\times 6\times 10^5$ lb. Hence at the sandstone and coal boundary $c = 0.21$.

In Section 2 general formulae are obtained for the stresses and displacements at a general point within the slab. Numerical values of the vertical stress transmitted to the underlying medium at the lower surface of the slab are calculated in Section 3 for values of the parameter c over the range 10^{-4} to infinity. The results are thus quite general, applying to discontinuous foundations that are extremely yielding as well as to those which are effectively rigid and to intermediate cases.

2. GENERAL FORMULAE FOR THE STRESSES AND DISPLACEMENTS WITHIN THE LOADED SLAB

Consider an elastic slab of infinite area and of thickness $2b$, its upper surface being the plane $z = -1$ and its lower surface being the plane $z = 1$, supported by a perfectly discontinous elastic foundation. Let the surface deflection of the foundation at any place be equal to $1/k$ times the vertical force per unit area between the lower surface of the slab and the foundation at that place. Let an x axis be chosen in the plane $z = 0$ and distances be measured along this axis in units of b, and suppose that a vertical load of amount $p(x)$ per unit area is applied to the upper surface of the slab.

If the modulus of elasticity of the plate is denoted by E and Poisson's ratio by σ, the stresses per unit area, in the usual suffix notation, may be written as complex Fourier transforms as follows (23, p. 404):

$$[1a] \qquad \sigma_x = (1/2\pi)\int \partial^2 G/\partial z^2 \exp(-isx)ds,$$

$$[1b] \qquad \sigma_z = -(1/2\pi)\int s^2 G \exp(-isx)ds,$$

$$[1c] \qquad \tau_{xz} = (i/2\pi)\int s\partial G/\partial z \exp(-isx)ds,$$

in which the integrations are from $-\infty$ to $+\infty$. G is a function of the form

$$[2] \qquad G(s, z) = [A(s)+B(s)sz]\cosh sz+[C(s)+D(s)sz]\sinh sz$$

where A, B, C, and D are arbitrary functions of s. The displacements u and w in the directions of x and z are given by

$$[3a] \quad u = (i/2\pi E)(1+\sigma)b\int[(1-\sigma)\partial^2 G/\partial z^2+\sigma s^2 G](1/s)\exp(-isx)ds,$$

$$[3b] \quad w=(1/2\pi E)(1+\sigma)b\int[(1-\sigma)\partial^3 G/\partial z^3+(\sigma-2)s^2\partial G/\partial z](1/s^2)\exp(-isx)ds.$$

The coordinates x and z are dimensionless, the displacements u and w have the dimension of b, while the stresses σ_x, σ_z, τ_{xz} also depend upon the dimension of b.

The stresses and displacements must satisfy the following boundary conditions:

(i) at $z = -1$, $\tau_{xz} = 0$ and $\sigma_z = -p(x)$,

(ii) at $z = 1$, $\tau_{xz} = 0$ and $\sigma_z = -kw$.

Substitution of the expressions [1], with G of [2], into the conditions (i) and

(ii) provides four equations for determining the functions A, B, C, and D. If $2kb(1-\sigma^2)/E$ is denoted by c, the values obtained for A, B, C, and D are

$$[4a] \qquad A = \frac{2[s(\sinh 2s - 2s) + 2c\cosh^2 s](\sinh s + s\cosh s)}{2s(\sinh^2 2s - 4s^2) + c(\sinh 4s + 4s)} q/s^2,$$

$$[4b] \qquad B = \frac{2[s(\sinh 2s + 2s) + 2c\sinh^2 s]\cosh s}{2s(\sinh^2 2s - 4s^2) + c(\sinh 4s + 4s)} q/s^2,$$

$$[4c] \qquad C = \frac{-2[s(\sinh 2s + 2s) + 2c\sinh^2 s](\cosh s + s\sinh s)}{2s(\sinh^2 2s - 4s^2) + c(\sinh 4s + 4s)} q/s^2,$$

$$[4d] \qquad D = \frac{-2[s(\sinh 2s - 2s) + 2c\cosh^2 s]\sinh s}{2s(\sinh^2 2s - 4s^2) + c(\sinh 4s + 4s)} q/s^2,$$

where

$$[5] \qquad q(s) = \int p(x)\exp(isx)\,dx.$$

Substitution of G from [2] and [4] into [1] and [3] leads to the following expressions for the stresses and displacements at the point (x, z):

$$[6a] \tfrac{1}{4}(\sigma_x + \sigma_z) = -(1/2\pi)\int s[\sinh 2s \sinh(1-z)s - 2s\sinh(1+z)s](q/F)\exp(-isx)ds - (c/2\pi)\int \sinh 2s\cosh(1-z)s(q/F)\exp(-isx)ds,$$

$$[6b] \quad \tfrac{1}{4}(\sigma_x - \sigma_z) = (1/2\pi)\int s^2[(1+z)\sinh 2s\cosh(1-z)s - 2s(1-z)\cosh(1+z)s] \times (q/F)\exp(-isx)ds + (c/2\pi)\int s[(1+z)\sinh 2s\sinh(1-z)s + 2\cosh(1+z)s](q/F)\exp(-isx)ds,$$

$$[6c] \quad \tfrac{1}{2}\tau_{xz} = -(i/2\pi)\int s^2[(1+z)\sinh 2s\sinh(1-z)s + 2s(1-z)\sinh(1+z)s] \times (q/F)\exp(-isx)ds - c(i/2\pi)\int s[(1+z)\sinh 2s\cosh(1-z)s - 2\sinh(1+z)s](q/F)\exp(-isx)ds,$$

$$[7a] \quad Eu/2(1+\sigma)b = (i/2\pi)\int s[(1+z)\sinh 2s\cosh(1-z)s - 2s(1-z)\cosh(1+z)s] \times (q/F)\exp(-isx)ds + c(i/2\pi)\int[(1+z)\sinh 2s\sinh(1-z)s + 2\cosh(1+z)s](q/F)\exp(-isx)ds - (1-2\sigma)(i/2\pi)\int[\sinh 2s\sinh(1-z)s - 2s\sinh(1+z)s](q/F)\exp(-isx)ds - c(1-2\sigma)(i/2\pi)\int \sinh 2s\cosh(1-z)s(q/F)\exp(-isx)(1/s)ds,$$

$$[7b] \quad Ew/2(1+\sigma)b = (1/2\pi)\int s[(1+z)\sinh 2s\sinh(1-z)s + 2s(1-z)\sinh(1+z)s] \times (q/F)\exp(-isx)ds + (c/2\pi)\int[(1+z)\sinh 2s\cosh(1-z)s - 2\sinh(1+z)s](q/F)\exp(-isx)ds + 2(1-\sigma)(1/2\pi)\int[\sinh 2s\cosh(1-z)s + 2s\cosh(1+z)s](q/F)\exp(-isx)ds + 2(1-\sigma)(c/2\pi)\int \sinh 2s\sinh(1-z)s(q/F)\exp(-isx)(1/s)ds,$$

where F denotes the expression

$$F(s) = 2s(\sinh^2 2s - 4s^2) + c(\sinh 4s + 4s).$$

For general values of c the approximation of factors in the above integrands by sums of the form $c_n s^n \exp(-\nu s)$, as in the method of Filon (8), Sneddon (22), and Biot (3), appears to require too many terms to justify the procedure. Likewise, evaluation in terms of residues by the method of Dougall (7) involves laborious calculation for general values of c.

3. VERTICAL STRESSES AND DISPLACEMENTS AT LOWER SURFACE OF SLAB

At the lower surface of the slab $z = 1$, $\tau_{zz} = 0$, and the equation for σ_z may be written as

$$[8] \quad -\sigma_z = p_z = (1/\pi)\int c(\sinh 2s + 2s \cosh 2s)(1/F)q \exp(-isx)\, ds,$$

the downward displacement w being $(1/k)p_z$. When c is infinite the equation [8] reduces to formula 10 of Biot (3).

The expression

$$[9] \quad c(\sinh 2s + 2s \cosh 2s)/F$$

is tabulated in Table I over a wide range of values of c. Multiplication by $q(s)$, dependent only upon the surface load, and by $\exp(-isx)$ leads to values of the integrand of [8], hence permitting integration to be performed numerically. In many instances of practical concern the function $q(s)$ is a relatively simple expression in s and the calculations are not unduly tedious.

If $p(x) = 1/2ab$ for $-a < x < a$ and $p(x) = 0$ otherwise, then $q(s) = (\sin as)/(asb)$. As a tends to zero $q(s)$ becomes $1/b$ and $p(x)$ represents a line load

TABLE I

NUMERICAL VALUES OF $c(\sinh 2s + 2s \cosh 2s)/F$ (EQUATION [9])

$2s$	$c = 0.0001$	$c = 0.001$	$c = 0.01$	$c = 0.1$	$c = 1$	$c = 10$	$c = 100$	$c = \infty$
0.0	.5000 0	.5000 0	.5000 0	.5000 0	.5000 0	.5000 0	.5000 0	.5000 0
0.1	.4616 1	.4958 7	.4995 9	.4999 6	.5000 0	.5000 0		.5000 0
0.2	.2152 5	.4415 7	.4934 6	.4993 2	.4999 1	.4999 8	.4999 8	.4999 8
0.3	.0655 16	.3005 6	.4687 3	.4965 0	.4994 8	.4997 7		.4998 1
0.4	.0230 65	.1629 4	.4139 8	.4893 7	.4984 6	.4994 0	.4994 9	.4994 9
0.5	.0098 735	.0838 08	.3335 9	.4752 3	.4962 9	.4985 1		.4987 6
0.6	.0049 074	.0450 72	.2482 8	.4521 2	.4925 6	.4970 1	.4974 5	.4975 1
0.7	.0027 220	.0259 38	.1763 1	.4195 2	.4866 7	.4945 8		.4954 8
0.8	.0016 401	.0159 24	.1233 5	.3790 6	.4781 9	.4910 4	.4923 6	.4925 1
0.9	.0010 536	.0103 36	.0868 21	.3339 6	.4668 5	.4862 0		.4884 5
1.0	.0007 1223	.0070 289	.0621 51	.2880 2	.4524 5	.4798 4	.4827 6	.4830 9
1.1	.0005 0172	.0049 701	.0454 35	.2444 8	.4350 8	.4718 8		.4763 5
1.2	.0003 6567	.0036 311	.0339 44	.2053 9	.4150 3	.4622 1	.4675 2	.4681 2
1.4	.0002 1060	.0020 971	.0201 22	.1432 2	.3689 0	.4379 2	.4462 6	.4472 0
1.6	.0001 3170	.0013 134	.0127 74	.1003 3	.3189 4	.4077 8	.4194 6	.4208 0
1.8	.0000 8752 9	.0008 7352	.0085 626	.0715 00	.2698 2	.3733 9	.3883 0	.3900 3
2.0	.0000 6089 4	.0006 0802	.0059 881	.0520 15	.2248 2	.3366 8	.3543 0	.3563 8
2.2	.0000 4387 5	.0004 3822	.0043 291	.0386 11	.1855 5	.2995 6	.3191 6	.3215 1
2.4			.0032 119	.0291 78	.1523 2	.2635 3	.2843 0	.2868 1
2.8			.0018 702	.0173 86	.1020 3	.1988 5	.2196 9	.2222 8
3.2			.0011 454	.0107 91	.0683 48	.1464 8	.1653 8	.1677 9
3.6			.0007 2366	.0068 761	.0459 20	.1062 5	.1223 2	.1244 1
4.0			.0004 6595	.0044 544	.0309 32	.0762 69	.0885 12	.0911 06
4.8			.0001 9933	.0019 210	.0140 97	.0385 03	.0465 63	.0476 72
5.6			.0000 8700 5	.0008 4299	.0064 303	.0190 70	.0237 35	.0243 98
6.4			.0000 3832 2	.0003 7276	.0029 285	.0093 153	.0119 14	.0122 95
7.2			.0000 1696 0	.0001 6548	.0013 210	.0045 014	.0059 092	.0061 220
8.0			.0000 0752 89	.0000 7363 9	.0006 0384	.0021 565	.0029 030	.0030 191
8.8			.0000 0334 96	.0000 3283 0	.0002 7356	.0010 259	.0014 149	.0014 771
9.6			.0000 0149 26	.0000 1465 2	.0001 2378	.0004 8508	.0006 8505	.0007 1792

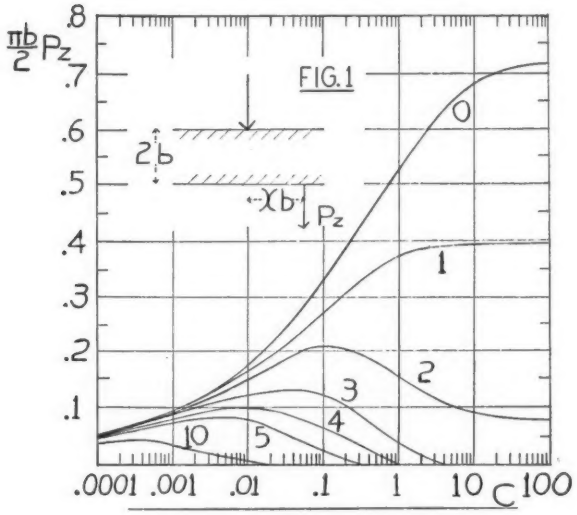

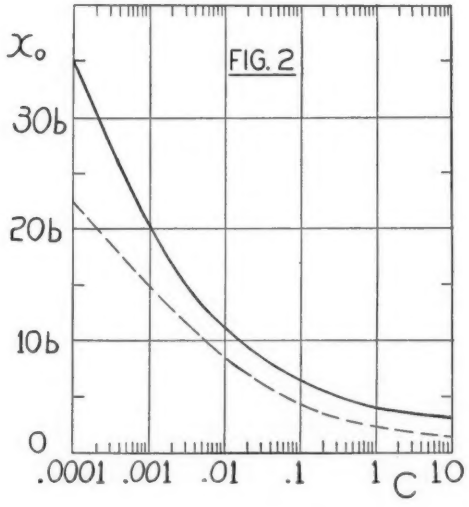

FIG. 1. Dependence of p_z upon the foundation modulus k (Equation [8]). The parameter c denotes $2kb(1-\sigma^2)/E$. Each curve applies to the value of x as indicated. The horizontal scale is logarithmic.

FIG. 2. Horizontal limit x_0 of the region within which the vertical stress transmitted to the foundation is one of compression. The continuous curve refers to a line load; the broken curve refers to a load distributed uniformly over a half plane.

of unit magnitude per unit length. The factor $\exp(-isx)$ may be replaced by $2\cos sx$ and the integration performed from zero to infinity by the method of Filon (9). The results are shown graphically in Fig. 1 where p_z is plotted as a function of c for various values of x.

In Fig. 1 the parameter c is represented by a logarithmic scale and it is apparent that for many practical estimations of p_z it is sufficient to know c, or k, only to within a factor of two. The condition for the underlying material to behave as a rigid base is approximately that c exceed 10.

Directly below the load the stress transmitted to the foundation is one of compression. As x increases, the transmitted stress decreases and eventually, at a distance x_0, becomes a tension, which may however be cancelled by the uniform compressive stress that supports the weight of the slab in the absence of surface loading. The variation of x_0 with the parameter c is shown by the continuous curve in Fig. 2.

The dependence of the transmitted stress upon the slab thickness is apparent from Fig. 3 in which both c and p_z are represented by logarithmic scales.

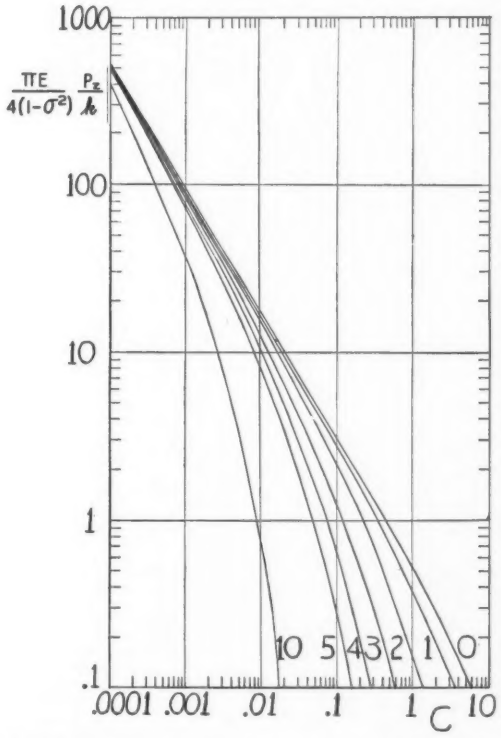

FIG. 3. Dependence of p_z upon the slab thickness $2b$. c denotes $2kb(1-\sigma^2)/E$. The value of x is indicated on each curve. Both horizontal and vertical scales are logarithmic.

The curve for $x = 0$ is essentially a straight line for c values below unity and fits the empirical equation

$$[10] \qquad \tfrac{1}{4}\pi E(1-\sigma^2)^{-1}p_z/k = 0.5293\, c^{-0.7495}.$$

If $p(x) = 1$ for $x > 0$ and zero otherwise, then $q(s) = \delta(s) - 1/is$ where $\delta(s)$ is the unit impulse function (23, p. 406). $p(x)$ represents a load distributed uniformly over the surface of the slab to the positive side of the line $x = 0$. Equation [8] becomes

$$[11] \qquad p_z = \tfrac{1}{2} + (4/\pi)\int c(\sinh 2s + 2s\cosh 2s)(1/F)(\sin sx)/(2s)\, ds$$

in which the integration is from zero to infinity. At $x = 0$, $p_z = \frac{1}{2}$, while for negative values of x the variation of p_z with c is as indicated in Fig. 4. The stress at a positive value of x may be determined by subtracting from unity the stress at the corresponding negative value of x.

As the magnitude of x increases from zero in a negative direction the compressive stress p_z decreases and becomes a tension at $x = -x_0$ where the variation of x_0 with c is as indicated by the broken curve in Fig. 2. The value of x_0 also indicates the positive value of x at which the pressure per unit area transmitted to the foundation begins to exceed that applied to the surface of the slab. Comparison of the two curves of Fig. 2 indicates that at the lower

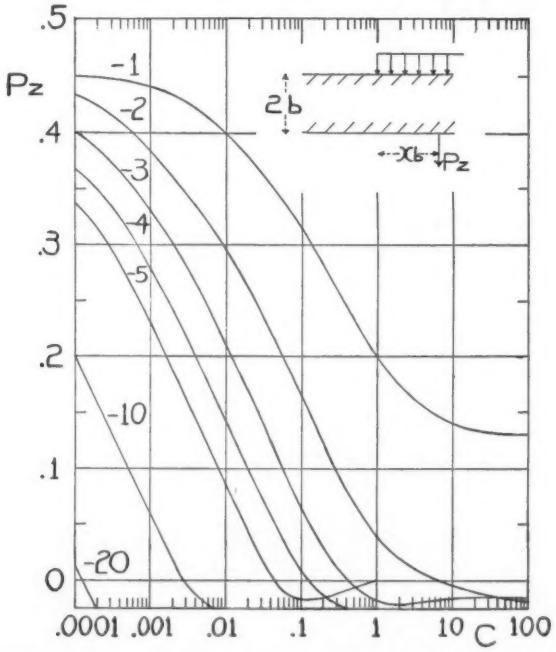

FIG. 4. Dependence of p_z upon the parameter $c = 2kb(1-\sigma^2)/E$ where k is the foundation modulus (Equation [11]). Each curve applies to the indicated value of x.

surface of the slab the compressive pressure due to a line load extends farther to the left than does that due to a load distributed uniformly to the right of the line. The difference in the horizontal limits is half the slab thickness if $c = 10$ and is six times the slab thickness if $c = 0.0001$.

4. CONCLUDING REMARKS

While for any surface load $p(x)$ the corresponding function $q(s)$ may be substituted into equation [8] and a numerical integration performed after use of Table I, there are some instances in which it is more convenient to regard

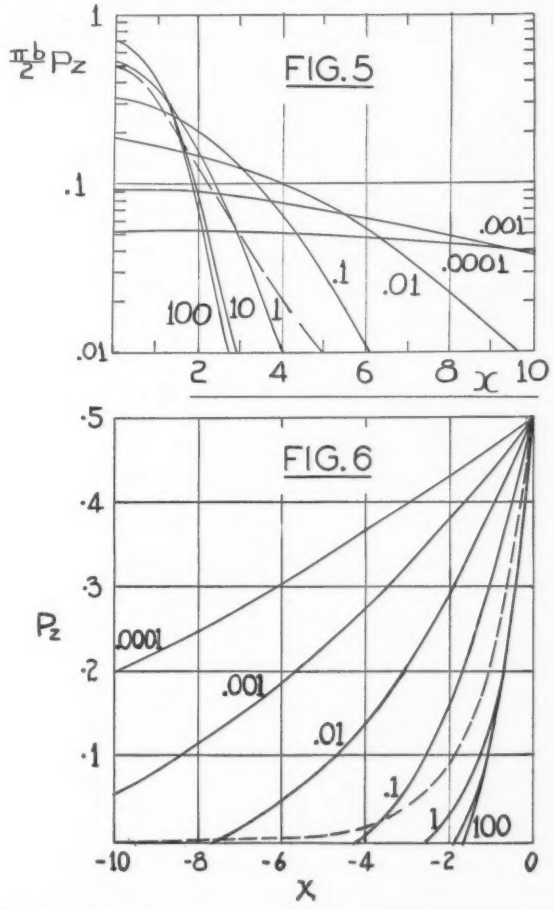

FIG. 5. Variation of p_z with the horizontal distance x for the case of a line load. The value of c is indicated on each curve. The broken curve applies to the corresponding Boussinesq stress. The vertical scale is logarithmic.

FIG. 6. Variation of p_z with the horizontal distance x for the case of a load distributed uniformly over a half plane. The value of c is indicated on each curve. The broken curve applies to the corresponding Boussinesq stress.

the surface load as a superposition of the two cases already treated. For example, the stress due to a load distributed uniformly over the surface strip $-a < x < a$ is the algebraic sum of the stress due to a load of amount $p(x) = 1$ to the right of $x = -a$ and the stress due to a load of amount $p(x) = -1$ to the right of $x = a$. Similarly the effect of a non-uniform load may be computed by addition of the stresses due to appropriate line loads acting over parallel narrow strips. To facilitate such calculations Figs. 5 and 6 are drawn to show the variation of p_z with x for the two types of surface loads previously considered. The broken curves are for the corresponding Boussinesq stresses.

If the surface load is axially symmetric the equations [6] must be replaced by equations 10 of Reference 12. Putting $z = 1$ the latter equations lead to

$$[12] \qquad p_z = 2c \int (\sinh 2s + 2s \cosh 2s)(q/F)sJ_0(sr)ds$$

where r denotes the radial distance from the axis of symmetry, J_0 is the Bessel function of zero order, and q may be found from the relation

$$[13] \qquad q(s) = \int p(r)rJ_0(sr)dr.$$

The integrations are from zero to infinity. Use of Table I allows numerical integration of [12] to proceed analogously to that of equation [8]. In the case of a point load of unit magnitude, $q(s) = 1/2\pi b^2$. When c is infinite the equation [12] reduces to that of Biot (3).

REFERENCES

1. Acum, W. E. A. and Fox, L. Geotechnique, 2: 293. 1951.
2. Benscoter, S. U. Proc. Am. Soc. Civil Engrs. 69: 691. 1943.
3. Biot, M. A. Physics, 6: 367. 1935.
4. Boussinesq, J. Application des potentiels à l'étude de l'équilibre et du movement des solides élastiques. Paris. 1885.
5. Burmister, D. M. Proc. Highway Research Board, 23: 126. 1943.
6. Deverall, L. I. and Thorne, C. J. J. Appl. Mechanics, 18: 152. 1951.
7. Dougall, J. Trans. Roy. Soc. Edinburgh, 41: 129. 1904.
8. Filon, L. N. G. Trans. Roy. Soc. (London), A, 201: 63. 1903.
9. Filon, L. N. G. Proc. Roy. Soc. Edinburgh, 49: 38. 1928.
10. Fletcher, H. J. and Thorne, C. J. J. Appl. Mechanics, 19: 361. 1952.
11. Fox, L. Dept. of Sci. and Ind. Research, Road Research Tech. Paper No. 9. 1948.
12. Heaps, H. S. Trans. Am. Geophys. Union, 34: 769. 1953.
13. Heaps, H. S. Trans. Roy. Soc. Can. IV, 47: 17. 1953.
14. Hetényi, M. Beams on elastic foundation. The University of Michigan Press, Ann Arbor, Mich. 1946.
15. Hogg, A. H. A. Phil. Mag. 25: 576. 1938.
16. Jeffreys, H. The earth. 2nd ed. The MacMillan Co., New York. 1929.
17. Kansas State Highway Commission. Comparison and nature of stresses in a concrete pavement due to different applied loads and axle spacings. Project 5001. 1952.
18. Livesley, R. K. Quart. J. Mech. and Appl. Math. 6: 32. 1953.
19. Merritt, R. G. and Housner, G. W. Bull. Seismological Soc. Amer. 44: 551. 1954.
20. Murphy, G. Iowa Eng. Expt. Sta. Bull. 135. June, 1937.
21. Shockley, W. G. Civil Eng. 20: 24. 1950.
22. Sneddon, I. N. Proc. Cambridge Phil. Soc. 42: 260. 1946.
23. Sneddon, I. N. Fourier transforms. 1st ed. McGraw-Hill Book Company, Inc., New York. 1951.
24. Terazawa, K. J. Coll. Sci., Imp. Univ. Tokyo, 37: Art. 7. 1916.
25. Timoshenko, S. Theory of plates and shells. McGraw-Hill Book Company, Inc., New York. 1940.

THE OXIDATION, DECOMPOSITION, IGNITION, AND DETONATION OF FUEL VAPORS AND GASES

XXV. THE TRANSITION FROM SPARK TO NUCLEAR IGNITION AS COMPRESSION RATIO IS RAISED[1]

By R. O. King[2] and A. B. Allan[3]

ABSTRACT

An experimental study of the characteristics of combustion during the transition from spark to nuclear ignition as compression ratio is raised is described in this Part. Heptane was used as the fuel for a C.F.R. engine operated at 400 r.p.m. Compression ratio was always adjusted for maximum power output as the mixture with air was varied from 65% weak to 25% rich. Charge densities of 64 and 78% of normal were used. The progressive changes in the relation between compression ratio and mixture strength and between thermal efficiency and mixture strength are shown by families of graphs. Pressure–time indicator diagrams are used to illustrate the changes that occur in the mean values of pressure during the transition from spark to nuclear ignition. Rate of pressure change diagrams taken simultaneously with a dual beam oscilloscope show the high frequency pressure vibrations due to the nuclear ignition of the part of the compressed charge adjacent to the combustion chamber surface of maximum temperature.

INTRODUCTION

A transition from spark to nuclear ignition can be obtained on increasing compression ratio if fuels are used which decompose (crack) in a manner to form material nuclei. The changes in the relation between thermal efficiency and compression ratio as the transition occurs cannot be determined in the usual conditions of engine operation because of the accompanying severity of knocking combustion commonly described as detonation. Nuclear ignition does not however occur simultaneously throughout the mass of the charge in an engine but begins in some part where the temperature and mixture conditions are such that decomposition can occur. In these circumstances the combustion knock due to the consequent pressure waves can be tolerated by the C.F.R. engine if charge density be reduced by approximately 20%. The relation between thermal efficiency and compression ratio can then be determined even when the engine is operated at the relatively low speed of 400 r.p.m., the heat of combustion added to the working fluid substantially at constant volume, and a correct mixture used. Then if the jacket coolant and the air supply be maintained at relatively low temperatures, surfaces in the combustion chamber do not attain temperatures required for oxidation of the fuel during compression and decomposition becomes the sole preflame reaction.

Experiments made accordingly with pentane, hexane, and heptane as engine fuels for the C.F.R. engine are described in Part XXI (5). It was indicated

[1]*Manuscript received February 15, 1955.*
Contribution from Defence Research Board, Ottawa, Canada, in association with the Department of Mechanical Engineering, University of Toronto, Toronto, Canada.
[2]*Research Scientist, Defence Research Board and Special Lecturer in the Department of Mechanical Engineering, University of Toronto.*
[3]*Principal Scientific Officer, Defence Research Board.*

by these experiments that nuclear ignition started in the part of the charge adjacent to the ceramic core of an unfired spark plug or, if the plug were removed, in the part adjacent to the exhaust valve.

The timing of nuclear ignition could always be regulated to obtain maximum power output by adjustment of compression ratio. The experiments were devoted mainly to showing that the relation between mixture strength and the compression ratio required for maximum power output, that is the optimum value, was represented by a graph of a W form instead of by the familiar U form obtained with spark ignition only.

It was found in the course of further experiments that sufficient time had not always been allowed between changes of mixture strength and compression ratio for the attainment of equilibrium temperatures by surfaces in the combustion chamber. Especial care was therefore taken when the experiments with heptane–air mixtures were carried out, as described in this Part, to run the engine at particular values of mixture strength until repeatable values were obtained for power output with the compression ratio adjusted to the optimum value. It is considered that reliable results were then obtained for the changes in the relation between thermal efficiency and compression ratio that occur during the transition from spark to nuclear ignition, as compression ratio is raised. Series of experiments were carried out with charge densities of 64 and 78% of normal.

EXPERIMENTAL CONDITIONS

The experimental arrangements and conditions were similar to those described in some detail in Part XIX (4, pp. 30–32, 33). The essential conditions were,—

air supply 50°F.; jacket coolant 95°F. at inlet, 100°F. at outlet; engine speed 400 r.p.m.; unshrouded inlet valve.

Charge densities of 64 and 78% of normal were obtained by fitting long choke tubes of suitable diameter into the standard C.F.R. carburetor. The tubes were curved to discharge into the well of the inlet valve, see Part XIX (4, p. 40).

Experiments were carried out at each of the subnormal charge densities with ignition by spark at 20°, 15°, 10°, and 5° in advance of t.d.c. with no spark, and with the spark plug replaced by a blank steel plug.

There were three spark plug holes in the wall of the cylinder of the C.F.R. engine. A C.F.R.-8 spark plug, which is a hot variety, was used in the standard position for experiments with spark ignition. The two other holes were fitted with blank plugs or used for pressure pickups when indicator diagrams were taken. The bouncing pin hole in the cylinder head was always fitted with a blank plug.

The fuel used for the experiments was the normal heptane supplied by Phillips Petroleum Company and approved by the A.S.T.M. as a reference fuel for knock rating. Calculations of thermal efficiency were based on the heptane having a lower calorific value of 19160 B.T.U./lb.

The abbreviations Opt. C.R., I.T.E., and M.S. are used in subsequent text for Optimum Compression Ratio, Indicated Thermal Efficiency, and Mixture Strength, respectively.

I. EXPERIMENTAL RESULTS: CHARGE DENSITY 64% OF NORMAL

Experimental results are given by the graphs of Fig. 1 for the relation between Opt. C.R. and M.S. and between I.T.E. and M.S.

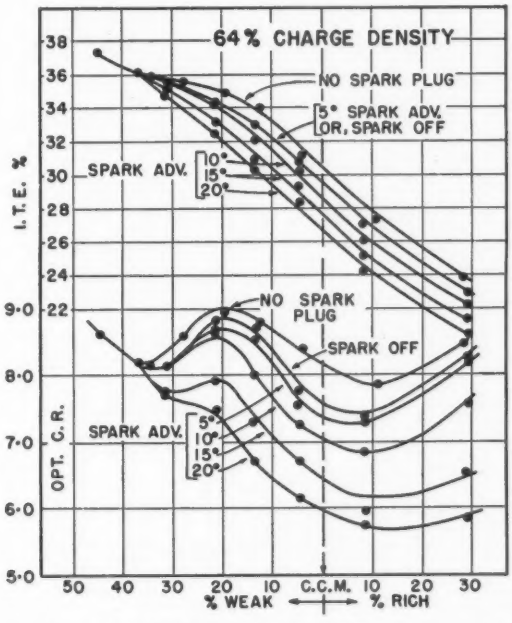

FIG. 1. Upper graphs, relation between I.T.E. and M.S.; lower graphs, relation between Opt. C. R. and M.S. Charge density, 64% of normal.

There was some degree of detonation with a spark advance of 20° when the mixtures were nearly correct or richer. Knock intensity increased as spark timing was retarded and Opt. C.R. increased accordingly. Repeatable values were obtainable for Opt. C.R. until spark advance was reduced to 5°. Ignition then tended to become independent of the spark and when C.R. was raised to the Optimum value ignition soon became of the runaway type characteristic of preignition and was accompanied by severe knock. Although the values thus obtained for Opt. C.R. with the spark off were somewhat higher than with it on, the differences in the corresponding values of I.T.E. were inappreciable. The relation between I.T.E. and M.S. is therefore given by a single graph.

When the spark plug was replaced by a blank plug, the higher values then required for Opt. C.R. remained substantially constant irrespective of time of

running. There was a slight degree of knock when a mixture 40% weak was used. Knock intensity increased as M.S. was increased and became medium heavy over the mixture range 20 to 15% weak. Intensity attained a maximum with mixtures within the M.S. range correct to 10% rich. It is of interest that with nuclear ignition, knock intensity varied with mixture strength, not with compression ratio. Thus the value of Opt. C.R. was 8.5 for mixtures 43% weak, 30% weak, 7.5% weak, and 30% rich although over this range of M.S. knock intensity varied from very light to very severe.

Spark ignition remained effective as timing was retarded from 20° to 10° in advance of t.d.c. and partially so as timing was further retarded to 5° advance, over the mixture range 25% rich to 25 or 30% weak. Within this range it was necessary to *raise* the C.R. to obtain an optimum value as M.S. was reduced from approximately 10% rich or as it was increased from that value and it will be seen by reference to Fig. 1 that the graphs for the relation between Opt. C.R. and M.S. were then of the conventional U shape.

As M.S. was reduced to be leaner than 25 to 30% weak, spark ignition became progressively ineffective until it failed completely when the mixture was 40% weak. Over this mixture strength range of failing spark ignition it was necessary to lower C.R. progressively in order to maintain an optimum value.

The transition from spark to nuclear ignition having been completed on reducing M.S. to be 40% weak, the engine continued to run on nuclear ignition only as M.S. was further reduced. It was then necessary to raise C.R. progressively in order to maintain an optimum value. A symmetrical W form was then obtained for the graph relating I.T.E. and C.R. with mixtures ranging from 45% weak to 50% rich.

The Relation Between I.T.E. and Opt. C.R.

It is now apparent that the graphs of Fig. 1, if plotted on a base of Opt. C.R. instead of M.S., will illustrate the transition from single to two stage ignition as well as the transition from spark to nuclear ignition. The series of graphs thus derived are shown by Fig. 2. The "points" on the graphs are for 5% changes of M.S. and the correct value is marked CCM.

The graphs move toward higher values of Opt. C.R. as spark timing is retarded from 20° to 5° in advance of t.d.c. and continue to do so as ignition is obtained without spark and with the spark plug replaced by a blank plug. In all of these ignition conditions the graphs for the relation between I.T.E. and Opt. C.R. are of the conventional form until M.S. is reduced to be approximately 20% weak, but the value of I.T.E. increased from a minimum of 32% with a spark advance of 20% to a maximum of 34.6% with nuclear ignition in the absence of a spark plug. The transition from single to two stage ignition then began and became complete on reducing M.S. to 40% weak. Then transition is indicated by a single inflection in the graph obtained with a spark advance of 20°. The beginning of a double inflection is shown by the graph obtained when the spark advance was 15°. The range of Opt. C.R. over which a double inflection occurred increased as spark timing was further retarded and succeeded by nuclear ignition. Finally when nuclear ignition

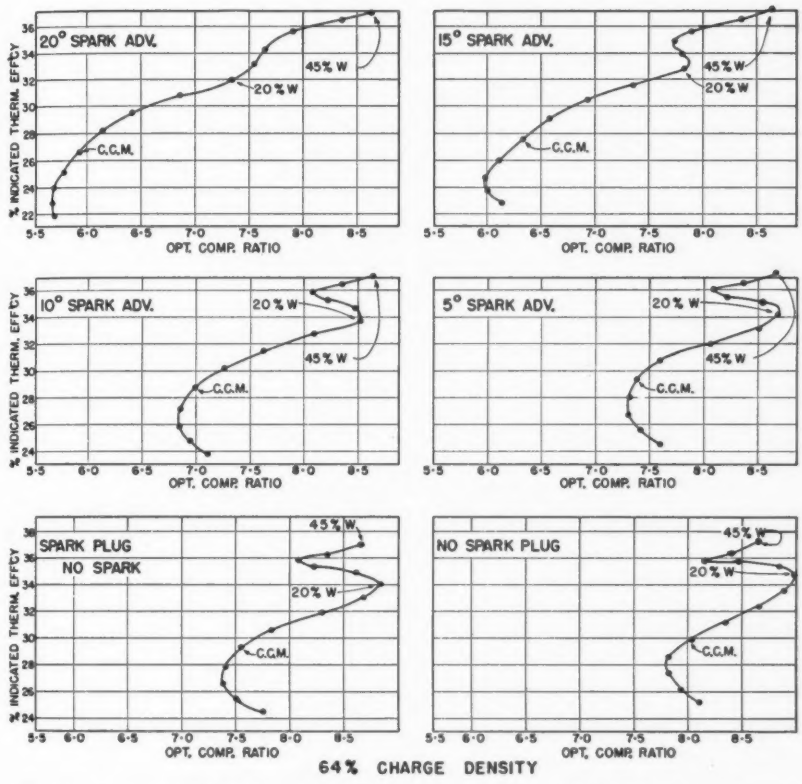

FIG. 2. Progressive change in the relation between I.T.E. and Opt. C.R. during the transition from spark to nuclear ignition. Charge density 64% of normal.

occurred in the absence of a spark plug, I.T.E. tended to become constant for values of Opt. C.R. *diminishing* from 9.0 to 8.4, while at the same time M.S. decreased from 25 to 40% weak. The explanation for this effect is as given in Part XXIV (3, p. 227), namely that as the transition from spark to nuclear ignition occurs, then as M.S. is reduced from 25 to 40% weak, the increase in I.T.E. to be expected is counteracted by the adverse effect on thermal efficiency of the heat absorbed by the endothermic reaction necessary for the provision of nuclei of ignition. It will be noted that after the transition to nuclear ignition is complete, at a M.S. of approximately 40% weak, I.T.E. increases as M.S. is further reduced and compression ratio raised to maintain an Optimum value.

II. EXPERIMENTAL RESULTS: CHARGE DENSITY 78% OF NORMAL

The experiments were carried farther into the weak mixture region than those of Section I. Results are given by the graphs of Fig. 3 for the relation

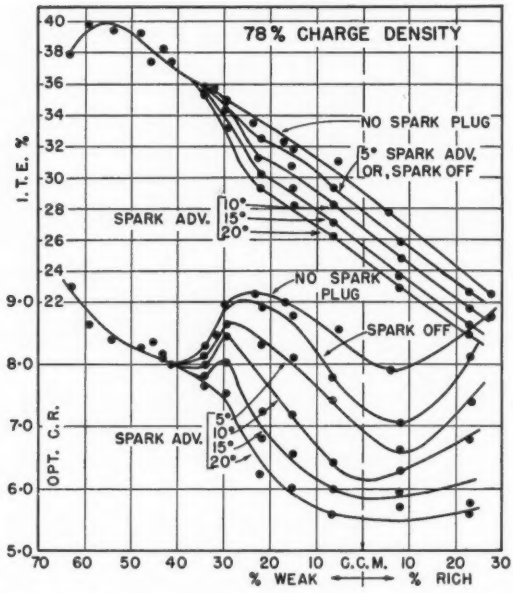

FIG. 3. Upper graphs, relation between I.T.E. and M.S.; lower graphs, relation between Opt. C.R. and M.S. Charge density, 78% of normal.

between C.R. and M.S. and between I.T.E. and M.S. They are similar in character to those obtained when a charge density of 64% of normal is used and the related description applies also to the results obtained with a charge density of 78% normal. The intensity of combustion knock at 78% charge density was the greater, as would be expected. It will be seen by reference to Fig. 3 that on decreasing M.S. to 65% weak I.T.E. passed through a maximum value of 40% for a mixture 55% weak.

The Change from Single to Two Stage Ignition

The series of graphs, Fig. 4, are similar to those of Fig. 2, and likewise illustrate the transition from spark to nuclear ignition as well as the transition from single to two stage ignition. The sole notable differences are that the transition from spark to nuclear ignition began with mixtures approximately 10% weaker than when the lower charge density was used and that the value of I.T.E. did not remain constant during the transition from spark to nuclear ignition but increased by one unit over the range of Opt. C.R. in which the transition occurred.

The Transition from Spark to Nuclear Ignition as Shown by Pressure–Time Indicator Diagrams

The diagrams, Fig. 5, were taken with spark timings of 20°, 15°, and 10°, and 5° before t.d.c., with no spark, and finally with the spark plug replaced by

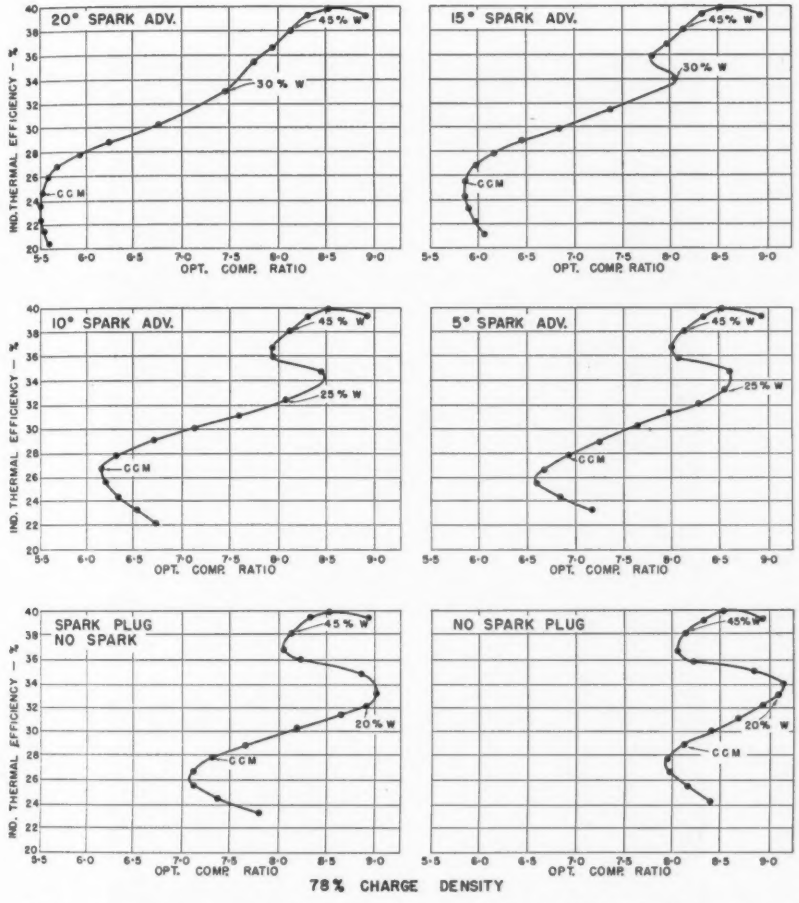

FIG. 4. Progressive change in the relation between I.T.E. and Opt. C.R. during the transition from spark to nuclear ignition. Charge density 78% of normal.

a steel blank. One series was taken with the heptane–air mixture 19% weak and another with a correct mixture. Reproductions of the diagrams are set out in the two vertical columns of Fig. 5. All were taken with C.R. adjusted for maximum power output. A "Sunbury" indicator was used for the experiments. The pressure scale is not linear, and a consequent effect is that, especially for the lower values of maximum combustion pressure, the expansion lines of the diagrams are nearly straight. The "blips" on the diagram occur at t.d.c. and at 10° of crank revolution for 30° before and after. The blip at t.d.c. is marked by a short vertical line. The blips on the upper and lower lines of the diagrams are out of step and spacing is somewhat irregular, because the inertia of

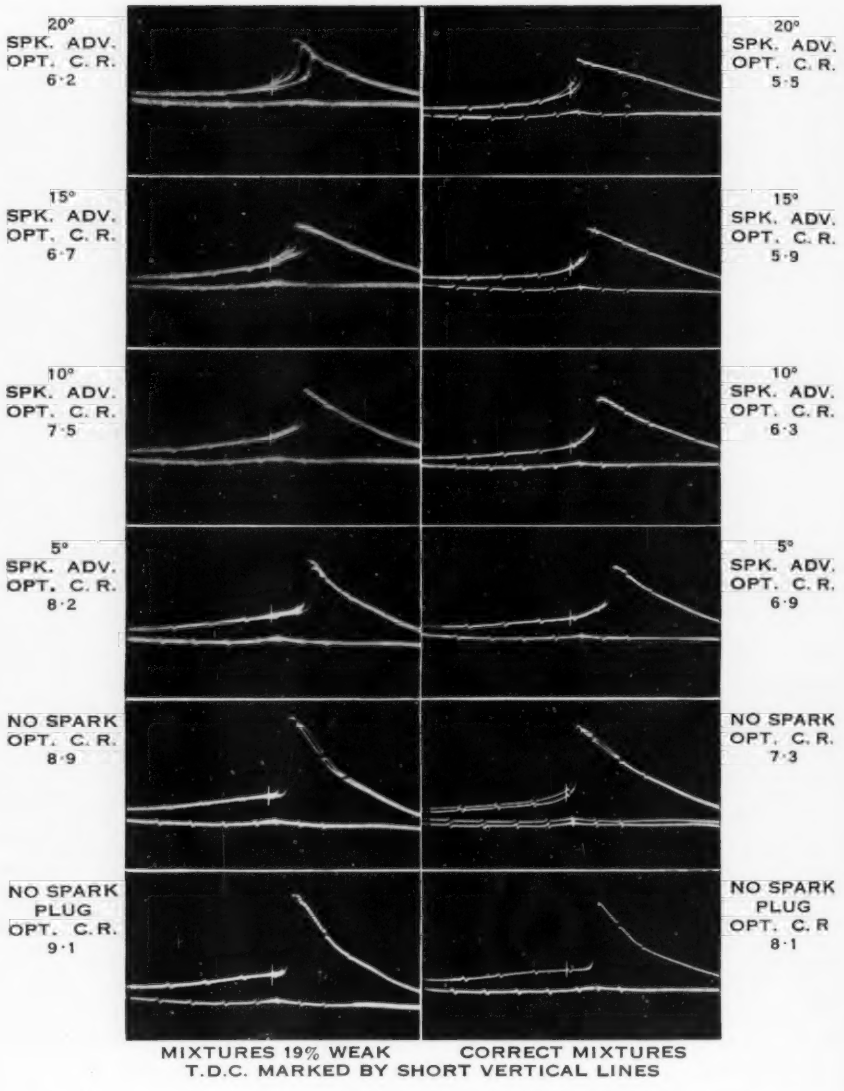

FIG. 5. Pressure–time diagrams. Charge density 78% of normal, transition from spark to nuclear ignition.

rotating parts of the C.F.R. unit is insufficient at the engine speed of 400 r.p.m. to damp out the effects of pressure changes in the cylinder.

The diagrams were taken when a charge density of 78% of normal was used. Values for Opt. C.R. and I.T.E. as given by Fig. 3 may therefore be used when comments are made on the corresponding combustion characteristics.

Diagrams for Mixtures 19% Weak

Starting with spark ignition 20° advance, Opt. C.R. was 6.2 and the diagram exhibits the irregularity of combustion commonly obtained when weak mixtures are ignited by spark. When spark ignition was retarded to 15° advance, Opt. C.R. increased to 6.7, combustion was more regular, and maximum combustion pressure was higher. When spark ignition was further retarded to 10° advance, a relatively large increase of C.R. to 7.5 was required in order to obtain maximum power output and the diagram shows that the consequent increase in the rate and magnitude of combustion pressure rise was accompanied by more regular combustion. Rate of pressure rise and maximum combustion pressure again increased when the spark was further retarded to 5° advance, and an increase of Opt. C.R. to 8.2 was required to maintain maximum power output. The engine would then run without spark ignition, but not indefinitely because of a continuing diminution of power output. The beginning of a complete transition from spark to nuclear ignition was thus indicated.

Continuous running without spark ignition required the relatively large increase of Opt. C.R. from 8.2 to 8.9. The related diagram shows that combustion pressure rise began at 2° to 5° after t.d.c. whereas, with the spark on, the rise began at from 12° to 15° after t.d.c. but varied from cycle to cycle. The last diagram of the series was taken after the spark plug was replaced with a mild steel blank plug. A small increase in Opt. C.R. of 8.9 to 9.1 was then required for continuous running with nuclear ignition. The diagram shows that combustion pressure rise began at 5° after t.d.c. with little variation of the position of maximum combustion pressure, which occurred at 8° after t.d.c. during the three cycles shown by the diagram.

The interval between t.d.c. and the crank angle position of maximum combustion pressure varied irregularly from 5° to 15° with spark timings of 20°, 15°, and 10° in advance of t.d.c. When however the spark plug was replaced by a mild steel blank, maximum combustion pressure occurred regularly at between 8° to 10° after t.d.c.

When ignition was by spark, 10° in advance of t.d.c., a C.R. of 7.5 was required for maximum power output. When the spark plug was removed and ignition became a nuclear effect entirely, it was necessary to raise the C.R. to 9.1 to obtain maximum power output. Then, although the heat of combustion was added to the working fluid the more nearly at constant volume with nuclear ignition, the increase in I.T.E. was from 31 to 33% only.

Diagrams for Correct Mixtures

The diaphragm of the Sunbury pressure pickup proved to be too thin for satisfactory use with the nuclear ignition of correct mixtures. One slightly

thicker was therefore fitted to the pickup and although amplification was increased to the limit of the indicator, the pressure scales of the diagrams for correct mixture differ little from those for mixtures 19% weak. Then because the indicated pressure increase is less than the real increase, the expansion lines of the diagrams tend to remain linear until ignition is a nuclear effect and relatively high values are obtained for maximum combustion pressure.

The diagrams taken with spark ignition, especially those with ignition timing 20° and 15° in advance of t.d.c., indicate a greater regularity of combustion than was obtained with mixtures 19% weak. The intervals in degrees of crank angle between t.d.c. and the attainment of maximum combustion pressure are more clearly defined. The interval is shown to have increased from 5° to 15° as spark timing was retarded from 20° to 5° in advance of t.d.c. That is, the time of burning had decreased from 25° to 20° of crank revolution on increasing Opt. C.R. from 5.5 to 6.9. When spark timing was 5° in advance of t.d.c. the Opt. C.R. was 6.9, then with ignition "off" an increase in Opt. C.R. of 0.30 only was required for complete transition to nuclear ignition. Burning of the mixture then occurred in approximately 2° of crank revolution. There was however an indication that nuclear ignition was accompanied by some degree of nuclear preignition. The spark plug was then replaced by a blank plug and preignition did not occur.

III. DISCUSSION

The transition from spark to nuclear ignition as compression ratio is raised was illustrated by experiments with heptane, hexane, and pentane described in Part XXI (5). These experiments formed part of a general survey of the characteristics of nuclear ignition and were therefore of a somewhat preliminary nature. The experiments of this Part were carried out with heptane only, in greater detail and with some improvement in method.

The indicator diagrams of Fig. 5, taken when heptane–air mixtures 19% weak and correct were used, show that after ignition was initiated by a spark, combustion pressure rose in the manner characteristic of a normal rate of flame propagation until a transition occurred to nuclear ignition. This was marked by a pressure rise so rapid that combustion pressure attained a maximum value in a further 2° of crank revolution.

The transition which thus occurred after spark ignition 20° in advance of t.d.c. of a mixture 21% weak is shown clearly by the pressure–time and rate of pressure change diagrams of Fig. 6. They were taken simultaneously during the use of a dual beam Dumont oscilloscope. Spark ignition was by a C.F.R.–8 plug in the standard position. The "Sunbury" electronic circuit with a magnetic flux pressure pickup was used for the rate of change diagram. A "Photocon" electronic circuit with an electrostatic pressure pickup was used for the pressure–time diagram. It was possible accordingly to restrict pressure indications to the nearly linear part of the pressure scale.

A compression ratio of 8 : 1 was required for maximum power output and a value of 32.2% was obtained for indicated thermal efficiency. Top dead center is marked on the pressure–time diagram by a short vertical line and the timing

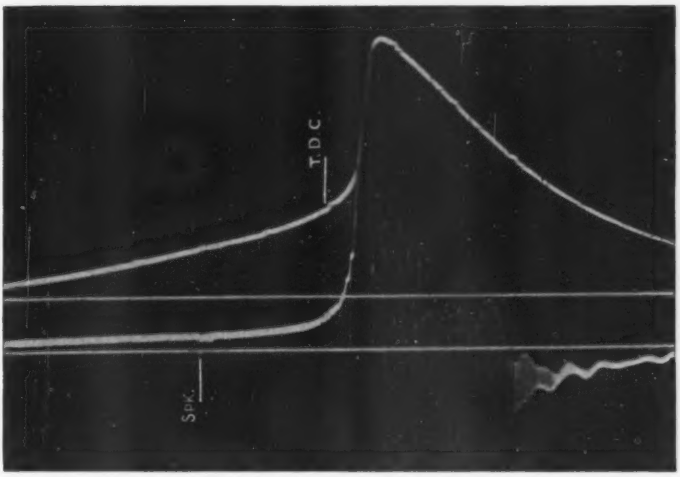

FIG. 6. Pressure–time and rate of change diagrams taken simultaneously; spark ignition 20° advance, followed by nuclear ignition. Mixture 21% weak, Opt. C.R. 8:1, I.T.E. 32.3%, speed 400 r.p.m. Charge density 64% of normal.

of the spark at 20° before t.d.c. is marked similarly on the rate of change diagram.

The pressure–time diagram is generally similar to those of Fig. 5, in that the gradual pressure rise following the spark ignition is succeeded by a sudden rise just prior to the attainment of maximum combustion pressure. This is attributed as before to the transition from spark to nuclear ignition. The pressure waves that necessarily accompanied nuclear ignition were, also as before, integrated to a mean value in the electronic circuit and do not show on the diagram. The approach of the expansion line to a true form is attributed to the use of superior indicating arrangements.

The diagram showing rate of change of pressure is of special interest. The rates of pressure change accompanying the pressure waves due to nuclear ignition are shown with exceptional clarity. Thus it will be seen that rate of change of pressure increased very slowly after spark ignition at 20° before t.d.c. until 5° before t.d.c. Rate of change then began to increase more rapidly as combustion continued in the normal manner without accompanying pressure waves. However after continuing for 10° of crank revolution, that is until 5° after t.d.c., explosive ignition occurred and the magnitude of the accompanying rate of pressure change was so great that it exceeded the pressure scale of the diagram. The high frequency pressure waves which followed explosive ignition are shown clearly by the accompanying rates of pressure change. They are attributed to reflections from surfaces and to the fact that nuclear ignition arose from more than a single source.

It is of interest that the process of combustion as illustrated by the rate of change diagram is in fair agreement with the knocking combustion that

followed spark ignition, as shown by the high speed photographs taken by Withrow and Rassweiler (6) and reproduced in Part IV (1).

Single Stage Nuclear Ignition

The characteristics of nuclear ignition when the consequent combustion occurred in a single stage are illustrated by the diagrams of Fig. 7. They were taken in the same operating condition and with the same mixture strength, namely 21% weak, but after the spark plug was replaced with a blank and the compression ratio was adjusted to the higher value of 9:1 then required for maximum power output without spark ignition.

The initiation of combustion without the aid of a spark required prior decomposition of the fuel to the extent necessary for the formation of an igniting concentration of nuclei in some part of the mixture with air, Part IV (1), Part XX (2, pp. 59–60). The occurrence of the decomposition reaction, which is endothermic, is indicated on the pressure–time diagram of Fig. 7 by the failure of pressure to rise during the final stage of compression and on the rate of change diagram by a zero value extending from t.d.c. to about 5° after. Small scale pressure waves are shown by that diagram to have then appeared early in the fillet joining compression pressure with combustion pressure. Combustion of the entire mixture then followed with such velocity that combustion pressure attained a maximum value in approximately 2° of crank revolution. The high frequency pressure waves which occurred during combustion are indicated by the rates of pressure change shown by the diagram and combustion appears to have been substantially completed before the beginning of expansion. In the absence of a spark or a spark plug core it

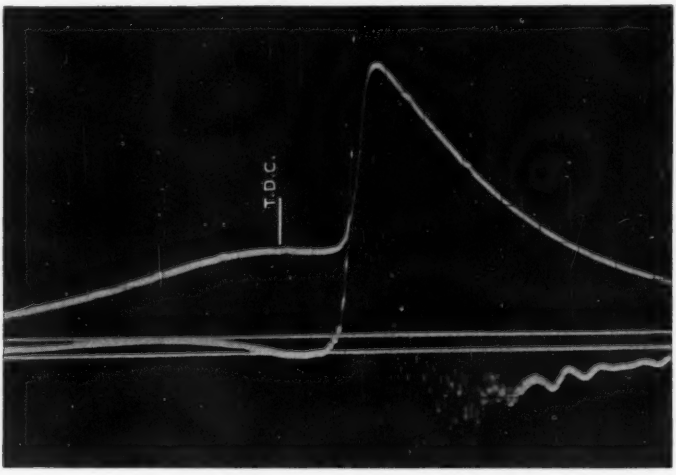

FIG. 7. Pressure–time and rate of change diagrams taken simultaneously; nuclear ignition only, mixture 21% weak, Opt. C.R. 9:1, I.T.E. 35.7%, speed 400 r.p.m. Charge density 64% of normal.

may be assumed that in the temperature conditions of the experiment, explosive nuclear ignition occurred in the part of the compressed mixture adjacent to the exhaust valve.

The heat of combustion was added to the working fluid more nearly at constant volume than when combustion of a similar mixture was initiated by a spark and completed with nuclear ignition. The consequent increase in thermal efficiency from 32.2% to 35.7% is greater than could be expected from the increase of Opt. C.R. from 8 to 9.1.

The rate of change diagrams show vibrations of relatively low frequency which become visible after expansion has proceeded for about 30° of crank revolution. These are due to mechanical vibration in the pressure pickup, set up by the prior explosive nuclear ignition.

Nuclear Ignition in One or Two Stages

The igniting effect has been shown by the experiments described in this Part to occur in a single stage for correct heptane–air mixtures and for mixtures 19 and 21% weak, engine speed being 400 r.p.m. It was shown to occur in two stages at the same engine speed when the mixture was 70% weak, by experiments described in Part XXI (4, p. 230). Thus a transition from single to two stage nuclear ignition must occur within the mixture range 21 to 70% weak when heptane is used as the fuel and the engine speed is 400 r.p.m. The decomposition of the fuel to provide the concentration of nuclei required for ignition involves a time factor. It would be expected therefore that the transition from single to two stage nuclear ignition of a particular fuel would be affected by engine speed as well as by mixture strength. Thus it has been shown by experiments to be described in a subsequent Part that two stage nuclear ignition continues into mixtures even richer than correct, on increasing the engine speed to 600 r.p.m.

ACKNOWLEDGMENTS

The experiments described in this Part were carried out in the Department of Mechanical Engineering, University of Toronto, with the co-operation of Professor E. A. Allcut, Head of the Department, and the assistance of Mr. R. W. P. Anderson, Instructor in the Department. The investigation was sponsored by the Defence Research Board (Canada). The authors are indebted to the Board for permission to publish the results.

REFERENCES

1. KING, R. O. Can. J. Research, F, 26: 228–240. 1940.
2. KING, R. O. and ALLAN, A. B. Can. J. Technol. 30: 44–60. 1952.
3. KING, R. O. and ALLAN, A. B. Can. J. Technol. 32: 220–241. 1954.
4. KING, R. O., DURAND, E. J., ALLAN, A. B., and HANSEN, E. J. T. Can. J. Technol. 30: 29–43. 1952.
5. KING, R. O., DURAND, E. J., ALLAN, A. B., HANSEN, E. J. T., and BOWEN, V. E. Can. J. Technol. 30: 222–257. 1952.
6. WITHROW, L. and RASSWEILER, S. M. Trans. Soc. Automotive Engrs. 31: 297–304. 1936.

THE DETERMINATION OF THE FLUORIDE CONTENT OF EDIBLE BONE MEAL[1]

By John C. Bartlet, Doris Kavanagh, and Ross A. Chapman

ABSTRACT

Fluoride is determined in edible bone meal by igniting a sample at a temperature between 550°C. and 750°C. A Willard and Winter distillation from perchloric acid is used to separate fluoride from interferences and the amount of fluoride in the distillate is measured by the amount of bleaching of a ferric salicylate solution at pH 3.1. The optimum conditions of acidity and reagent concentration were investigated and the effects of interfering substances were determined. The standard error of the method as applied to bone meal is ±2.3%. The sensitivity of the procedure is not as high as that of other colorimetric procedures for fluoride ion but the method has the advantages of being rapid and using easily obtainable reagents.

INTRODUCTION

In a previous paper (1) a method for the determination of fluoride in edible bone meal was described. The method used a thorium nitrate titration with gallocyanine as indicator (16). It was found, however, that since gallocyanine deteriorated even in the dry state, and was not uniform from batch to batch, reproducible results were not obtainable and the end point of the titration was often obscure. Therefore, a relatively sensitive rapid colorimetric method was sought.

In the past few years numerous colorimetric procedures for the determination of fluoride have been proposed. All of them depend on the formation of a colored compound of a metal such as iron, zirconium, thorium, and aluminum which is bleached by fluoride ion through the formation of a metal–fluoride complex. The reactions may be summarized as follows:

$$M^+ + R^- \rightleftharpoons MR \qquad \text{(colored)}$$
$$M^+ + F^- \rightleftharpoons [MF] \qquad \text{(colorless)}$$
$$\text{or } MR + F^- \rightleftharpoons [MF] + R^-$$

Since there are two competing equilibrium reactions, these methods will, in general, be particularly sensitive to small changes in temperature, pH, and ionic strength. Also, since the colored complex must be readily broken down by fluoride, other complex-forming anions such as sulphate, chloride, and phosphate will interfere. This means that most of the colorimetric methods for fluoride follow a Willard and Winter distillation (17) to separate the fluoride from interfering material. The numerous methods that have been proposed for the determination of fluoride have been reviewed (3, 9, 10, 11, 12). However, a few of the more widely used methods should be mentioned specifically. The zirconium – alizarin lake procedure (4, 13) has won wide acceptance and the

[1]*Manuscript received May 26, 1955.*
Contribution from Food and Drug Laboratories, Department of National Health and Welfare, Ottawa, Ontario.

thorium–thoron procedure (7) is one of the most sensitive procedures. Other methods using various iron complexes (14) and aluminum lakes (2, 15) have also been proposed.

For the determination of fluoride in bone meal a method does not need to be extremely sensitive since the bone meal contains several hundred parts per million (1). Preliminary experiments with a method based on the bleaching of ferric salicylate (5, 8), while not as sensitive as the zirconium – alizarin sulphonate procedure, gave promising results and therefore the procedure was examined in greater detail.

EXPERIMENTAL

Optimum conditions for the ferric salicylate procedure of Greenspan and Stein as outlined by Busch *et al.* (5) and other details of the method as applied to bone meal were investigated. The colorimetric method was then used for the determination of fluoride in distillates obtained from perchloric acid solutions of ashed bone meal as described in our previous paper (1).

1. Sample Preparation

The original method used in this laboratory for ashing bone meal required calcium hydroxide as a fixative for fluoride. However, samples ashed with and without added calcium hydroxide gave the same recoveries of fluoride, within the experimental error, as shown in Table I. The addition of calcium hydroxide was then omitted as unnecessary.

TABLE I

RECOVERY OF FLUORIDE FROM BONE MEAL SAMPLES WITH AND WITHOUT ADDED CALCIUM HYDROXIDE

	F, p.p.m.	
Sample	$Ca(OH)_2$ added	No $Ca(OH)_2$
1	340	330
2	520	530
3	470	460
4	420	410
5	610	620

The recovery of fluoride after ignition of bone meal at different temperatures was investigated. An ignition temperature of at least 550°C. was necessary to burn off the organic material. Between 550°C. and 750°C. recovery was constant within experimental error, as shown in Table II.

2. Distillation

The distillation procedure of Willard and Winter (17) was followed, using perchloric acid and the apparatus of Churchill (6).

TABLE II

RECOVERY OF FLUORIDE FROM BONE MEAL SAMPLES IGNITED AT DIFFERENT TEMPERATURES

Sample	Ignition temperature, °C.	Fluoride, p.p.m.
1	400*	467
1	550	487
1	750	480
2	400*	340
2	550	347
2	750	333

**Perchloric acid solution of ignited sample was dark brown apparently caused by incompletely-ignited carbonaceous material.*

3. Colorimetric Procedure

The optimum conditions for the ferric salicylate procedure were investigated using the basic procedure given under "Procedure". This method was modified for each of the conditions investigated.

(*a*) *Acidity.*—The optimum pH was determined using 3 to 15 ml. of 0.025 *N* perchloric acid or 0.0025 *N* sodium hydroxide with samples containing 0, 20, and 100 micrograms (μgm.) of fluoride in 25 ml. final volume. The range covered was from pH 1.80 to pH 4.55. The data are plotted in Fig. 1 and show that the optimum pH is 3.0 to 3.1.

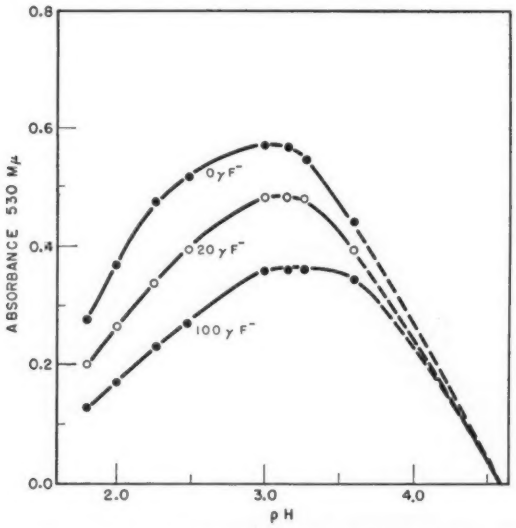

FIG. 1. The effect of pH on the determination of fluoride with ferric salicylate.

(*b*) *Concentration of Reagents.*—Greenspan and Stein (5) recommended a ferric salicylate reagent with ferric iron and salicylic acid in the weight ratio of 0.22 with the amount of salicylic acid held constant. This ratio was varied from 0.16 to 0.52 with the results shown in Fig. 2. The sensitivity (change in absorbance per p.p.m. of fluoride per cm. of light path) is plotted against the weight ratio of iron to salicylic acid. The optimum weight ratio is 0.404, which corresponds to 1.00 on a molar basis. When the concentration of ferric salicylate is lowered, the sensitivity was decreased. The effect of a higher concentration of ferric salicylate was not studied, since a higher absorbance would introduce greater photometer error.

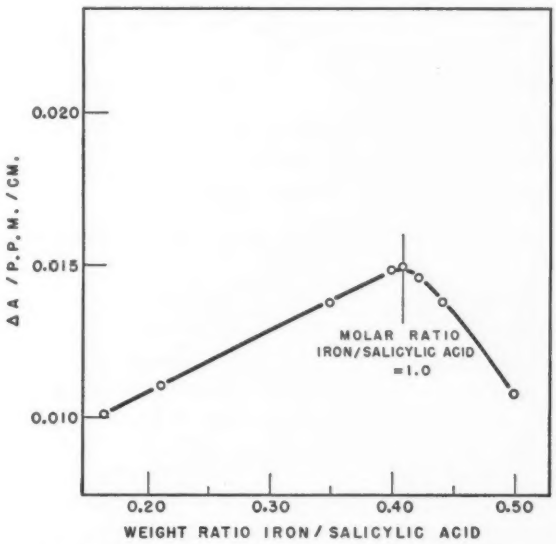

FIG. 2. The effect of a change in iron – salicylic acid ratio on the sensitivity of fluoride determination.

(*c*) *Buffer.*—A buffer system to hold the pH constant at 3.1 was necessary. Any buffer which included a complexing acid such as citric, phosphoric, or tartaric would, of course, be unsuitable since the ferric ions would be complexed and the color decreased. It was found that a monochloroacetic acid – sodium hydroxide system was suitable since this acid complexes iron to only a very slight extent. The effect of the slight complexing property of the buffer was to make the calibration curve linear. Fig. 3 shows calibration curves obtained with and without buffer present. These curves show that, although the sensitivity of the procedure below 20 μgm. of fluoride is decreased by the buffer, the useful upper limit is increased from 40 μgm. to 100 μgm. The sensitivity of the procedure at 70 μgm. is increased from 0.005 to 0.015 change in absorbance per μgm. of fluoride per cm. of light path.

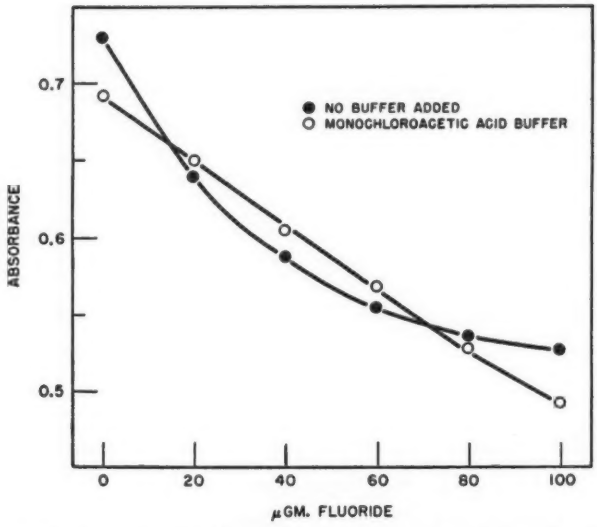

FIG. 3. Calibration curves obtained with and without monochloroacetic acid buffer.

It was found that some batches of monochloroacetic acid contained an impurity which complexed ferric ion strongly and hence were not suitable. On standing for more than two weeks, buffer solutions slowly developed a similar impurity which decreased the sensitivity. The impurity in each case was presumably glycolic acid formed by the hydrolysis of the chloroacetic acid. This assumption was strengthened by the fact that chloride ion could be detected in old buffer solutions but not in freshly prepared solutions. The sensitivities obtained with a buffer solution stored for five weeks decreased from 0.0135 to 0.0117 at room temperature and to 0.0064 at 40°C.

(*d*) *Interferences.*—Although the procedure is designed to follow a distillation, the effect of different ions on the color of ferric salicylate was felt to be of interest for possible application to waters containing small amounts of other ions. Table III shows the effects of possible interfering substances on the procedure. In general, reducing agents and complex-forming anions bleached the color giving high apparent fluoride results. Some oxidizing agents increased the color slightly giving slightly low fluoride results. Cations such as aluminum competed with the ferric iron of the reagent for fluoride and gave high results. The tolerated amount is defined as that amount of interfering material which caused an error of not more than one microgram of fluoride. Where no interference is noted the amount given is the highest amount tested. Calibration curves in the presence of up to 5 mgm. of sulphate and 50 mgm. of chloride were parallel to curves obtained in their absence. Hence, if the concentration of these anions is known, corrections may be made and amounts considerably larger than shown in Table III may be tolerated.

TABLE III

INTERFERENCE OF VARIOUS MATERIALS WITH THE FERRIC SALICYLATE PROCEDURE FOR FLUORIDE

Material	Tolerated amount, mgm./25 ml.	Remarks	Material	Tolerated amount, mgm./25 ml.	Remarks
Pyrophosphate	0.001	High fluoride results	Free chlorine	0.04	Low fluoride results
Phosphate	0.012	" " "	Aluminum	0.001	" " "
Citrate	0.025	" " "	Ferric	0.002	" " "
Tartrate	0.05	" " "	Cupric	0.2	No interference noted
Sulphate	0.3	" " "	Calcium	1	" " "
Chloride	3	" " "	Magnesium	1	" " "
Bromide	5	" " "	Ferrous	1	" " "
Hydroxylamine	0.01	Causes fading	Nitrate	10	" " "
Sulphite	0.03	" "	Chlorate	10	" " "
Iodide*	10 or 1	" "	Perchlorate	10	" " "
Thiosulphate*	10 or 1	" "	Hydrazine	0.5	" " "
Nitrite	1	Low fluoride results			

**The larger amount can be tolerated if read immediately but fading is pronounced within three minutes.*

PROCEDURE

Reagents

1. *Perchloric acid.* Reagent grade, 70%.
2. *Silver sulphate or perchlorate.* Reagent grade.
3. *Ferric nitrate solution.* Dissolve 0.608 gm. of pure iron wire in 13 ml. of concentrated nitric acid. When the wire has dissolved, add 20 ml. of water. Boil to expel oxides of nitrogen and dilute to 500 ml. in a volumetric flask.
4. *Ferric salicylate solution.* Dissolve 0.75 gm. salicylic acid in water. Add 25.0 ml. of the ferric nitrate solution and dilute to 1000 ml. in a volumetric flask. Store in an amber glass or low-actinic glass bottle. This gives a solution in which the iron salicylic acid ratio is 0.404 on weight basis and 1.00 on a molar basis. Prepare a fresh solution every two weeks.
5. *Buffer solution.* Dissolve 6.1 gm. of monochloroacetic acid and 1.7 gm. of sodium hydroxide in water. Dilute to about 200 ml. and adjust the pH to 3.1 with monochloroacetic acid or sodium hydroxide if necessary. Prepare a fresh solution every two weeks.
6. *Standard fluoride solution.* Dissolve 0.2211 gm. of sodium fluoride in water and dilute to 500 ml. Ten milliliters of this solution diluted to 200 ml. contains 10 μgm. fluoride per ml.

Method

Ignite a weighed sample of 4 to 6 gm. in a platinum dish at 650°C. for at least two hours. Cool and transfer the sample to a 250 ml. modified Claisen Flask (6) and dissolve in 30 ml. of perchloric acid, add 0.2 gm. of silver sulphate or perchlorate and a small amount of sea sand. Distill the fluosilicic acid at 135–137°C. according to the method of Churchill (6). Collect about 190 ml. of distillate, maintaining a basic condition to phenolphthalein in the receiving flask with 1 *N* hydroxide solution. Neutralize the distillate with 1 *N* perchloric

acid adding five or six drops excess. Make up to 200 ml. in a volumetric flask. The pH of this solution should be between pH 3 and 5. A 5 ml. aliquot is placed in a 25 ml. volumetric flask and 1.0 ml. of buffer solution and 5.0 ml. of ferric salicylate solution are added. The sample is diluted to the mark, and the absorbance is measured at 530 mμ in a 5 cm. cell with a Beckman Model B spectrophotometer, with distilled water in the reference cell. The absorbance of a blank containing ferric salicylate solution, buffer, and distilled water should also be measured. The absorbance of the samples is subtracted from the absorbance of the blank and the amount of fluoride in the sample determined from the calibration curve. If the fluoride content exceeds 100 μgm. the colorimetric test should be repeated using a smaller aliquot. The sample flasks should be protected from direct light after the addition of the ferric salicylate solution.

Calibration Curve

Twenty-five milliliter volumetric flasks containing 0 to 12 ml. of standard fluoride solution corresponding to 0 to 120 μgm. of fluoride are carried through the procedure. The absorbance versus μgm. of fluoride is plotted. The relationship is linear from 0 to 80 μgm. but deviates slightly when the fluoride concentration is above 80 μgm.

RESULTS AND DISCUSSION

The recovery of fluoride added to samples of bone meal is given in Table IV. The fluoride content of the bone meal was determined in quadruplicate by the procedure given here and an average value of 340 p.p.m. was obtained. Standard sodium fluoride solution was added to samples after ignition and the recovery of fluoride in the distillate was measured. The per cent recovery in Table IV is given in terms of the total fluoride expected rather than of the added fluoride. The standard error of the method when applied to two samples taken from separate barrels of 10 commercial batches of bone meal was ±2.3%, and the standard deviation on 17 samples taken from 17 barrels of one shipment consisting of two or more batches was 4.7%.

TABLE IV

RECOVERY OF FLUORIDE ADDED TO BONE MEAL*

F added per gm., μgm.	Recovery of F per gm., μgm.†	% Recovery
83	429	101.4
83	426	100.7
167	498	98.2
167	523	103.1
250	580	98.3
250	582	98.6

**The fluorine content of the bone meal was 340 p.p.m. as determined by the ferric salicylate procedure.*

†Determined on aliquots of the distillate containing from 50 to 85 μgm. of fluoride ion.

REFERENCES

1. BARTLET, J. C., COUTU, C., LIST, E., and WOOD, M. Can. J. Technol. 30: 137–142. 1952.
2. BEVERIDGE, J. S., HUNTER, G. J., and MACNULTY, B. J. Anal. Chim. Acta, 9: 330–337. 1953.
3. BRIDGER, G. L. Anal. Chem. 25: 17–24. 1953.
4. BUMSTEAD, H. E. and WELLS, J. C. Anal. Chem. 24: 1595–1597. 1952.
5. BUSCH, G. W., CARTER, R. C., and MCKENNA, F. E. Analytical chemistry of the Manhattan project, Natl. Nuclear Energy Ser. Div. VIII. Vol. 1. McGraw-Hill Book Company, Inc., New York. 1950. pp. 226–248.
6. CHURCHILL, H. V. Ind. Eng. Chem. Anal. Ed. 17: 720–721. 1945.
7. HORTON, A. D., THOMASON, P. F., and MILLER, F. J. Anal. Chem. 24: 548–550. 1952.
8. KORTÜM-SEILER, M. Angew. Chem. A, 59: 159–160. 1947.
9. LOVE, S. K. and THATCHER, L. L. Anal. Chem. 25: 65–74. 1953.
10. MCKENNA, F. E. Nucleonics, 8 (No. 6): 24–33. 1951.
11. MCKENNA, F. E. Nucleonics, 9 (No. 1): 40–49. 1951.
12. MCKENNA, F. E. Nucleonics, 9 (No. 2): 51–58. 1951.
13. MEGREGIAN, S. and MAIER, F. J. J. Am. Water Works Assoc. 44: 239–248. 1952.
14. NICHOLS, M. L. and CONDO, A. C. Anal. Chem. 26: 703–707. 1954.
15. PRICE, M. J. and WALKER, O. J. Anal. Chem. 24: 1593–1595. 1952.
16. RICKSON, J. B. Analyst, 75: 84–91. 1950.
17. WILLARD, H. H. and WINTER, O. B. Ind. Eng. Chem. Anal. Ed. 5: 7–10. 1933.

A LOW TEMPERATURE ATTACHMENT FOR AN X-RAY GONIOMETER[1]

By R. G. Butters and H. P. Myers

ABSTRACT

A simple low temperature attachment for use with a Philips high angle X-ray diffraction goniometer is described. The attachment allows spectrometer plots to be obtained between room and liquid oxygen temperatures.

INTRODUCTION

In order to determine crystal structures at low temperatures a means for X-ray examination is essential. Several methods utilizing conventional photographic recording are available but these have inherent disadvantages. In particular there is the relatively long exposure time that is needed with the attendant difficulty of accurate temperature control over large time intervals. The use of high intensity microfocus X-ray tubes offsets this limitation to some extent but the construction of an X-ray camera still demands extreme mechanical precision and the facilities of a fully equipped workshop.

The study of phase changes does not necessarily require that the whole diffraction pattern be recorded and in this respect the X-ray goniometer, which can be used to scan all or any particular line of the pattern, has distinct advantages. A single important line may be scanned and the intensity directly recorded in a period of time dependent only upon the scanning speed; temperatures need be kept constant for short intervals and control conditions are more easily maintained. The features of mechanical design of a low temperature attachment for such an instrument are on the whole simple, there being few aspects demanding precision in arrangement. The apparatus described below uses only readily available materials and has been found to work satisfactorily.

THE APPARATUS

The attachment is comprised of two parts, the specimen holder and the outer casing. Fig. 1 shows the details of the design. The specimen plate is machined from a solid cylinder of brass $1\frac{1}{2}$ in. $\times$ $\frac{3}{4}$ in. diameter, the central $\frac{1}{2}$ in. of this is milled away until a diametral plane is exposed. A cooling chamber is prepared by suitable drilling. The specimen plate is silver soldered to a stainless steel tube, this being done in a lathe to ensure alignment of the tube axis and the specimen plane. This steel tube is coaxial with a surrounding brass tube $\frac{5}{8}$ in. outer diameter, which is the means whereby the arrangement is attached to the goniometer. The end of this tube remote from the specimen plate is silver soldered to the steel tube so that they are coaxial; it is also

[1]*Manuscript received May 13, 1955.*
Contribution from the Department of Mining and Metallurgy, University of British Columbia, Vancouver, B.C.

threaded at this end for clamping to the goniometer assembly. This outer brass tube is also silver soldered to a brass end plate which carries the $\frac{1}{8}$ in. O ring used for the vacuum seal; the thermocouple wires pass through this end plate, a rubber seal being used.

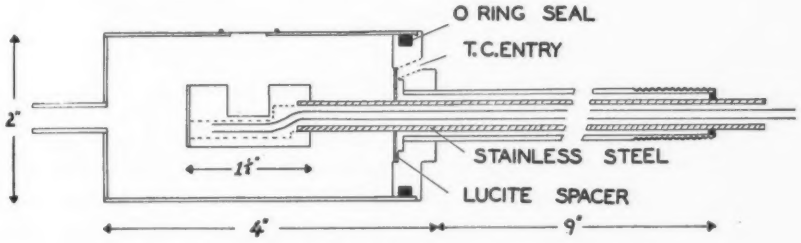

FIG. 1. Scale drawing of the low temperature attachment.

Although the inner steel tube is only fixed at one end it remains rigid; if necessary it may also be fixed at the brass end plate provided an opening is left for evacuation of the space between the steel and brass tubes. In the present design a lucite spacer was used. The complete specimen holder is attached to the goniometer by the brass tube which replaces the mounting shaft of the Philips specimen holder; the specimen plate is aligned in the 0° plane of the goniometer and then clamped in position by a nut working in the threaded part of the brass tube.

The outer case is of brass open at one end where it fits and seals by the O ring to the end plate; a pumping stem is soft soldered to the closed end. The X-ray window is a $\frac{7}{16}$ in. slot cut almost half way around the circumference of the case and covered by a thin sheet of seran plastic. This window is secured by scotch tape and held fixed by two binding wires sitting in small grooves machined in the circumference of the case. This window is extremely transparent to X-rays and very strong having withstood repeated evacuations without failure. The whole apparatus may be evacuated and the coaxial brass and steel tubes then form a Dewar assembly for introducing the coolant. The temperature of the specimen plate is controlled by coolant led through a thin walled brass tube passing inside the steel tube and into the cooling chamber itself. The coolant passes back over the inlet tube thereby minimizing losses. The thin brass inlet tube is kept from contact with the steel tube by small rubber washers.

The low temperature of the specimen plate is maintained by a continuous flow of coolant. Cold oxygen gas has been used to obtain temperatures down to -100°C., the gas is led from an oxygen boiler, and the flow (and thereby the temperature) adjusted by controlling the power input to a small heater element (100Ω, 10 watt resistor) immersed in the liquid oxygen. With a constant power input the temperature remains constant within ± 0.5°C. In our experiments the oxygen was brought to the apparatus through a length of lagged glass tubing, lower temperatures than -100°C. can be obtained but it would be

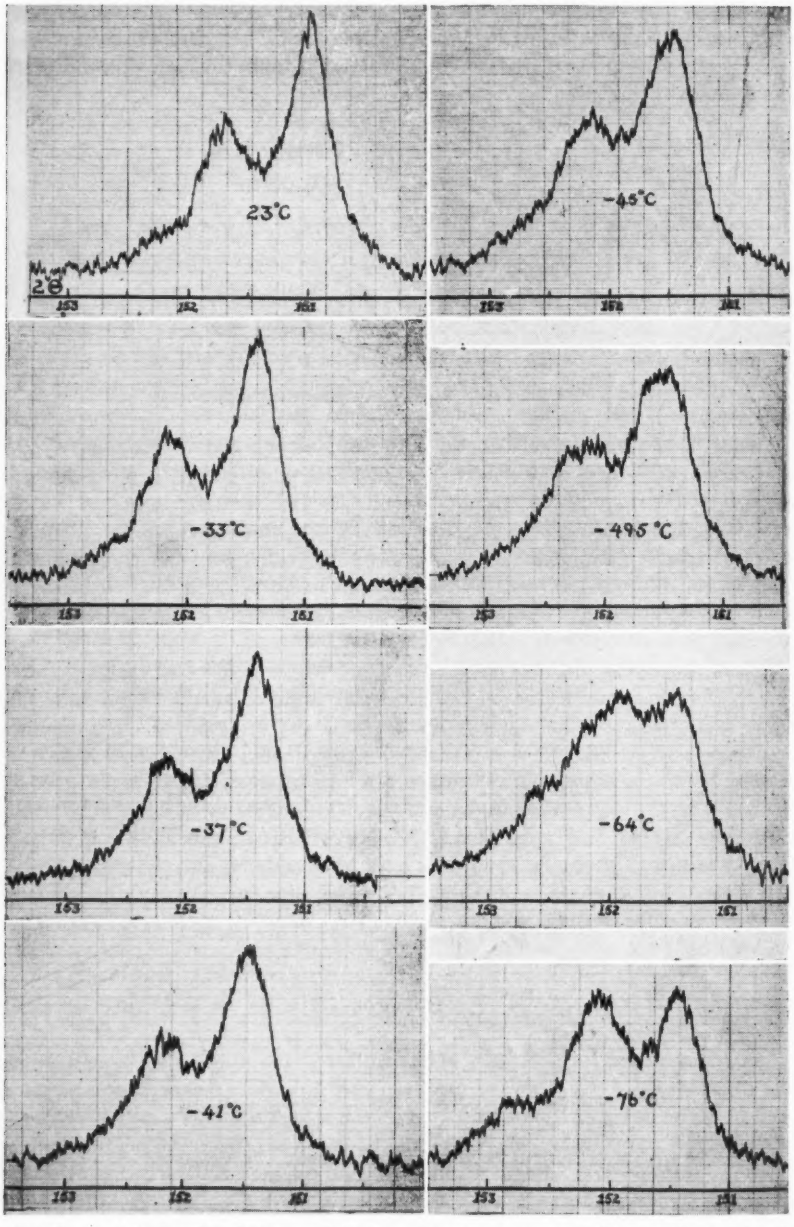

FIG. 2. A second order phase transition in a manganese ternary alloy is indicated by the change in structure of the line 311 at low temperatures.

desirable to use a double walled lead in tube for this purpose. Measurements at liquid oxygen temperature are straightforward; it is not necessary to maintain a continuous flow since the cooling chamber can contain a small volume of liquid which is replenished periodically.

TEMPERATURE MEASUREMENT

The temperature of the specimen is measured by a copper constantan thermocouple lying in the specimen plane, it is fixed to and insulated from the specimen holder by scotch tape. The specimen plate is covered with a thin layer of vacuum grease and the powdered specimen spread uniformly from a sieve. The grease serves to hold the powder in place when large values of θ are being used and in addition provides good thermal contact between the specimen, the thermocouple, and the specimen plate.

OPERATION

Fig. 2 shows spectrometer plots obtained at low temperatures on a manganese ternary alloy which undergoes a second order transition at $-42°$C. (1). The structure of this alloy at room temperature is face centered cubic but changes to face centered tetragonal at $-42°$C., the axial ratio becoming progressively less than 1 the lower the temperature. The axial ratio is 0.994 at $-196°$C. so the change in structure is slight. Fig. 2 shows the change in intensity profile of line 311 of the cubic structure as determined with the apparatus described. It will be seen that a reduction in peak intensity and an angular broadening of the line occurs in the temperature interval $-37.5°$C to $-45°$C. indicating the transition region.

ACKNOWLEDGMENT

This work was carried out in connection with a research project, 281, sponsored by the Defence Research Board of Canada.

REFERENCES

1. BUTTERS, R. G. and MYERS, H. P. Phil. Mag. 46: 132. 1955.

THE AIR BLOWING OF REDWATER ASPHALT BASE STOCK

THE USE OF PHOSPHORUS PENTOXIDE AS AN ADDITION AGENT[1]

By J. Eng,[2] G. W. Govier, and D. Quon

ABSTRACT

Redwater asphalt base stock was air blown in a conventional vertical cylindrical still approximately 10 in. in diameter and 30 in. in height. The base stock was blown initially without "catalyst" at temperatures of 465°F. and 525°F. and with air rates of 55 and 75 cubic feet per minute per ton of charge. Subsequently, the base stock was air blown with amounts of phosphorus pentoxide "catalyst" varying between 0.25 and 1.0%. Various methods of catalyst dispersion were employed. The straight air blowing gave a product which had a higher softening point, a lower penetration, a lower ductility, and a higher viscosity than the base stock. With small amounts of phosphorus pentoxide as an addition agent, the blown product, at a given softening point, had a higher penetration and a higher viscosity than the product obtained by air blowing alone. There was, however, no marked effect on the ductility – softening point relationships. The penetration increase was dependent on the amount of pentoxide used. The method of dispersion of the phosphorus pentoxide was found to be comparable in importance to the amount used. In both the non-catalytic and the catalytic air blowing, the blowing temperature and the air rate each had a significant effect on the time required to produce an asphalt with a given softening point. The effect of these variables on the relationships between the softening point of the product and the other physical properties was found to be small. Air blowing produced a marked increase in the mean molecular weights of the asphaltene, resin, and oily constituent fractions. The oily constituent content remained substantially constant but the asphaltene content showed an increase and the resin content a decrease.

INTRODUCTION

Asphalt has been known to man for some five or six thousand years. For centuries the only asphalt used was a native asphalt formed by the natural distillation of oil. Today, although there are still large deposits of native asphalt, most asphalt is manufactured and is a product of the refining of crude oil. Because of the great variety in the present-day uses of asphalt, it is necessary to prepare products which differ widely in certain important physical properties. One of the most important processes for preparing such products is carried out by blowing air at elevated temperatures through residual petroleum oils. The resulting "air blown" asphalts acquire a certain amount of pliability, elasticity, and resilience. While less ductile at ordinary temperatures than residual asphalts of the same hardness they are less susceptible to temperature changes and are favored where wide temperature ranges are to be met. For equal softening points the penetration of blown asphalts is greater than that of residual asphalt.

The characteristics of the "blown" asphalt can however be controlled only to a certain extent. For example, Canadian refiners have had difficulty in making certain grades of asphalt from a vacuum reduced Redwater base stock.

[1]*Manuscript received April 12, 1955.*
Contribution from the Department of Chemical and Petroleum Engineering, University of Alberta, Edmonton, Alberta.
[2]*Shell Oil Fellow, University of Alberta. Present address: Imperial Oil Co., Sarnia, Ontario.*

The softening point and penetration specifications of roofing asphalts could not simultaneously be met by the air blowing of this stock, and an asphalt finished to a given softening point had too low a penetration. This problem is of particular interest since the Redwater field represents Canada's largest fully developed field, having an average daily production of some 63,000 barrels.

Considerable interest has developed in the United States in work done by Hoiberg (5) of the Lion Oil Co. who in his patent claims that certain compounds, especially some phosphorus containing compounds, when used as addition agents would modify the course of the air blowing reaction and result in products having a higher penetration for a given softening point.

The present work deals with the application of Hoiberg's claims to the problem of manufacturing roofing asphalt from a Redwater base stock. The objectives of the investigation were, firstly, to determine the range of products obtainable by conventional air blowing and, secondly, to obtain a quantitative measure of the effect on the product properties of phosphorus pentoxide as a catalyst.

LITERATURE REVIEW

In 1865, Gesner (4) reported that the properties of petroleum products changed when the products were treated with oxidizing agents or air. However, it was not till 1894 that Byerley (2) first manufactured blown asphalt on a commercial scale. Since he used only a small quantity of air, this process was essentially a distillation process, with the air used principally for agitation. Culmer (3) later described a process which was the forerunner of the present methods used in air blowing of asphalt. A large amount of air was passed through petroleum residuum at low temperatures, the air being introduced into a single perforated pipe laid along the bottom of the still. Because of the character of the light gravity residuum used in these early experiments and the poor distribution of air, the time of blowing was lengthy, varying from 20 to 60 hr.

Although blown asphalts are often referred to as oxidized asphalts, the essential process, as postulated by Katz (9), is not oxidation but condensation followed by polymerization to form products of higher molecular weight. It is believed that the small amount of hydrogen removed combines with the oxygen to form water. Ultimate analyses of the blown asphalts showed no appreciable fixation of oxygen, suggesting that the latter probably acts as a catalyst.

The use of addition agents to modify the air blowing process dates back to Jenny (8) in 1876, but it was not until 1930 that Abson (1) pointed out that the use of salts such as ferric chloride and zinc chloride not only accelerated the blowing process but also changed the physical properties of the finished asphalt. The term "catalytic asphalt" is generally used to describe an air blown asphalt obtained with the use of addition agents—although the reaction may not strictly be a catalytic one. The reaction rate may or may not be increased and in some cases it may even be decreased. In many instances,

the addition agents act by forming complexes or intermediate products and hence cannot be recovered at the end of the reaction. Abson was followed by a number of patentees who found various advantages in the use of different agents or catalysts. Among these patentees, the most important is Hoiberg (5). He found that blown asphalt prepared by air blowing Smackover crude residua in the presence of red phosphorus or phosphorus-containing catalysts, such as P_2O_5, P_4S_3, P_4S_7, and P_2S_5, had a much higher penetration for a given softening point than is the case for an asphalt produced by air blowing alone. The product was found suitable for protective coatings and roofing applications.

Attempts have been made to relate the changes in physical properties of the asphalt with the changes in chemical constitution. The composition of natural asphalt is extremely complex, but by means of solvent extraction Marcusson (10), following the early work of Richardson, has distinguished oily constituents, resins, and asphaltenes. Although this division is used widely, any slight variations in analytical techniques will lead to significantly different results. Also, the nature of the oily constituents, resins, and asphaltenes in different asphalts varies considerably.

Marcusson and Picard (11) found that the fractional composition changed with air blowing, the resins decreasing and the asphaltenes increasing. The oily constituents changed comparatively little. Sachanen (13) suggested that the oily constituents were oxidized to resins, which in turn were oxidized to asphaltenes. In addition to variations in the fractional composition, Katz (9) found that the mean molecular weight of the individual fractions increased markedly on air blowing.

Practically nothing is known about the mechanism by which certain addition agents change the physical properties of the blown asphalt. Hoiberg (6) analyzed Arkansas asphalts blown with and without phosphorus pentoxide. Although the pentoxide blown asphalt showed a very much higher penetration for a given softening point than the straight air blown asphalt, the fractional compositions of the two asphalts appeared almost identical. Hoiberg states that perhaps the increase in penetration is due to the formation of asphaltene molecules of higher molecular weight than produced by straight air blowing. Such fractions could be expected to be less susceptible to peptization by the resin fractions. Evidently any changes brought about by addition agents are primarily the result of changes in the colloidal nature of the asphalt, although chemical reaction may still be a factor.

EXPERIMENTAL PROGRAM

Three series of tests were planned to determine the nature of the products obtainable by normal air blowing of Redwater asphalt base stock and to evaluate the effect of phosphorus pentoxide as a "catalyst". The first of these was designed to obtain basic data on the effect of air rate and blowing temperature under conditions near those of industrial practice, i.e. air rates of 55 and 75 cubic feet per minute (c.f.m.) per ton of charge and temperatures of 465 and 525°F.

In the second group of tests, various amounts of phosphorus pentoxide (from 0 to 1.0% by weight of the total charge) were added as catalysts. Both fresh phosphorus pentoxide and catalyst residues were used. The air rate was held constant at 55 c.f.m. per ton of charge and the blowing temperature was maintained at 525°F. Dispersion of catalyst into the asphalt was by a mortar-and-pestle technique. In the third group of tests, two other methods of dispersion were tried. One involved the use of a small laboratory stirrer or mixer. The other method consisted of first dispersing the phosphorus pentoxide in carbon tetrachloride (to overcome the hygroscopic tendencies of the pentoxide) and then pouring the resultant mixture into the hot asphalt.

Materials and Equipment

The physical properties of the Redwater asphalt base stock were determined by standard ASTM test procedures. The composition of the base stock, in terms of asphaltenes, resins, and oily constituents, was obtained by the procedure of Strieter (14). The molecular weights of these constituents were determined cryoscopically using water-saturated benzene as suggested by Hoiberg *et al.* (7). A summary of the properties appears in Table I.

TABLE I

PROPERTIES OF REDWATER ASPHALT BASE STOCK

		ASTM test procedure
Softening point (ring and ball)	107.0°F.	D36–26
Penetration at 32°F., 200 gm., 60 sec.	24 mm.	D243–36
77°F., 100 gm., 5 sec.	148 mm.	
100°F., 100 gm., 5 sec.	Too soft	
Saybolt Furol viscosity 210°F.	540 sec.	D88–44
250°F.	138 sec.	
Ductility at 77°F.	150 cm. plus	D113–44
Specific gravity at 77°F.	1.007	D70–27
Solubility in carbon tetrachloride	99.60%	D165–42
Flash point (Cleveland open cup)	350°F.	D92–46
Asphaltenes		
Per cent by weight	18.1	
Mean molecular weight	1299	
Resins		
Per cent by weight	43.4	
Mean molecular weight	601	
Oily constituents		
Per cent by weight	38.5	
Mean molecular weight	525	

The blowing tests were conducted in a conventional vertical cylindrical still illustrated in Figs. 1 and 2. The still was approximately 10 in. in diameter, 30 in. in height, and was mounted on a 1-in. angle iron support. The charge was introduced at the top upon removing the ½-in. thick cover plate. Samples were withdrawn from one of the three sampling connections located at different levels on the still. Attached to the bottom of the still was a firebox made of 16-gauge steel plate through which heat was applied directly by a 7-in. diam-

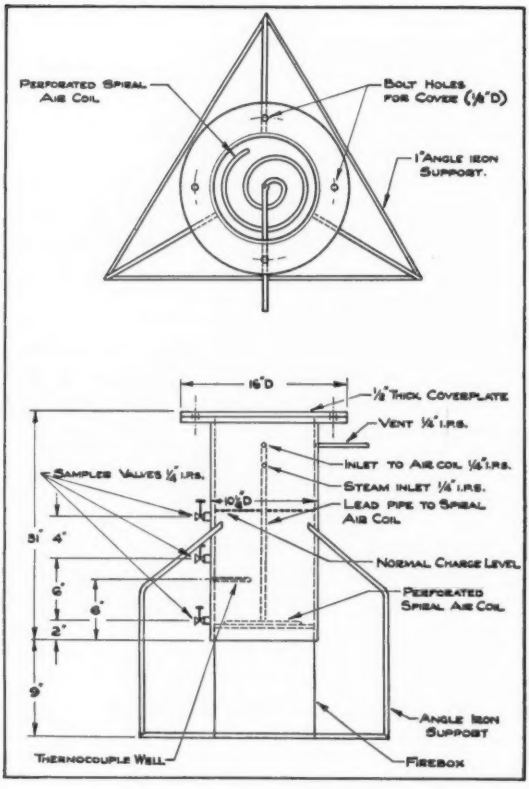

FIG. 1. Sketch of asphalt still.

eter ring-type gas burner. Air was admitted into the charge through a spiral air coil set at the bottom of the still. This air coil was made of $\frac{1}{4}$-in. o.d. mild carbon steel tubing, perforated with 7 1/32-in. diameter holes spaced 5 in. apart. The thermocouple well was located 4 in. from the bottom of the still. Standard $\frac{1}{4}$-in. piping was used for all lines and connections.

The air rate was controlled manually, the flow measuring device being a calibrated sharp-edged orifice. The temperature of blowing was controlled automatically by means of an on–off pyrometer controller actuated by a chromel–alumel thermocouple. The controller operated a solenoid gas valve in a bypass of the main fuel gas line. This permitted the heating gas supply to be varied between preset limits and enabled the blowing temperature to be controlled within about three Fahrenheit degrees.

Procedure

A charge of approximately 30 lb. of the asphalt base stock was weighed, heated until fluid, and poured into the still where it was then heated to the

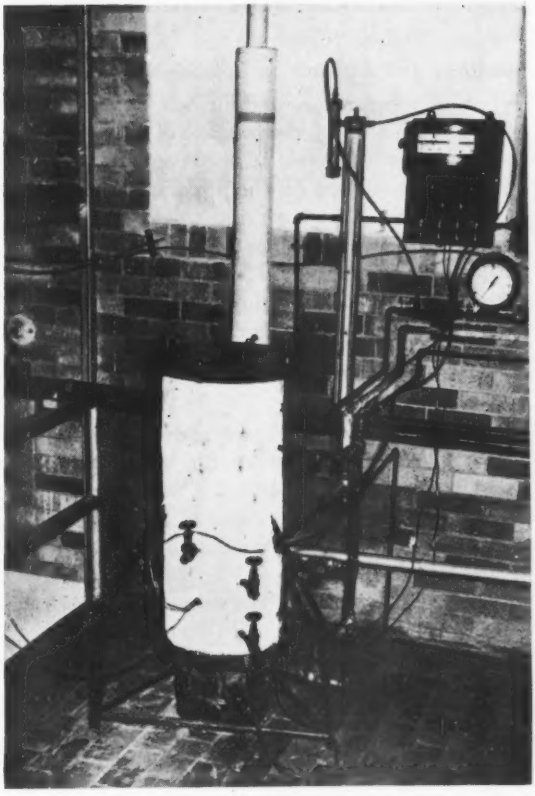

FIG. 2. Photograph of asphalt still and accessory equipment.

desired temperature. When the charge reached the proper temperature the desired air blowing rate was set and the test was considered started. At regular time intervals, 1-lb. samples were withdrawn for testing. When an asphalt of at least 220°F. softening point was obtained, the blowing was discontinued and the contents of the still were discharged.

In the tests where catalysts were employed, about three pounds of asphalt was heated to about 400°F. and mixed with the phosphorus pentoxide. This mixture was then added to the main charge in the still when the charge had reached the blowing temperature. Dispersion methods included hand grinding with a mortar-and-pestle, mechanical stirring for half an hour with a laboratory motor stirrer, and finally, immersion of the phosphorus pentoxide in carbon tetrachloride prior to adding it to the charge.

The samples taken during each of the tests were examined for essentially the same properties as were determined on the original base stock.

EXPERIMENTAL RESULTS

Series 1—Air Blowing Without "Catalyst"

Effect of Temperature and Air Rate on Reaction Time

Data on the effect of temperature and air rate on the reaction time in the Series 1 tests are presented in Fig. 3, the progress of the reaction being measured by the change in the softening point. It is convenient to illustrate the effect of time, temperature, and air rate on the physical properties by reference to the softening point, which is perhaps the single most important physical property of an asphalt. The data indicate that increasing the blowing temperature from 465°F. to 525°F. reduces the time required to reach a 220°F. softening point to almost one-half. A similar effect occurs when the blowing temperature is fixed and the air rate increased.

Effect of Temperature and Air Rate on Penetration –, Ductility –, Viscosity – Softening Point Relationships

The data indicate that the temperature and air rate have comparatively little effect on the relationships between the softening point (chosen as a reference property) and the other properties. Thus, Figs. 4, 5, and 6 show only a very slight effect of the blowing temperature, within the range of 465° to 525°F., on the penetration – softening point, ductility – softening point, and viscosity – softening point relationships. Fig. 4 also shows the corresponding small effect of the air rate, at least in the range of 55 to 75 c.f.m. per ton of charge, on the penetration – softening point relationship.

Series 2—Air Blowing with Phosphorus Pentoxide "Catalyst"

Effect of Phosphorus Pentoxide on Reaction Time

The results of the Series 2 tests, conducted with phosphorus pentoxide as an addition agent, are shown in Fig. 7. It will be noted that a longer reaction time is required to achieve a given softening point than in the case of the Series 1 tests, the degree of increase being dependent on the amount of phosphorus pentoxide used. While it requires approximately six hours to produce a 230°F. softening point asphalt with straight air blowing, more than 10 hr. are necessary to produce the same softening point in the presence of 1.0% phosphorus pentoxide. From the industrial point of view, this increase in reaction time is most undesirable since it would both decrease equipment capacity and increase air requirements. It is interesting to note that the phosphorus pentoxide has its retarding effect on the reaction rate chiefly in the early stages of the blowing.

Effect of Phosphorus Pentoxide on Penetration –, Ductility –, Viscosity – Softening Point Relationships

With the addition of small amounts of phosphorus pentoxide in the blowing process, the relationships between the other physical properties of the blown asphalt and the softening point are changed substantially. Fig. 8 indicates that the penetration of the blown asphalt is increased appreciably for a given softening point, the increase being approximately proportional to the amount

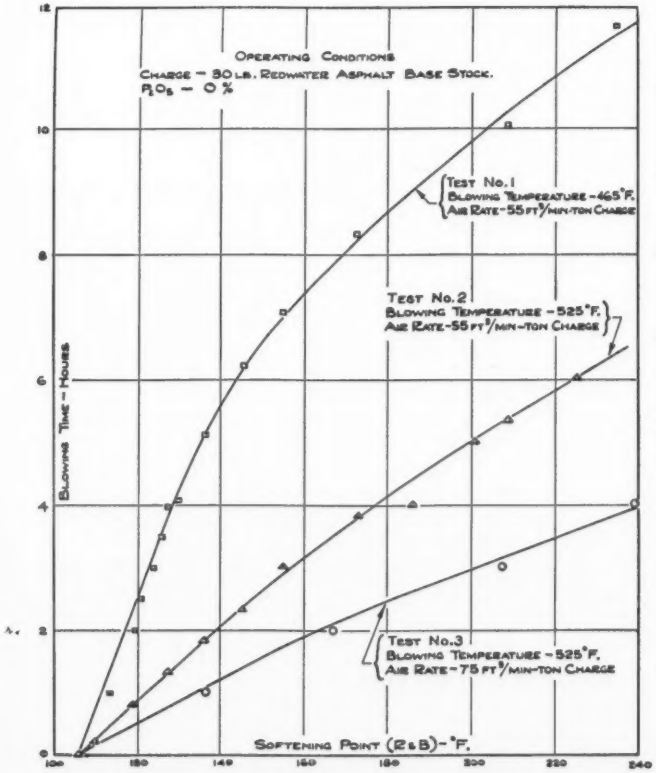
OPERATING CONDITIONS
CHARGE – 30 LB. REDWATER ASPHALT BASE STOCK.
P_2O_5 – 0 %
TEST No. 1
BLOWING TEMPERATURE – 465°F.
AIR RATE – 55 FT³/MIN-TON CHARGE
TEST No. 2
BLOWING TEMPERATURE – 525°F.
AIR RATE – 55 FT³/MIN-TON CHARGE
TEST No. 3
BLOWING TEMPERATURE – 525°F.
AIR RATE – 75 FT³/MIN-TON CHARGE
BLOWING TIME – HOURS
SOFTENING POINT (R & B) – °F.

FIG. 3. Time – softening point relationships: effect of blowing temperature and air rate.

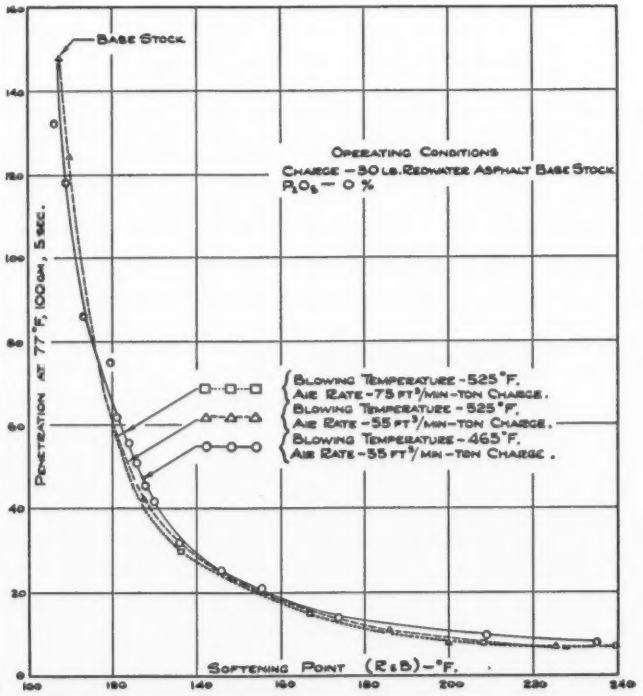
BASE STOCK
OPERATING CONDITIONS
CHARGE – 30 LB. REDWATER ASPHALT BASE STOCK.
P_2O_5 – 0 %
BLOWING TEMPERATURE – 525°F.
AIR RATE – 75 FT³/MIN-TON CHARGE.
BLOWING TEMPERATURE – 525°F.
AIR RATE – 55 FT³/MIN-TON CHARGE.
BLOWING TEMPERATURE – 465°F.
AIR RATE – 55 FT³/MIN-TON CHARGE.
PENETRATION AT 77°F, 100 GM., 5 SEC.
SOFTENING POINT (R & B) – °F.

FIG. 4. Penetration – softening point relationships: effect of blowing temperature and air rate.

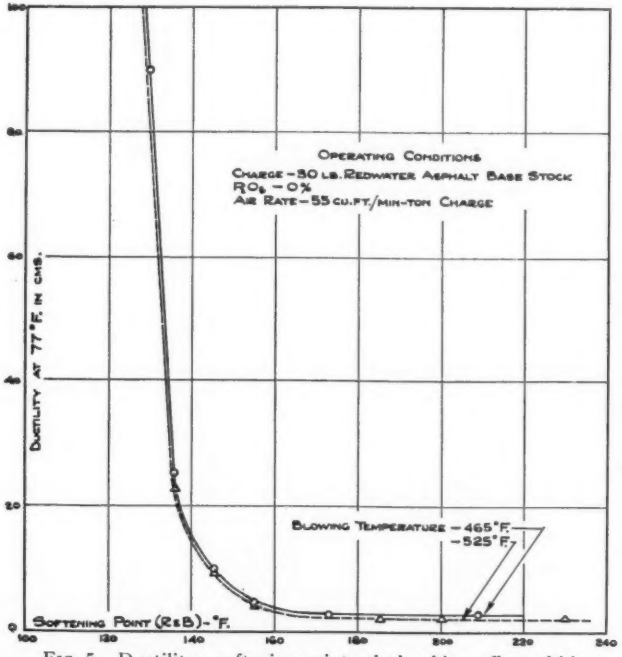

FIG. 5. Ductility – softening point relationships: effect of blowing temperature.

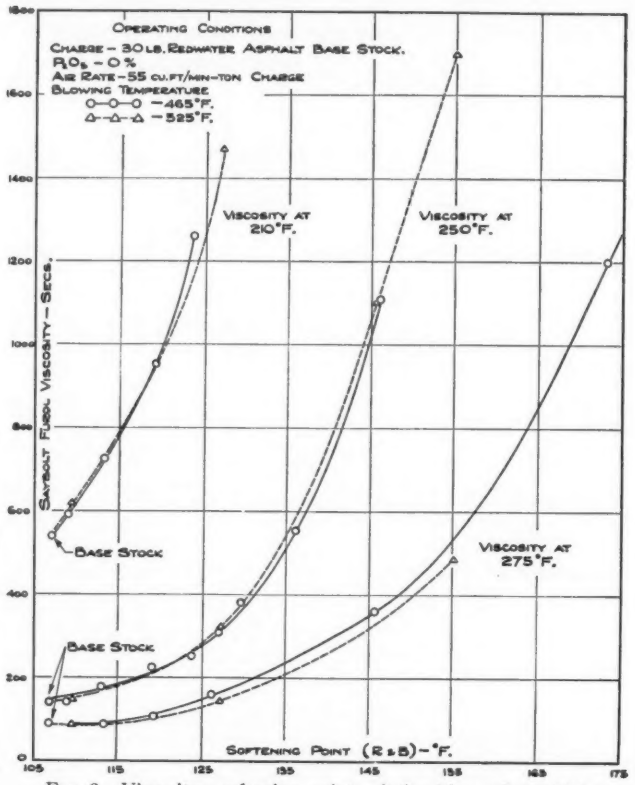

FIG. 6. Viscosity – softening point relationships: effect of blowing temperature.

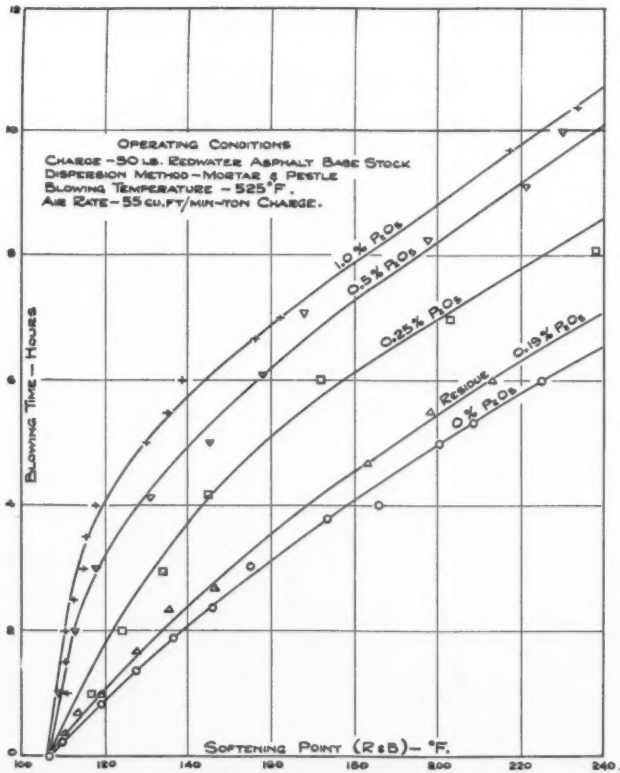

FIG. 7. Time – softening point relationships: effect of phosphorus pentoxide "catalyst" concentration.

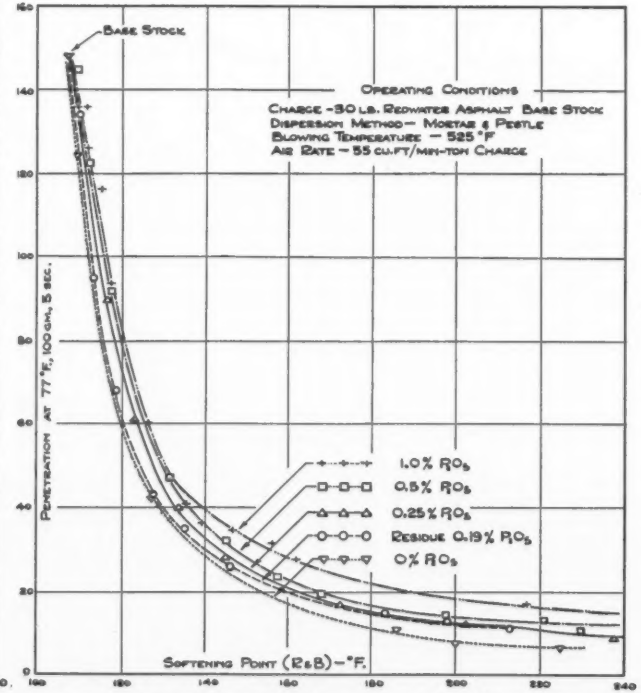

FIG. 8. Penetration – softening point relationships: effect of phosphorus pentoxide "catalyst" concentration.

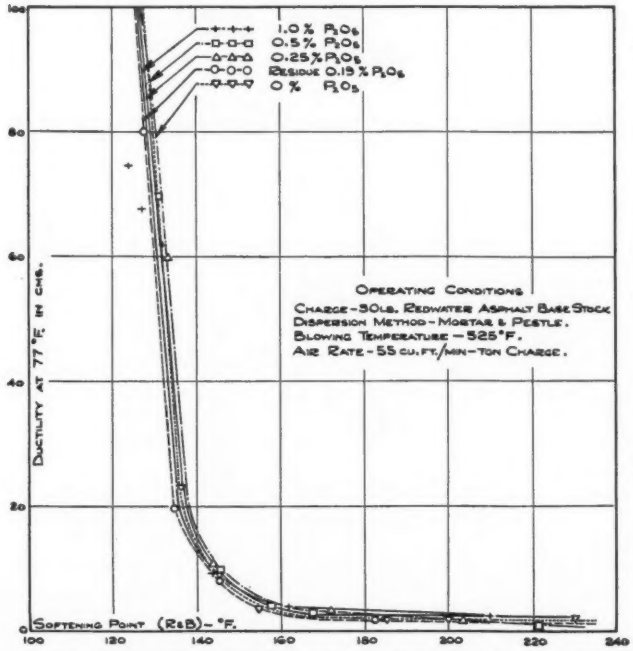

FIG. 9. Ductility – softening point relationships: effect of phosphorus pentoxide "catalyst" concentration.

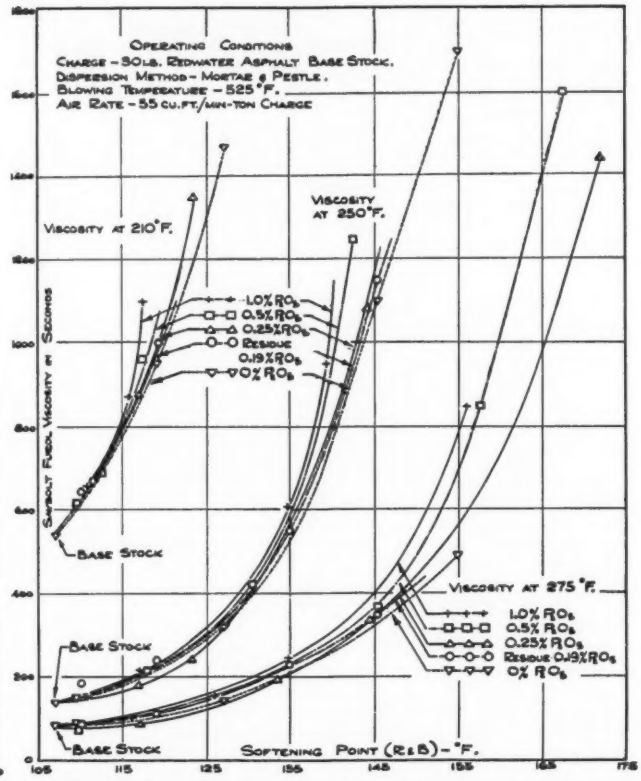

FIG. 10. Viscosity – softening point relationships: effect of phosphorus pentoxide "catalyst" concentration.

of pentoxide added, for the range tested. For 1.0% pentoxide, the increase is of the order of 10 penetration units (at 77°F.) for a 220°F. softening point asphalt, representing a 130% increase over the penetration for a straight blown product of the same softening point.

Results of the ductility measurements on the pentoxide blown asphalts are shown in Fig. 9. There is a "critical range" at a softening point of approximately 130°F. during which the ductility changes very abruptly from over 80 to less than 10 cm. No clear trend is to be seen in the effect of phosphorus pentoxide on the ductility – softening point relationships.

Fig. 10 shows the effect of phosphorus pentoxide on the viscosity – softening point relationship of the blown asphalt. For a given softening point, the viscosity is increased with increased percentages of phosphorus pentoxide used. Some difficulty was encountered in the determination of viscosity at the higher temperatures (250°F. and above) but the trend shown is believed to be real.

Effect of the Pentoxide Residue

The high phosphorus content of the solid residue from the "catalyst" tests suggested the possibility of residue reuse. Accordingly, part of the residue from one test was added to fresh asphalt, using the mortar-and-pestle technique of dispersion. The amount added corresponded to an equivalent phosphorus pentoxide content of 0.19%. The results of this test have been plotted with the results of the other "catalyst" tests (using fresh phosphorus pentoxide). The phosphorus pentoxide in the residue is seen to have about the same effect as an equal amount of fresh phosphorus pentoxide. In all the plots, the curve for the "residue catalyst" test fell between the curve for 0% phosphorus pentoxide and the one for 0.25% pentoxide. This is true both in its effect on reaction time and in its effect on the penetration – softening point, the viscosity – softening point, and the ductility – softening point relationships.

Effect of Phosphorus Pentoxide on Asphaltenes, Resins, and Oily Constituents

Samples of straight blown and 1.0% pentoxide blown asphalts covering the softening point range from 107°F. to 210°F. were analyzed and separated into three major fractions—asphaltenes, resins, and oily constituents. Fig. 11 shows the change in the fractional composition of the asphalt base stock as it is air blown with and without the use of phosphorus pentoxide. The air blowing increases the asphaltenes from about 20 to 40% and at the same time reduces the resins from approximately 45 to 25%. Only a slight change in the proportion of oily constituents occurs. The fractional compositions of the straight blown and the pentoxide blown asphalts are found to be almost identical, at least within two per cent. This is consistent with Hoiberg's observations (6) but does not explain the difference in the physical properties of the straight blown and pentoxide blown asphalts.

The properties of the different fractions were examined and found to be consistent with those reported in the literature (12, 13, 15). The asphaltenes are dark brown to black powdery solids. Upon heating, they do not melt but

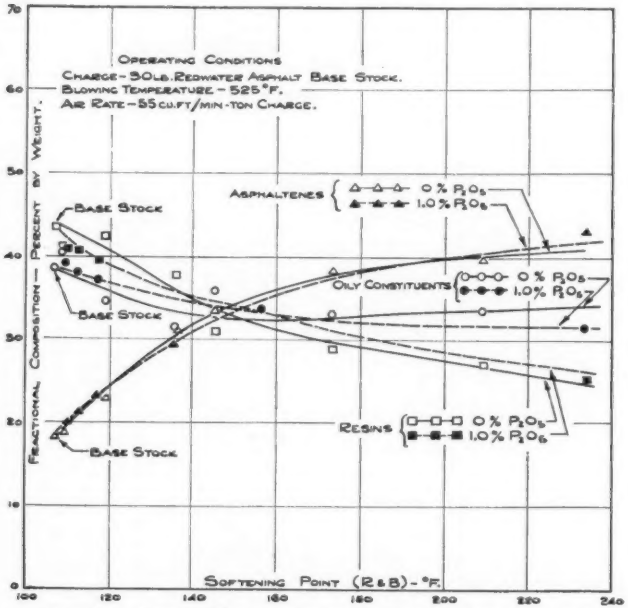
OPERATING CONDITIONS
CHARGE – 30 LB. REDWATER ASPHALT BASE STOCK.
BLOWING TEMPERATURE – 525 °F.
AIR RATE – 55 CU. FT/MIN.-TON CHARGE.
FRACTIONAL COMPOSITION — PERCENT BY WEIGHT.
ASPHALTENES 0 % P2O5
1.0 % P2O5
OILY CONSTITUENTS 0 % P2O5
1.0 % P2O5
RESINS 0 % P2O5
1.0 % P2O5
BASE STOCK
BASE STOCK
BASE STOCK
SOFTENING POINT (R & B) - °F.

FIG. 11. Composition – softening point relationships: effect of phosphorus pentoxide "catalyst" concentration.

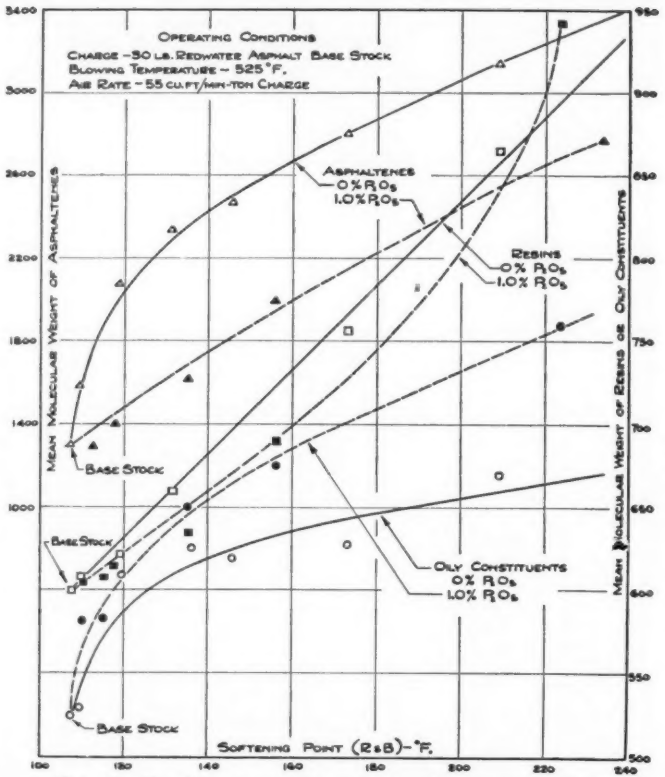
OPERATING CONDITIONS
CHARGE – 30 LB. REDWATER ASPHALT BASE STOCK
BLOWING TEMPERATURE – 525 °F.
AIR RATE – 55 CU. FT/MIN.-TON CHARGE
MEAN MOLECULAR WEIGHT OF ASPHALTENES
MEAN MOLECULAR WEIGHT OF RESINS OR OILY CONSTITUENTS
ASPHALTENES 0 % R2O5
1.0 % R2O5
RESINS 0 % R2O5
1.0 % R2O5
OILY CONSTITUENTS 0 % R2O5
1.0 % R2O5
BASE STOCK
BASE STOCK
BASE STOCK
SOFTENING POINT (R & B) - °F.

FIG. 12. Constituent molecular weight – softening point relationships: effect of phosphorus pentoxide "catalyst" concentration.

sinter and eventually decompose into a hard cake-like material. They are soluble in benzene, carbon tetrachloride, and carbon disulphide, but insoluble in alcohol, ether, acetone, and petroleum naphtha. The asphaltenes are the substances that impart "body" and "hardness" to the asphalt.

The resins are reddish brown, low melting point solids which are soluble in petroleum naphtha, benzene, carbon tetrachloride, and carbon disulphide, but are only sparingly soluble in acetone. The resins give the asphalt its ductility and tensile strength.

The oily constituents at room temperature exhibit the properties of a viscous liquid. They are light yellow in color and have the appearance of a heavy lubricating oil. Their primary function is to act as a dispersing medium for the asphaltenes and resins. As a general rule, the softer the asphalt, the higher will be its content of oily constituents.

In addition to these properties, the mean molecular weights of the three fractions were determined by a cryoscopic method (7). Fig. 12 shows that the mean molecular weights of all the fractions increase markedly with air blowing —that of the asphaltenes from about 1000 to 3000, that of the resins from approximately 600 to 900, and that of the oily constituents from 500 to 700. It is also seen that air blowing with pentoxide produces asphaltenes with a lower mean molecular weight, resins with about the same molecular weight, and oily constituents with a higher mean molecular weight than that of those fractions produced by air blowing without catalyst. Hoibergs' suggestion (6) that in the pentoxide tests, the increased penetrations are due to the formation of asphaltenes having higher molecular weight than those produced in the absence of catalyst is not borne out in this investigation.

Series 3—Various Dispersion Methods

Three methods of dispersing the phosphorus pentoxide into the asphalt—mortar-and-pestle, motor stirring, and preliminary immersion with carbon tetrachloride—were investigated. These methods were described earlier.

Effect of Dispersion Method on Reaction Time

The reaction time data are presented in Fig. 13. No significant difference in the reaction rate was observed between the mortar-and-pestle and the motor stirring methods of stirring. Dispersion by means of carbon tetrachloride produced an appreciable increase in the reaction rate which was even higher than that for straight air blowing. More than likely this was due to the chemical effects of the carbon tetrachloride itself rather than due to the degree of dispersion.

Effect of Dispersion Method on the Penetration –, Ductility –, Viscosity – Softening Point Relationships

The method of dispersing the phosphorus pentoxide in the asphalt was found to be comparable in importance to the amount of phosphorus pentoxide used. Fig. 14 shows the effect of the dispersion method on the penetration – softening point relationship. Clearly, the motor stirring and carbon tetrachloride methods of dispersion are not nearly as effective as the mortar-and-pestle method. The

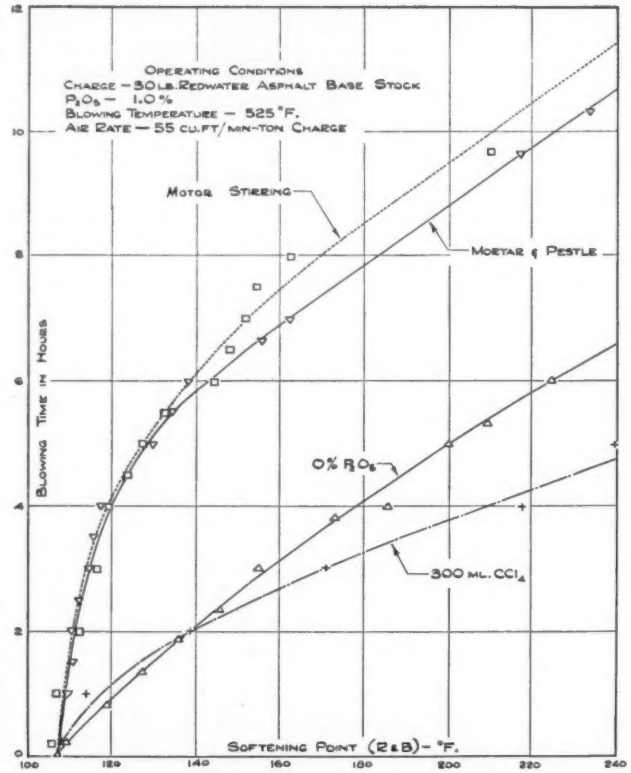

FIG. 13. Time – softening point relationships: effect of method of "catalyst" dispersion.

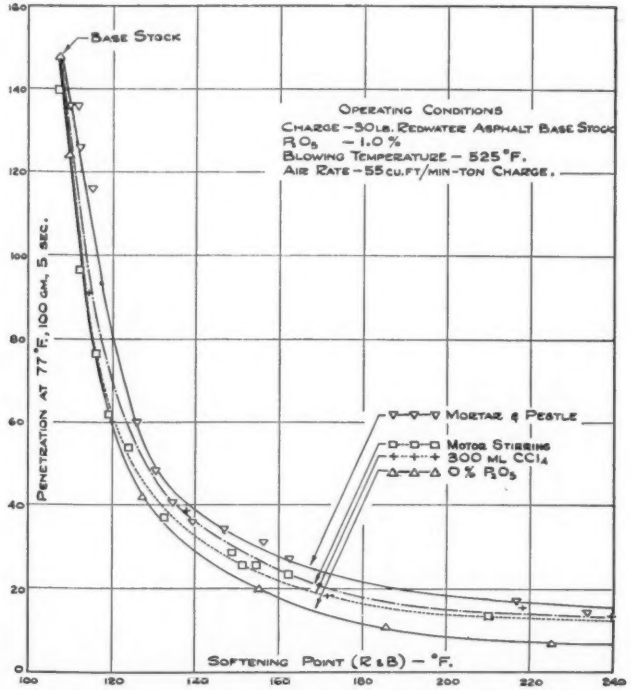

FIG. 14. Penetration – softening point relationships: effect of method of "catalyst" dispersion.

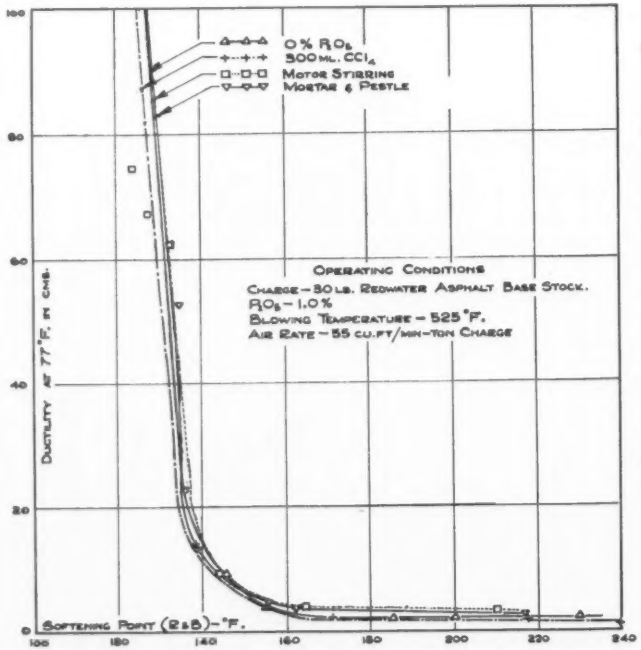

FIG. 15. Ductility – softening point relationships: effect of method of "catalyst" dispersion.

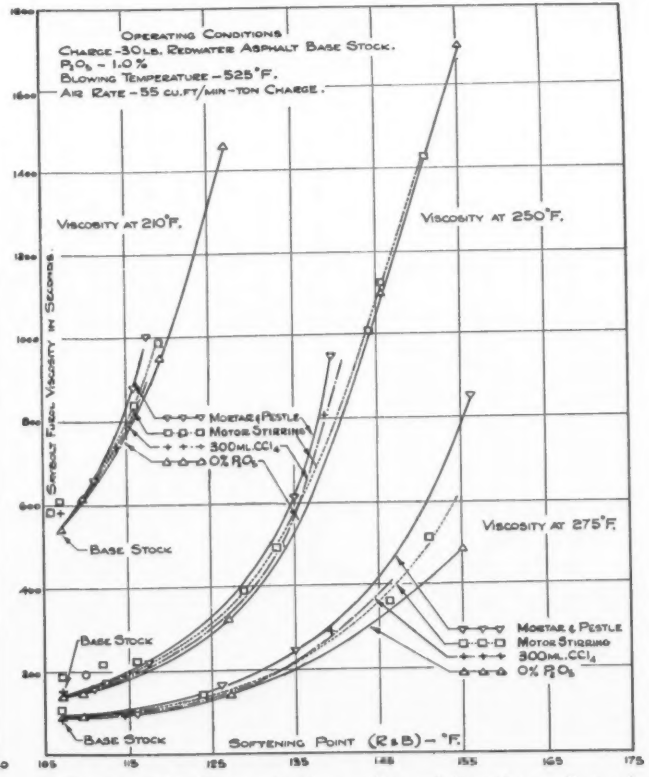

FIG. 16. Viscosity – softening point relationships: effect of method of "catalyst" dispersion.

same conclusion may be drawn from the ductility – softening point and viscosity – softening point curves shown in Figs. 15 and 16. In commercial operation, dispersion comparable to that by mortar-and-pestle could readily be obtained with a ball mill.

CONCLUSIONS

From this investigation of the air blowing of vacuum reduced Redwater asphalt base stock and of the use of phosphorus pentoxide the following conclusions may be drawn:

(1) The properties of the base stock are changed by air blowing. The product is harder (lower penetration), heavier, lower in ductility, higher in viscosity, and higher in softening point than before the blowing.

(2) The fractional composition of the asphalt is changed with air blowing—the asphaltenes increasing, the resins decreasing, and the oily constituents changing comparatively little.

(3) The mean molecular weights of the three fractions (asphaltenes, resins, and oily constituents) are increased markedly on air blowing.

(4) Increasing the blowing temperature or the air rate, or both, does not change the properties of the final asphalt with relation to a given softening point, but does significantly decrease the reaction time.

(5) With the addition of small amounts of phosphorus pentoxide, the reaction time, penetration, and Saybolt Furol viscosity of the blown asphalt are increased appreciably for a given softening point. With the same method of dispersing the phosphorus pentoxide, the increase is dependent on the quantity of phosphorus pentoxide, at least in the range 0–1%.

(6) The use of the residue formed from a previous phosphorus pentoxide test produces effects proportionate to the actual phosphorus pentoxide content.

(7) The method of dispersing the phosphorus pentoxide in the asphalt base stock is comparable in importance to the amount of phosphorus pentoxide used. The mortar-and-pestle method of dispersion was far more effective in changing the penetration – softening point, viscosity – softening point, and ductility – softening point relationships than dispersion by a laboratory stirrer or by preliminary immersion in carbon tetrachloride.

In evaluating the commercial practicabilities of the "catalytic" oxidation of Redwater asphalt base stock, the advantage of improved penetration properties must be weighed against the disadvantages of increased operating expenses due both to the "catalyst" costs and to the significant decrease in over-all reaction rates.

REFERENCES

1. Abson, G. To Chicago Paving Laboratory. U.S. Patent No. 1,782,186. 1930.
2. Byerley, F. X. U.S. Patent No. 524,130. 1894.
3. Culmer, G. F. and Culmer, G. C. K. U.S. Patent No. 635,430. 1899.
4. Gesner, A. A practical treatise on coal, petroleum, and other distilled oils. Baillière Brothers, New York. 1865. p. 128.
5. Hoiberg, A. J. To Lion Oil Co. Can. Patent No. 448,758 and U.S. Patent No. 2,450,756. 1948.
6. Hoiberg, A. J. Proc. Assoc. Asphalt Paving Technol. 19: 225. 1950.

7. HOIBERG, A. J., HOUGEN, O. A., and ZAPATA, J. The properties and compositions of asphalts of the slow curing type. Univ. of Wisconsin Eng. Expt. Sta. Bull. 86. p. 27. 1939.
8. JENNY, W. P. U.S. Patent No. 190,762. 1877.
9. KATZ, M. Can. J. Research, 10: 435–451. 1934.
10. MARCUSSON, J. Die naturlichen and kunstlichen Asphalte. Leipzig. 1931. p. 92.
11. MARCUSSON, J. and PICARD, M. Chem. Ztg. 48: 338. 1924.
12. MURPHY, B. A. J. Inst. Petroleum, 31: 475–485. 1945.
13. SACHANEN, A. N. Chemical constituents of petroleum. Reinhold Publishing Corporation, New York. 1945. p. 385.
14. STRIETER, O. G. J. Research Natl. Bur. Standards, 26: 415. 1941.
15. SWANSON, J. M. J. Phys. Chem. 46: 141–150. 1942.

PHYSICOCHEMICAL STUDIES ON ALBERTA COALS

II. ON THE PHYSICAL BEHAVIOR OF COAL IN ULTRASONIC FIELDS[1]

By N. Berkowitz[2]

ABSTRACT

'Spot' experiments, designed to test the response of coal to ultrasonic irradiation, have been carried out at 250 kc./sec. and 1 Mc./sec. The results indicate an essentially stable structure at these frequencies: while limited changes are induced in the X-ray pattern and colloid structure of the coal, its density appears to remain sensibly unaffected, and no 'cavitation' and macroscopic breakdown has been observed. Estimates of the energetics of irradiation suggest that *ca.* 99% of the theoretically available input energy is elastically reflected.

INTRODUCTION

Some years ago, in the course of a study of the action of some 50 organic solvents on a Pittsburgh Seam coal, Kiebler (10) observed that there existed a well-defined statistical correlation between the extract yield x and the internal pressure p_i of the solvents. The relationship assumed the linear form $x = a+bp_i$ (where a and b are temperature-dependent constants), and it was shown that the statistical correlation coefficient for this relationship, while ranging as high as 0.98 for small groups of chemically similar solvents, never fell below 0.73. Thus, for 44 solvents examined over the range 150°–300°C., the correlation coefficient varied between 0.73 and 0.75.

In view of Dryden's conclusion (7) that extract yields are largely determined by the presence of specific chemical configurations in the solvent molecule, an extension of Kiebler's observation (from the specific case of the Pittsburgh coal to coal in general) may well be hazardous. But it is worth noting that Kiebler's relationship is in broad conformity with the demands of Hirst's isogel model (9), and on this as well as other grounds, some basic correlation between extract yields and the energy content of a given coal–solvent system would not be unexpected. Indeed, the effects of pressure and temperature on extract yields (8) are such as to imply some such dependence.

If Kiebler's results are accepted as indicative of general behavior and expressed in the form $x = f(e)$, where e = total energy of the coal–solvent system, it becomes consequently a matter of some interest to replace elevated pressures and temperatures by other sources of energy and to examine, as one example, possible interactions between coal and solvents in ultrasonic fields. The application of such fields is, in fact, of particular interest in view of the powerful effects which they are known to exert upon certain depolymerization reactions and upon the dispersal of complex colloidal substances.

Some work along these lines is already in progress. Thus, Berkowitz (3) has reported substantial solubility of the pyridine-insoluble fraction of coal when this fraction is suspended in pyridine and exposed to frequencies of the order

[1]*Manuscript received April 12, 1955.*
Contribution No. 44 from the Research Council of Alberta, Edmonton, Alberta.
[2]*Senior Research Chemist, Research Council of Alberta.*

of 250 kc./sec.; and Sarjant *et al.* (11) have more recently applied ultrasonic fields to solvent extraction of coal in a study of the composition of such extracts. A similar study, and an examination of the kinetics of coal–solvent interactions in ultrasonic fields, is moreover currently under way in the laboratories of the Alberta Research Council. But as yet, no information about the physical behavior of coal *per se* in such fields has been made available. The only indication of change is provided by Vucht *et al.* (13) who have used cavitation effects (at *ca.* 20 kc./sec.) to produce ultrafine coal suitable for infrared spectroscopy.

The survey reported below—which was designed to explore the *type* and *magnitude* of changes induced by ultrasonic irradiation rather than to provide a reasonably complete picture of any *one* change under varying conditions—was undertaken in order to help fill this gap. Since preliminary experiments failed to show cavitation and size degradation at the frequencies attainable with the available generator, attention was confined (i) to the energetics of ultrasonic irradiation with a view to estimating the efficiency of the treatment and (ii) to changes induced in the ultrafine structure of the coal.

The ultrasonic generator employed for the experimental work was a Mullard Type E. 7562 instrument, using an oscillating quartz crystal mounted in a

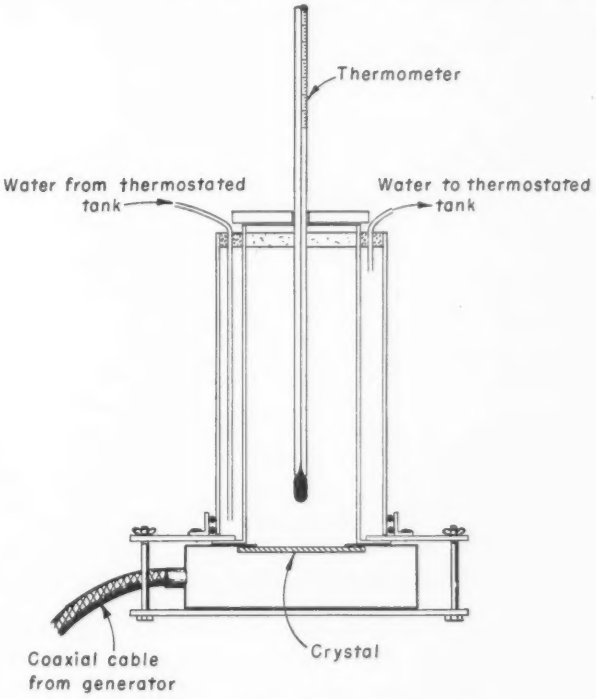

FIG. 1. Diagrammatic view of reaction chamber.

sealed transducer head. The radiating surface of the crystal was approximately 14.9 cm.[2] The reaction chamber was mounted above the transducer as shown in Fig. 1; and since direct transmission of ultrasonic waves from the crystal into the solid involves danger of crystal fracture, the coal was in each case irradiated in suspension in a 0.25% 'Aerosol O.T.' solution in water. The use of this neutral carrier liquid eliminated undesirable solvent effects.

A description of the various coals used for experimentation and some relevant analytical data are given in Table I.

TABLE I

COMPOSITION OF COALS

Coal No.	Description of coal	Volatile matter,* %	Carbon,* %	Hydrogen,* %
1	Lignite; Taylorton, Sask.	55.80	73.86	4.85
2	Subbituminous coal; Drumheller area, Alta.	40.20	75.71	5.12
3	Medium-volatile bituminous coal; Crows Nest Pass area, Alta.	28.60	87.26	4.87
4	Subbituminous coal; Edmonton area, Alta.	38.36	75.22	4.58

**Expressed on the "dry, ash-free" basis.*

ENERGETICS OF ULTRASONIC IRRADIATION

In general, the power emitted from a tuned oscillating crystal can be calculated with fair accuracy from the expression

$$e = v^2/r,$$

where e = power emitted, v = R.F. voltage output of the generator, and r = crystal resistance. (r varies directly with the acoustic impedance of the liquid into which the crystal radiates and inversely with the square of the frequency; for the instrument used in the present study, r = 50,000 ohms at 1 Mc./sec. when radiating into water.) As a precursor to an examination of possible structural changes accompanying ultrasonic irradiation of coal, there arises the question as to what proportion of the energy output of the crystal is available to the solid and actually utilized by it for change.

Possibly because of the theoretical complexity of the system used in these experiments (a solid suspended in a liquid), this problem does not appear to have been previously examined. But it is not an intrinsically very difficult one, and it can in principle be solved by an empirical calorimetric approach. Suppose the reaction chamber containing the suspension to be so mounted that the suspension is (as in the case under review here) in direct contact with the vibrating crystal, and that the chamber is suitably insulated. The energy

radiated into it from the crystal will then cause a temperature rise proportional to e, and if

ΔT = the temperature rise (°C./min.) in the carrier liquid *per se*,
$\Delta T'$ = the temperature rise (°C./min.) in the suspension,
a = temperature rise (°C./min.) equivalent to the energy 'absorbed' by the suspended solid,
j = temperature rise (°C./min.) equivalent to the energy scattered and dissipated by the solid,
c_s = specific heat of suspended solid,
w = weight of suspended solid,
V_L = volume of carrier liquid,
c = specific heat of the carrier liquid,
and d = density of the carrier liquid,
one may write:—

$$[1] \qquad \Delta T-\Delta T' = a+j+\frac{\Delta T\, c_s w}{V_L\, cd+c_s w}.$$

The term j in equation [1] allows for the attenuation of the ultrasonic shock waves by reflection from the solid particles; and the third term in the equation introduces a correction for the heat capacity of the suspended solid. It will be noted that this last term becomes a 'second order' term if w is small, and that equation [1] then reduces to

$$[2] \qquad \Delta T-\Delta T' = a+j.$$

It will also be observed that

$$[3] \qquad j = f(w,\ s),$$

where s = mean particle size of the suspended solid, and further, that

$$[4] \qquad a = f(1/E,\ 1/R),$$

where E = elastic modulus of the suspended solid and R = its rigidity modulus. The statement in [4] implies that if $R \rightarrow \infty$, *all* energy reaching the solid will be reflected; i.e. $a \rightarrow 0$ and $\Delta T-\Delta T' = j$. The same net effect will result when E is high, and it follows that in the case of coal, theory would require an inverse variation of a with coal 'rank', i.e. $a = f(1/\mathrm{C})$, where C = carbon content.

Strictly speaking, equation [1] or [2] needs to contain an additional term expressing the energy required to maintain the solid particles in suspension. But this term has been omitted because of the virtual impossibility of analyzing its components in a system in which a uniform wave front leaving the crystal is disturbed not by one, but by many particles. The same applies to the structure of j and only an empirical correction has therefore been attempted. This has been done by measuring $\Delta T-\Delta T'$ with a suspension of pure silica sand in Aerosol.* Since, for this substance, R is very high, a may be assumed to approach zero, and

$$\Delta T-\Delta T' = j+e_s,$$

**The size analysis of this sand approximated closely to that of the coal samples used in the measurement of* a.

where e_s is a measure of the energy required to maintain the particles in suspension. It turns out that $j+e_s$ lies within the limits of experimental error incurred in the measurements reported below and that one is justified, as a first approximation, in equating $\Delta T-\Delta T'$ with a only.

The foregoing treatment is in itself adequate for the evaluation of a. For comparative purposes, however, it is convenient to express a in more appropriately 'unitized' parameters, and these may be defined as follows:—

(i) The *specific energy absorption* is given by a/w;

(ii) The *volume fraction*, which expresses the concentration of suspended solid in terms of the total material contained in the reaction chamber, is written as

$$\bar{v} = 100\ \frac{w/D}{V_L+w/D} = 100w/(DV_L+w),$$

where D = density of the solid; and

(iii) *The utilization efficiency*, which gives the fraction of input energy e 'absorbed' by unit weight of suspended solid, is given by

$$q = 100(a/w)/\Delta T = 100a/(\Delta T\, w).$$

Measurements of a were made in the assembly shown in Fig. 1. Cooling of the reaction chamber, which became necessary when working at >250 kc./sec., was achieved by circulating water at 30°C. through the outer jacket. ΔT and $\Delta T'$ were in each case calculated from the usual time vs. temperature curves after these had been corrected for heat losses by the standard graphical methods. The results obtained with coals No. 1 and 2 (cf. Table I) at 250 kc. and 1 Mc./sec. are summarized in Table II; they represent an arithmetic mean value of between 6 and 10 measurements per coal.

In view of the experimental errors incurred in the measurement of ΔT and $\Delta T'$, values of q—particularly those calculated at the lower frequency—are probably correct only as to order of magnitude. But even at this lowest estimate of the significance of q, three features emerge quite clearly:

First, in general conformity with equation [4], a/w (and hence q) decreases with increasing carbon content.

Secondly, values of q appear to increase with e: thus, comparing the data for coal No. 2 at 250 kc. and 1 Mc., one finds q = 0.28 and 1.51% respectively. (Because of the greater uncertainty in the measurement at 250 kc./sec., the actual values of q can here—depending upon the value assigned to ΔT—vary between 0.15 and 0.40%; but this variation does not alter the broad picture.)

And thirdly, and this is the most significant point, energy changes involved in irradiation at either frequency are low and barely sufficient to disrupt surface forces. By far the greatest part of the input energy e is evidently merely reflected from the coal particles; and unless the major portion of the 'absorbed' energy a is regarded as concentrated at specific valency bonds (e.g. at weak valency bonds such as occur at certain intervals in butadiene structures), it is quite inadequate to break such bonds.

TABLE II

ENERGY ABSORPTION BY COAL SUSPENSIONS IN ULTRASONIC FIELDS

Coal	Ultrasonic field	D_{30}, gm./cc., uncorr.	$\bar{v}$, %	ΔT, °C./min.*	$\Delta T'$, °C./min.*	a/w, °C./min./gm.	q
No. 1 C = 73.86%	Frequency = 250 kc./sec. R.F. output = 5.0 kv. e = 34 w.	1.55	1.6	0.373±0.003	0.357±0.002	0.003	0.85% (≡2.1 × 10^8 ergs/min.)
No. 2 C = 75.71%		1.59	1.55	0.373±0.003	0.368±0.002	0.001	0.28% (≡7 × 10^7 ergs/min.)
No. 2 C = 75.71%	Frequency = 1 Mc./sec. R.F. output = 4.0 kv. e = 300 w.	1.59	3.1	3.91 ±0.05	3.32 ±0.02	0.059	1.51% (≡2.7 × 10^9 ergs/min.)
No. 3 C = 87.26%		1.30	3.8	3.91 ±0.05	3.61 ±0.03	0.030	0.75% (≡1.3 × 10^9 ergs/min.)

**Calculated from the temperature-rise produced by a 10-min. ultrasonic "burst".*

DENSITY MEASUREMENTS

The structural stability indicated by the energy measurements reported above is, to some extent, supported by the observation (made in this laboratory) that ultrasonic irradiation leaves the infrared spectra of coal quite unchanged. But it is also, and perhaps more directly, suggested by the results of density determinations made with irradiated coal. The experimental method selected for these determinations was the simplest consistent with the empirically imposed condition that the experimental error between duplicates should not exceed $\pm 0.5\%$. It employed coal samples ground to pass a 65-mesh Tyler screen and a 0.5% aqueous Aerosol solution (D_{30} = 1.0049 gm./cc.) as dilatometric fluid. The coal samples were in each case dried for two hours at 105°C., weighed into pycnometers, mixed with *ca.* 10 cc. Aerosol solution, and allowed to stand for one hour at 80°–85°C. After that time, the pycnometers were topped, transferred to a water bath maintained at 30.0±0.1°C., and allowed to equilibriate for a further hour. Approximately 2 gm. of coal were used for each determination.

The experimental results (uncorrected for mineral matter) are summarized below; where they refer to 'irradiated' coal, they refer to coal samples that were, prior to drying, suspended in 200 cc. 0.25% aqueous Aerosol and exposed to oscillations of a tuned 250 kc./sec. crystal at 5.0 kv. All measurements were made in quadruplicate.

Irradiation time	Density	Deviation
Series A: coal No. 4, D_{30} = 1.5944±0.0006 gm./cc.; deviation = ±0.038%		
2 × 5 min.	1.5973±0.0014 gm./cc.	±0.089%
4 × 5 min.	1.5920±0.0005 gm./cc.	±0.031%
6 × 5 min.	1.6012±0.0008 gm./cc.	±0.050%
Range of mean densities:	1.5920−1.6012 gm./cc.	
Average mean density:	1.5966±0.0046 gm./cc.	
Deviation:	±0.29%	
Series B: coal No. 2, D_{30} = 1.5104±0.0031 gm./cc.; deviation = ±0.21%		
2 × 5 min.	1.5075±0.0055 gm./cc.	±0.37%
3 × 10 min.	1.4945±0.0025 gm./cc.	±0.16%
Range of mean densities:	1.4945−1.5104 gm./cc.	
Average mean density:	1.5024±0.0079 gm./cc.	
Deviation:	±0.53%	

It is clear from these results that ultrasonic irradiation at the frequencies and intensities employed in the current experiments does *not* cause a significant shift in densities: while the experimental errors between repeat determinations on a single sample are invariably very much smaller than the set limits of $\pm 0.5\%$, it is important that the set limits do, in fact, encompass the entire range of mean densities. Although the steady trend towards lower densities in Series B may conceivably be indicative of a real change, the over-all effect must thus be considered negligible. (It is important to note here that Series A density values do *not* show the consistent trend of those of Series B.)

HEAT OF WETTING MEASUREMENTS

But if ultrasonic irradiation leaves the density of coal sensibly unchanged, it causes very considerable increases in the extent of *accessible surface area* (S). The magnitudes of these increases are shown in Table III, which summarizes experimental values of S recorded with coal No. 2 before and after irradiation at 250 kc. and 1 Mc./sec. The ultrasonic treatment involved, as before, irradiation of the coal in suspension in a 0.25% aqueous Aerosol solution; and S was in each instance determined (in duplicate) by means of the heat of wetting technique described in an earlier paper (4).

TABLE III

EFFECT OF ULTRASONIC IRRADIATION ON HEAT OF WETTING (COAL NO. 2)

Treatment	Heat of wetting, cal./gm. dry coal	ΔS, % on raw coal
None	6.75±0.10	—
3 × 10 min. at 250 kc., 5.0 kv.	7.63±0.06	13.0
3 × 5 min. at 1 Mc., 4.0 kv.	7.37±0.03	8.6
3 × 10 min. at 1 Mc., 4.0 kv.	8.75±0.10	29.6
Repeat measurement with fresh coal sample: 3 × 10 min. at 250 kc., 5.0 kv.	7.56±0.10	12.0

Two quantitative aspects of these results are of interest here: (i) the increment in surface area (ΔS) varies directly with the frequency (or the input energy e), and (ii) the structural change accompanying irradiation and causing an increase in S is not instantaneous but requires a fairly lengthy period of time for its completion.

That ΔS is connected with a *structural change* follows from the observation (cf. above) that ultrasonic fields under the conditions employed in these experiments do not induce cavitation. ΔS can, in other words, not be associated with size degradation and the production of *new* surface. But without reference to a particular structural model, such as the micellar model developed by Bangham *et al.* (2), it is difficult to speculate on the nature of the change causing an increase in S. All that can at this stage be asserted with confidence is that the change is physical rather than chemical, i.e. that ultrasonic treatment appears to open up part of a previously more or less inaccessible pore space. It is worth noting that this observation may in itself go some way towards explaining the greatly accelerated rate of solvent extraction of coal in ultrasonic fields.

CRYSTALLOGRAPHIC STUDIES

Significant changes (even though possibly quite unrelated to those mentioned above) appear also to be induced by ultrasonic treatment in the crystallographic structure of coal.

Riley *et al.* (5), among others, have suggested that coal resembles a turbostratic system of randomly disposed graphite crystallites and that the most prominent X-ray diffraction peak given by a powdered coal sample ($\theta = 8°–10°$) can be identified with the 002 reflection of graphite. On the basis of this identification, the average 'height' of the crystallites (i.e. their average *c*-dimension) can be calculated from the half peak width of the 002 reflection. Using Laue's formula:

$$c = k\lambda/(B \cos \theta),$$

where c = 'height' of crystallites, k = constant (taken as unity for the 002 reflection), λ = wave length of X-radiation, B = half peak width, and θ = Bragg angle, c has thus been shown to increase with the carbon content of coal (i.e. with coal rank) and to range from *ca.* 8 to 15 Å (5). The lattice parameter d (i.e. the average interplanar spacing) has also been found to depend upon rank (12) and to vary from *ca.* 3.35 Å (in Ceylon and Acheson graphite) to 3.95 Å in coal containing around 75% carbon.

Because of the limited information obtainable from X-ray diffraction diagrams of coal, and because of the virtually complete lack of unequivocal stereochemical data, a *definite* identification of the diffraction maxima with graphitic structures is fraught with some danger. For example, Nelson (12) has recently pointed out that the most intense X-ray diffraction maximum of polyethylene terephthalate (—O—$(CH_2)_2$—O—CO—C_6H_4—CO—) occurs at d = 3.4 Å (1), and the second strongest diffraction maximum of polyethylene (—CH_2—CH_2—) at 3.7 Å (6), i.e. within the range of d-values assigned to coals and graphite. Despite these difficulties, however, interpretations such as those of Riley *et al.* have become customary, and in the absence of further information, Riley's method has been used in the present investigations.

Only one departure was made from the 'standard' techniques: instead of exposing a film strip to the diffracted X-ray beam and then photometering the film, a 'Norelco' X-ray spectrometer, coupled to a strip chart recorder and capable of scanning over the range $\theta = 1°–90°$, was used. Owing to the 'noise' recorded on the chart, precise calculations are probably somewhat more difficult than from a photometer trace of a film, but it is doubtful whether the error thereby incurred exceeds 5%. Duplicate calculations made on separate scans suggest, in fact, that the error is very much smaller than this if operating conditions are kept constant. (In the current experiments, CuK_α radiation with λ = 1.5402 Å has been employed; the scanning speed was 1°/min.; and dial settings on the spectrometer were: scale factor = 2, multiplier = 1.0, time constant = 8.)

Table IV shows values of c calculated from scans on coal No. 2 before and after ultrasonic irradiation. The data suggest that such treatment can cause significant crystallite 'growth' along the *c*-dimension (i.e. that it can induce

more extensive 'stacking' of layer planes), and—in view of the relative magnitude of this effect at 250 kc. and 1 Mc./sec.—point to the possible existence of a resonance frequency at well below 250 kc./sec.

From a theoretical standpoint, considerable interest attaches to the fact that the values of c and d here recorded are, respectively, significantly lower and higher than reported for British coals of equivalent rank, and that crystallite growth along the c-dimension appears to take place without an observable concurrent reduction in d. This latter feature (which suggests that a closer approach to the interplanar spacing of graphite is opposed by short side chains attached at a finite angle to essentially planar molecules) is currently being investigated in greater detail.

TABLE IV

EFFECT OF ULTRASONIC IRRADIATION ON CRYSTALLITE 'HEIGHT'

Treatment	c, Å	θ_{002}	d, Å	$4\pi \sin\theta/\lambda$
None	6.41 6.49	10.2°	4.35	1.448
3 × 10 min. at 250 kc., 5.0 kv.	8.16			
3 × 10 min. at 1 Mc., 4.0 kv.	6.79			

ACKNOWLEDGMENTS

I am indebted to Mr. J. Fryer for the analyses shown in Table I and to Dr. P. J. S. Byrne for the X-ray scans.

REFERENCES

1. ASTBURY, W. T. and BROWN, C. J. Nature, 158: 871. 1946.
2. BANGHAM, D. H., FRANKLIN, R. E., HIRST, W., and MAGGS, F. A. P. Fuel, 28: 231. 1949.
3. BERKOWITZ, N. Nature, 163: 809. 1949.
4. BERKOWITZ, N. Can. J. Technol. 33: 169. 1955.
5. BLAYDEN, H. E., GIBSON, J., and RILEY, H. L. Proc. Conf. Ultrafine Structure Coals and Cokes. Brit. Coal Utilisation Research Assoc. London. p. 176 et seq. 1944.
6. BUNN, C. W. Trans. Faraday Soc. 35: 482. 1939.
7. DRYDEN, I. G. C. Fuel, 30: 145. 1951. Nature, 163: 141. 1949; 166: 561. 1950; 166: 606. 1950.
8. FISCHER, F. and GLUUD, W. Ber. 49: 1460. 1916.
9. HIRST, W. Proc. Conf. Ultrafine Structure Coals and Cokes. Brit. Coal Utilisation Research Assoc. London. p. 35. 1944.
10. KIEBLER, M. W. Ind. Eng. Chem. 32: 1389. 1940.
11. KIRKBY, W. A., LAKEY, J. A. R., and SARJANT, R. J. Fuel, 33: 480. 1954.
12. NELSON, J. B. Fuel, 33: 153. 1954.
13. VUCHT, H. A. VAN, RIETVELD, B. J., and KREVELEN, D. W. VAN. Fuel, 34: 50. 1955.

THE OXIDATION, DECOMPOSITION, IGNITION, AND DETONATION OF FUEL VAPORS AND GASES

XXVI. THE EFFECT OF FLOW CONFIGURATION ON THE OXIDATION AND IGNITION OF HYDROGEN IN MIXTURES WITH AIR SUPPLIED TO VERTICAL COMBUSTION TUBES OF VARIOUS MATERIALS[1]

By R. O. King,[2] S. Sandler,[3] and R. Strom[4]

ABSTRACT

Experiments to determine the effect of flow configuration on the oxidation and ignition of hydrogen in mixtures with air, described in this Part, are the second of a new series carried out with a method described in Part XXIII and used for experiments with acetaldehyde and pentane. Oxidation and ignition of hydrogen in mixtures with air occurred solely on the surface of the combustion tube. The wall temperature required for ignition, as measured on the outer surface, exceeded a minimum of 590°C. to an extent increasing with increases in hydrogen concentration, with increases in the catalytic activity of the tube surface, and with decreases in the rate of mixture supply if that rate were lower than the value required for turbulent flow. The effect of these factors depended to a remarkable degree on whether flow configuration was due to the convection circulations which existed at relatively low rates of mixture supply or to the turbulence accompanying greatly increased rates. When, for example, a mixture containing 50% of hydrogen was supplied to combustion tubes of silica and of stainless steel with an aged surface, at 200 cc./min. the surface temperatures required for ignition were 600° and 790°C. respectively. When, however, the rate of supply was increased to 1000 cc./min. and flow configuration became turbulent, ignition temperatures were in the same order but the total difference was 30°C. and diminished to approximately 15°C. only, as rate of mixture supply was further increased to 2500 cc./min. The increase in ignition temperatures, as measured on the outer surface of the combustion tubes, that always occurred after turbulence had been established and rate of mixture supply further increased was probably due to the increase in the rate of heat transfer required to maintain the inner surface at an igniting temperature. It was found by associated experiments that the premature ignition commonly obtained when hydrogen is used as the fuel for an Otto cycle engine is, in accordance with the experiments of this Part, due to an igniting temperature having been attained by the exhaust valve or the ceramic core of the spark plug. The engine experiments will be described in the next of the present series of papers.

INTRODUCTION

The combustion tube method used for experiments made to determine the effect of flow configuration on the oxidation and ignition of acetaldehyde and *n*-pentane in mixtures with air, described in Part XXIII (9), was again used for experiments with the hydrogen–air mixtures of this Part. It was shown by the experiments with acetaldehyde and pentane that ignition occurred at two temperature levels if the combustion tube was of silica but not if it was of steel.

When a chemically correct acetaldehyde–air mixture was supplied to the silica tube at 100 cc./min. the first igniting effect occurred when the maximum

[1]*Manuscript received April 27, 1955.*
Contribution from Defence Research Board, Ottawa, Canada, and the Department of Chemical Engineering, University of Toronto, Toronto, Ontario.
[2]*Scientific Officer-in-charge Combustion Research, Defence Research Board, Ottawa, and Special Lecturer, Department of Chemical Engineering, University of Toronto.*
[3]*Principal Scientific Research Officer, Defence Research Board.*
[4]*Senior Scientific Research Officer, Defence Research Board.*

temperature of the wall, as measured on the outer surface, was 260°C. The second ignition occurred at a maximum wall temperature of 679°C. When a "correct" *pentane–air mixture* was supplied at the same rate, the first and second igniting temperatures were 321° and 574°C. respectively.

The first igniting effect was in both cases preceded and followed by cool flames which caused pressure fluctuations as they traversed the mixture. They disappeared before the occurrence of the second igniting effect. The temperature of the first ignition varied little with change of mixture strength or as rate of mixture supply was increased.

The temperature of the second igniting effect diminished rapidly as mixture strength was increased from weak to correct or as rate of mixture supply was increased from 100 cc./min. It was found also that the second igniting effect was not a consequence of the first. That is, the effects were not related and the characteristics of the second indicated that it occurred on the wall of the tube.

The first igniting effect, when obtained with the usual methods of experiment, is generally attributed to a chain reaction and mistakenly as preliminary to the second. The experiments mentioned above indicated however that the first ignition occurred when material nuclei were present in the reacting mixture. Thus it was evident that formaldehyde was formed by the partial oxidation of *n*-pentane or acetaldehyde on the wall of the tube at the temperatures of the first igniting effects. The formaldehyde was necessarily carried into the mixture ascending the tube by circulating convection currents. It is assumed that condensation products and the sudden decomposition of organic peroxide, if then formed, would provide the nuclei required for ignition. This hypothesis was supported by the results of engine experiments on the compression ignition of mixtures with air of acetaldehyde and of *n*-paraffins (7, 5, 8, 6).

Hydrogen cannot provide material nuclei of ignition in the manner described. The characteristics of its combustion and ignition in vertical combustion tubes and in engines are therefore of exceptional interest. The former are described in this Part; the latter are to be described in the next of the series.

A hydrogen–air mixture is always turbulent after admission to an engine cylinder. Combustion tube experiments with flow configuration dependent on turbulence as well as on heat convection are therefore described in this Part.

I. THE FLOW CONFIGURATION DUE TO HEAT CONVECTION IN VERTICAL COMBUSTION TUBES WITH TEMPERATURE GRADIENTS

Experimental Arrangements

The diagram of Fig. 1 was drawn with the horizontal scale double that of the vertical. It shows a combustion tube supported concentrically in a tubular electric furnace, and the ends of the annulus between the heated wall of the furnace and the tube closed by transite washers. The heated length of the furnace was 6½ in. and the combustion tube projected three inches from its ends. The temperature gradients over the length within the furnace were determined by using a slidable wire ring of chromel and alumel with diametrically opposite junctions. A precision potentiometer was used to balance

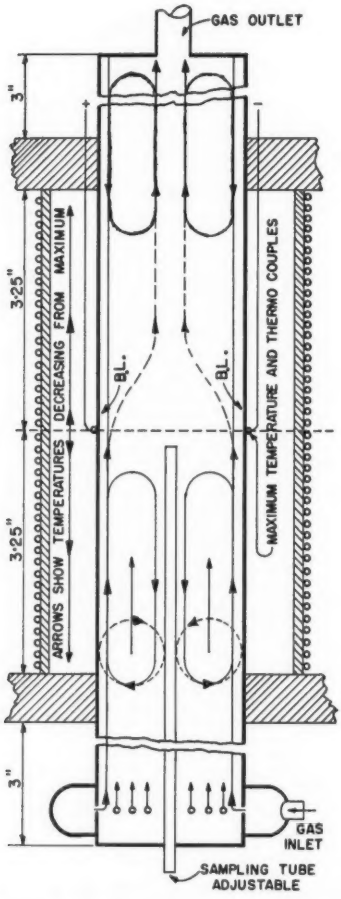

FIG. 1. Diagram showing the arrangement of a combustion tube concentrically in an electric furnace, the position of measurement of the apparent ignition temperature, the method of admitting gaseous mixtures, the convection circulations with non-turbulent gas flow, and the axis sampling device.

the thermoelectric potential against a standard cell. The equilibrium temperature gradients thus measured along a stainless steel tube, 28 mm. internal diameter and 1.58 mm. wall thickness, supported in a 2 in. diameter furnace are shown by the graphs of Fig. 2 for rates of heat input to the furnace varying from 135 to 344 watts; air or nitrogen was supplied at 200 cc./min. The graphs show that maximum wall temperature of the stainless steel tube was always attained at approximately the midsection of the tube length within the furnace. The position of maximum temperature was approximately half an inch above the midsection when the tube was of silica.

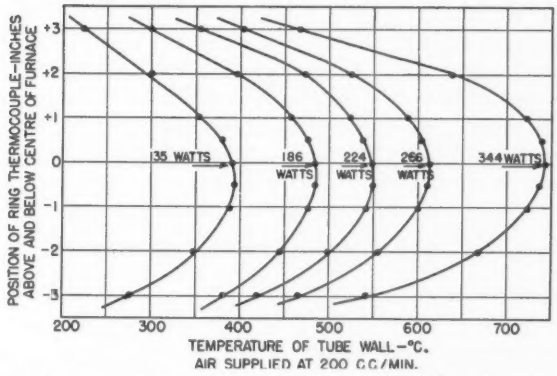

FIG. 2. Graphs showing surface temperature gradients from the midsection of the tube to the cool ends.

Hydrogen–air mixtures were admitted to the lower end of the combustion tube through a ring of holes in the periphery of a distributor type of inlet. When a mixture was supplied at rates commonly used for combustion experiments it tended to ascend along the heated wall of the tube and flow configuration depended on heat convection. The direction of flow through the distributor holes was however normal to the longitudinal axis of the tube and it was thus possible by increasing rate of mixture supply to create turbulence in the mixture passing through the tube while its space velocity was far less than would be required to exceed the critical Reynolds Number.

Flow Configuration Due to Heat Convection

An outline of the flow configuration in a transparent combustion tube when nitrogen was supplied through the distributor inlet at 100 cc./min. and the maximum wall temperature maintained at 500°C. was made visible by the method described in Part XXIII (9, p. 105). This outline, as shown by the solid flow lines of the diagram, Fig. 1, comprised a lower convection circulation extending over the rising temperature gradient below the midsection of the length of tube within the furnace and a shorter upper circulation over the falling temperature gradient above the midsection. The circulations are separated from actual contact with the tube wall by a boundary layer (B.L.) moving relatively slowly. The temperature of the mixture in the lower circulation is raised by heat from the wall, transmitted through the boundary layer. The mixture in the upper circulation, which passes over a falling temperature gradient, loses heat by transmission through the boundary layer to the wall before leaving the upper end of the tube. Thus its direction of motion was seen to be opposite to that of the lower circulation.

It was not possible to observe the pattern of flow within the convection circulations nor in the space between them. That within the lower circulation determines rate of heat transfer from the boundary layer to the mixture passing through the tube and the rate of reaction of the electrolytic gas in the

mixture as it ascends the tube. The ascending stream of this circulation receives initially all of the mixture supplied to the tube at rates which permit its existence. Its space velocity must therefore be higher than that of the descending stream in the constant pressure conditions of the experiments and also because temperature is raised continuously as it passes up the tube. It would be expected from considerations of gas dynamics that flow configuration within the circulation would comprise a procession of toroidal vortices moving upwardly with the mean space velocity of the mixture. A single vortex is shown in cross section by broken line circles, Fig. 1, and its upward movement indicated by arrows. The vortex is shown as penetrating the boundary layer. The thickness of the layer is shown to remain unchanged over the length of the combustion tube. The thickness would however diminish as penetration by the vortices increased. The degree of penetration would depend on the tendency of the diameter of the vortices to increase as the rotational velocity about their horizontal axis increased. This in turn would vary with the difference in temperature between the ascending and descending streams of the convection circulation.

II. TOROIDAL VORTICES AND RATES OF REACTION OF HYDROGEN–AIR MIXTURES ASCENDING A VERTICAL COMBUSTION TUBE OF STAINLESS STEEL

The procession of vortices ascending the rising temperature gradient of the lower convection circulation removes heated gas from the boundary layer and replaces it with cooler gas from the descending central stream. The rate of surface reaction as the hydrogen–air mixture passed up the tube could then be measured by the analysis of samples taken at points along the vertical axis. Experiments were carried out accordingly with the mixtures supplied to the stainless steel combustion tube at the relatively low rates required for the formation of convection circulations rather than general turbulence. The tube was 28 mm. internal diameter. The wall was 1/16 in. thick. The vertically adjustable sampling tube is shown by Fig. 1. It was of silica, 1/8 in. diameter and 1/16 in. bore. It is considered that samples remained unaltered while being drawn through the tube. Hydrogen was used in various concentrations in mixtures with air and corresponding concentrations of electrolytic gas, $2H_2+O_2$, are given by the graphs of Fig. 3. Electrolytic hydrogen, as supplied

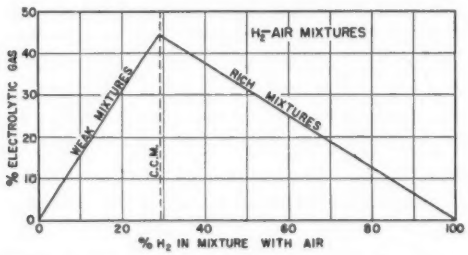

FIG. 3. Graph showing the relation between the concentration of hydrogen in a mixture with air and that of the electrolytic gas in the mixture.

by the Canadian Liquid Air Company, compressed to 2000 lb./sq. in. in steel cylinders, was used for the experiments. It was purified of oxygen before compression. It was then 99.95% hydrogen and nearly dry, the dew point being below minus 100°F. Experimental results are given by the graphs of Figs. 4, 5, and 6, and are described below in related paragraphs.

Fig. 4, Maximum Wall Temperature 550°C., Hydrogen Concentration 49%, Electrolytic Gas 32%, Mixture Supplied at 100 cc./min.

It is shown by Fig. 4 that reaction of the 32% of electrolytic gas in the mixture with air containing 49% of hydrogen began at approximately 3 in. below the midsection. That position is 0.25 in. within the furnace, and wall temperature would be 425°C. according to the relevant graph of Fig. 2. The

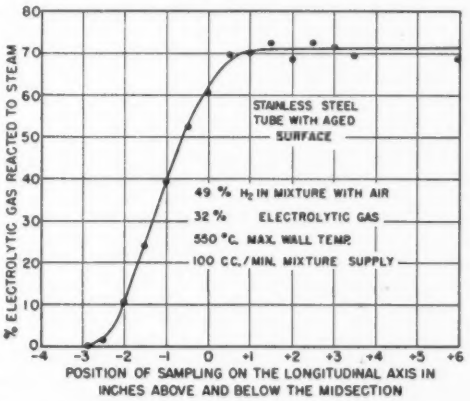

FIG. 4. Rate of reaction to steam on the surface of a stainless steel combustion tube. Maximum temperature 550°C., and 49% of hydrogen in mixture with air, supplied at 100 cc./min.

graph of the figure shows that rate of reaction increased slowly at first and then rapidly with the result that 60% of the concentration of electrolytic gas was reacted in the length of tube below midsection, over which wall temperature had increased from 425° to 550°C. Wall temperature then diminished and rate of reaction decreased to become zero at 1.5 in. above the midsection. Of the electrolytic gas in the mixture supplied to the tube, 71% had then been reacted to steam.

Fig. 5, Maximum Wall Temperature 755°C., Hydrogen Concentration 45%, Electrolytic Gas 34.6%, Mixture Supplied at 100 cc./min.

The temperature gradient below the midsection of the length of stainless steel combustion tube within the furnace was determined and is shown by graph B of the figure. Rates of surface reaction are given by graph A. It will be noted that the temperature of the tube wall was 605°C. at 3.0 in. below the midsection, that is 0.25 in. within the furnace, and that 30% of the electrolytic gas in the mixture had previously been reacted. The rate of reaction became so great that 80% of the electrolytic gas had been reacted at a position 2.6 in.

below the midsection. That is, a further 50% of the electrolytic gas was reacted while the boundary layer passed over 0.4 in. length of tube wall; the corresponding increase in wall temperature being from 615° to 715°C. over this length, see graph B. The increase in the reaction rate then diminished as the boundary layer passed over a length of 2.1 in. before reaction of the electrolytic gas was

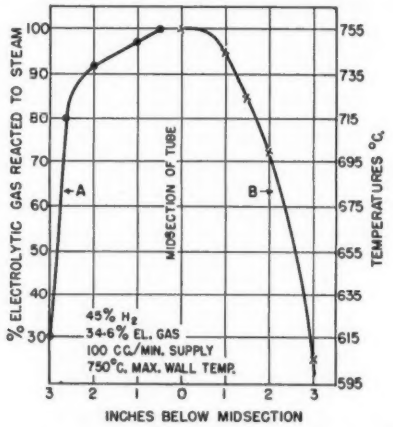

FIG. 5. Graph A. Rate of reaction to steam on the surface of a stainless steel combustion tube. Maximum temperature 750°C., 45% of hydrogen in mixture with air supplied at 100 cc./min.

Graph B. Temperature gradient on wall from midsection to 3 in. below that position.

100% complete at 0.5 in. below the midsection, which was at a temperature of 755°C. It will be seen by comparing graphs A and B that rate of reaction was generally similar to rate of increase of wall temperature.

Fig. 6, Maximum Wall Temperature 585°C., Differing Hydrogen Concentrations, Mixtures Supplied at 200 cc./min.

In addition to an experiment with a correct mixture, others were made with mixtures containing hydrogen in concentrations of 19 and 52%. These will be described as "weak" and "rich", and each contained 30% of electrolytic gas. Experimental results for rates of reaction are given by the graphs of Fig. 6.

The remarkable increase in rate of reaction that occurred on increasing the hydrogen concentration from 19 to 52% is shown by a comparison of Graphs A and B of the figure.

Reaction of the rich mixture began at 1.5 in. below the midsection of the tube and increased with such rapidity that 79% of the electrolytic gas had been reacted to steam at 2.0 in. above the midsection. There was no appreciable reaction between that position and the tube outlet. Reaction of the weak mixture began at a position one half inch closer to the midsection and 25% only of the electrolytic gas had been reacted at 2.0 in. above the position. There was no further reaction. The especially significant feature is that at the midsection of the tube where wall temperature had attained a maximum value

of 585°C., 42% of the electrolytic gas in the rich mixture had been reacted and 11% only of that in the weak mixture. As each contained 30% of electrolytic gas when supplied to the tube, this means that at the position of maximum wall temperature where ignition is generally assumed to occur, the rich mixture contained 17.4% and the weak mixture 26.7% of electrolytic gas. Inflammability and the surface temperature required for ignition would vary accordingly.

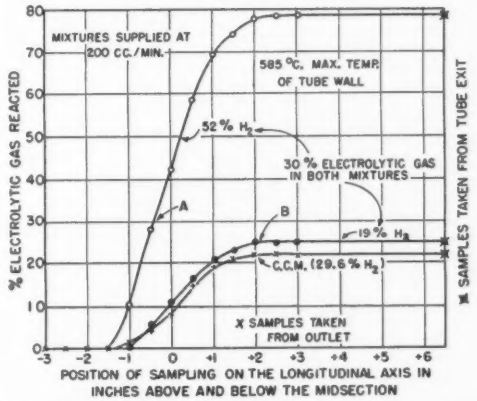
MIXTURES SUPPLIED AT 200 CC./MIN.
585 °C. MAX. TEMP. OF TUBE WALL
52 % H2
30 % ELECTROLYTIC GAS IN BOTH MIXTURES
A
B
19 % H2
C.C.M. (29.6 % H2)
X SAMPLES TAKEN FROM OUTLET
% ELECTROLYTIC GAS REACTED
% SAMPLES TAKEN FROM TUBE EXIT
POSITION OF SAMPLING ON THE LONGITUDINAL AXIS IN INCHES ABOVE AND BELOW THE MIDSECTION

FIG. 6. Rates of reaction to steam on the surface of a stainless steel combustion tube. Maximum temperature 585°C.; 52, 19, and 29.6% of hydrogen in mixtures with air supplied at 200 cc./min.

A comparison of results for a chemically correct mixture with those for the mixture containing hydrogen in the concentration of 19% is of interest. The former contains hydrogen in the concentration of 29.6% and electrolytic gas in the concentration of 45%; the latter contains 30% of electrolytic gas. It is shown, however, by the relevant graphs of Fig. 6 that the rate of reaction of electrolytic gas was approximately 3% the greater for the mixture containing the smaller concentration of hydrogen.

III. THE IGNITION OF HYDROGEN–AIR MIXTURES SUPPLIED AT 100 CC./MIN. TO COMBUSTION TUBES OF VARIOUS MATERIALS

The combustion tubes were of stainless steel, silica, sillimanite, and carbon. The steel tube was $1\frac{1}{8}$ in. internal diameter and the others approximately 1.0 in. The wall of the carbon tube was 1/4 in. thick, that of the others 1/16 in. The tubes were arranged in a vertical electric furnace as shown by Fig. 1, with thermocouples set at the midsection of the length within the furnace in order to measure the maximum temperature attained by the wall. The object of the experiments was to determine the temperature at that position when ignition occurred. Thus an approximate temperature having been obtained, the tube was allowed to cool until the temperature fell from 30° to 40°C. It was then reheated very slowly until ignition occurred again. Ignition temperatures thus

measured at the midsection of the tube must, according to the experiments of Section II, be higher than real values to an extent which varies with the degree of surface activity, with the concentration of hydrogen in excess of that required for a correct mixture, and with the time of contact of the mixture with the surface below the midsection, at a temperature such that reaction of electrolytic gas to steam can occur. The measured igniting temperatures will therefore be described as "*apparent ignition temperatures*" and the term abbreviated to A.I.T.

The Silica Tube

It is shown by Graph A, Fig. 7, that the A.I.T. was substantially constant with hydrogen concentration diminishing from 30 to 20%. Then as the concentration was further reduced to 8% and the concentration of excess oxygen increased accordingly, the increase in A.I.T. was 3°C. only. When however hydrogen concentration was *increased* from 30 to 80%, the A.I.T. rose slowly

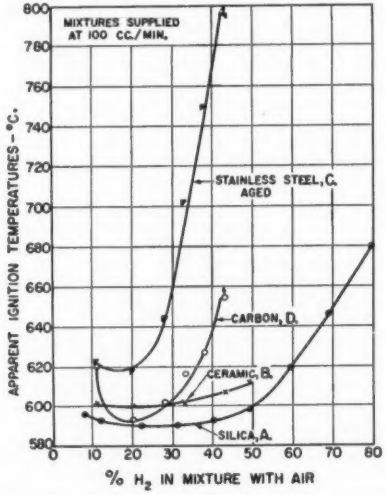

FIG. 7. Apparent ignition temperatures, combustion tubes of various materials, hydrogen concentration increasing from 10% in mixtures with air supplied at 100 cc./min.

at first and then rapidly to a value of 680°C. The concentration of electrolytic gas was approximately 12½% in mixtures containing either 8 or 80% of hydrogen, but the values for A.I.T. were 595° and 680°C. respectively. This result, obtained with a low rate of mixture supply and what is reputed to be a stable surface of minimum activity, illustrated the rise in A.I.T. due to the increase in rate of reaction below the midsection of the tube that is obtained as hydrogen concentration is increased.

The Sillimanite (Ceramic) Tube

The material was reputed to be a mixture of 62% alumina, 35% silica, and

3% oxides of other metals. The tube was used for the purpose of demonstrating the effect of spark plug cores of similar material in igniting hydrogen–air mixtures in an engine. Values for A.I.T. were determined accordingly for mixtures with air containing hydrogen in concentrations ranging from 10 to 50%. This is equivalent to mixtures ranging from 75% weak to 140% rich, as used in an engine. Graphs A and B show that values obtained for A.I.T. varied in the same manner for sillimanite and silica but that those for sillimanite were approximately 10°C. the higher.

The Stainless Steel Tube, Aged Surface

The tube had been used for experiments described in Section II. The surface had become oxidized and is therefore described as "aged". It will be seen by Graph C of Fig. 7 that a minimum of 620°C. was observed for the A.I.T. when the mixture with air contained hydrogen in the concentration of 20% and that a slight rise in A.I.T. occurred on reducing the concentration to 10%. However on increasing the hydrogen concentration, values for A.I.T. increased so rapidly that with 42% of hydrogen in the mixture, ignition was not obtained until the midsection was heated to 828°C.; not shown, Fig. 7. This ignition must therefore have occurred in the tube below the midsection of maximum temperature. This result is as would be expected from the experimental results shown by Fig. 5. These were obtained with the same combustion tube and the same rate of mixture supply, and all of the electrolytic gas in a mixture containing 45% of hydrogen was reacted to steam below a midsection temperature of 755°C.

The Carbon Tube

It will be seen by reference to Graph D of Fig. 7 that a minimum value of 592°C. was obtained for the midsection temperature required for the ignition of a hydrogen–air mixture in the carbon tube. The mixture then contained hydrogen in the concentration of 20% and the ignition temperature was approximately that obtained with the silica tube and the same concentration of hydrogen. Carbon tube ignition temperatures unlike those obtained for the silica tube rose rapidly as the concentration of hydrogen was either increased or diminished and ignition temperatures of 620° and 627°C. were obtained with hydrogen concentration of 10 and 38% respectively. On increasing the hydrogen concentration to 42% a temperature higher than 654°C. was required for ignition. The carbon surface was then glowing brightly and values for ignition temperatures were not obtainable.

It was found however that the carbon and graphite tubes used for the experiments were in some degree transparent to hydrogen. It is probable therefore that the rise in A.I.T. that occurred on increasing hydrogen concentration was affected accordingly.

The experimental results are however of significance, because it was shown by those given in Part XXIII (9, p. 108) that mixtures of air with pentane or acetaldehyde were not ignited in the carbon tube or in a graphite tube although the midsection temperature was raised to 760°C.

IV. IGNITION TEMPERATURES AS AFFECTED BY SURFACE STATE AND COMBUSTION TUBE MATERIAL, FLOW CONFIGURATION BEING DEPENDENT ON HEAT CONVECTION

Difficulties have been encountered in the obtaining of repeatable values for A.I.T. of hydrogen–air mixtures, especially when the steel combustion tubes are used, and rates of supply are such that flow configuration is governed by heat convection. The difficulties are due to changes in surface state that occur in the course of a series of experiments for which hydrogen concentration is varied. The extent to which observed values are not repeatable increases as hydrogen concentration increases.

Numerous methods of surface treatment were tried in attempts to obtain repeatable values for A.I.T. The methods, in addition to those commonly applied to vitreous surfaces, included the reduction of surface oxide by long exposure to hydrogen while the midsection of the tube was maintained at 680°C. as well as the formation of surface oxide by a similar treatment with oxygen. Nearly repeatable, but relatively low values for A.I.T. were obtained if, before beginning experiments with a stainless steel tube, the surface were cleaned by the usual method of pickling with a hot 10% solution of hydrochloric acid in water. Nearly repeatable but relatively high values for A.I.T. were obtained if the stainless steel surface were aged by continuous use after a coating of oxide had been formed. The "activity" of the surface thus formed was responsible for the relatively high values for A.I.T. obtained when hydrogen was in excess of the concentration required for a correct mixture with air. The activity of the surface diminished during a period of disuse and a period of reuse was required to regain repeatable values for A.I.T.

Values for A.I.T., Aged and Clean Stainless Steel Tubes

Mixtures containing hydrogen in concentrations rising from 10% were supplied to the tubes at rates of 200 cc./min. Experimental results are given by Fig. 8.

Graph A of the figure shows the values obtained for A.I.T. when the mixtures were supplied to the aged stainless steel tube. This tube had been used for the experiments described in Sections II and III.

Graph B shows the results obtained when a similar stainless steel tube was used after the surface had been cleaned by the pickling method. The experimental results for the similar tubes with different varieties of surfaces show differences in values of A.I.T. increasing to a remarkable extent as hydrogen concentration in the mixture supply was increased. Thus when a correct mixture was supplied, the values for A.I.T. were 640° and 610°C. for the aged and clean tubes respectively. When the hydrogen concentration was 40% the respective values for A.I.T. were 745° and 615°C. and 790° and 635°C. when hydrogen concentration was 50%. Values for A.I.T. were not obtainable below 800°C. when the mixture supplied to the aged tube contained hydrogen in greater concentration than 52% but were obtained for concentrations increasing to 80% in mixtures supplied to the clean tube.

Values for A.I.T. lying between those shown by the graphs of Fig. 8 were

obtained after various other methods of treatment had been used but were not repeatable. Pretreatment of the aged surface with hydrogen led to higher values being obtained for A.I.T. when oxygen was in excess in the mixtures supplied, but the values were not repeatable.

Graph A of Fig. 8 may be taken to represent the upper limit of repeatable values for A.I.T. and Graph B, the lower.

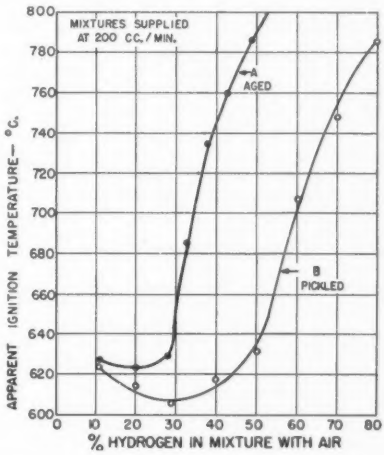

FIG. 8. Apparent ignition temperature as affected by the surface state of a stainless steel combustion tube. Hydrogen concentration increasing from 10% in mixtures with air, supplied at 200 cc./min.

Values for A.I.T. Mild and Stainless Steel and Silica Tubes

The mild steel tube was cleaned by pickling before being used. The silica surface was not treated in any way. The hydrogen–air mixtures were supplied at 200 cc./min. and an additional experiment with the silica tube was carried out with mixtures supplied at 100 cc./min. The experimental results are shown by Graphs A, C, and D of Fig. 9. Graph B for the clean stainless steel tube is reproduced from Fig. 8.

The surface of the mild steel tube oxidized rapidly and tended to pit and scale. It will be seen, Graph A, that a minimum of 650°C. was obtained for the A.I.T. with a hydrogen concentration of 20%. The values then increased so rapidly as the concentration of hydrogen was increased or diminished that A.I.T. values less than 800°C. were not obtained with a hydrogen concentration greater than 33%, or less than 700°C. when the concentration was less than 10%. Graph C, obtained for the silica tube with mixtures supplied at 100 cc./min., follows the pattern of Graph B for the stainless steel tube and the A.I.T. for a correct mixture was lower by 10° only. Moreover the values for A.I.T. varied little for hydrogen concentrations ranging from 10 to 40%. An especially significant result is the relatively rapid rise in A.I.T. obtained as

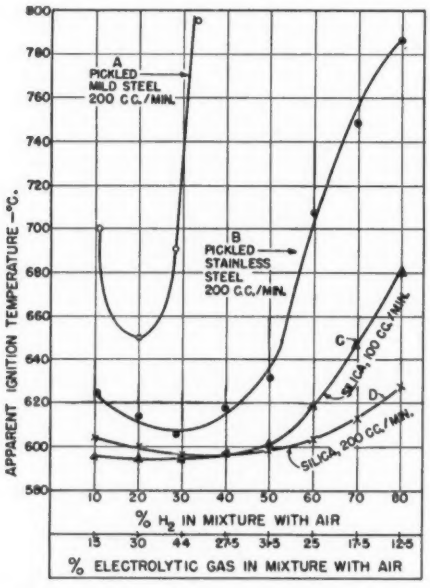

FIG. 9. Apparent ignition temperatures, hydrogen increasing in concentrations from 10% in mixtures with air supplied to combustion tubes of mild steel, stainless steel, and silica at 200 cc./min. and to the silica tube at 100 cc./min.

hydrogen concentration was increased from 40 to 80% in the mixture supplied at 100 cc./min. as compared with that obtained over the same range of hydrogen concentration when the mixtures were supplied at 200 cc./min. as shown by Graph D.

V. APPARENT IGNITION TEMPERATURES AS AFFECTED BY REPLACING CONVECTION CURRENTS WITH TURBULENCE

The design of the distributor inlet used for admitting hydrogen–air mixtures to the lower ends of vertical combustion tubes was described in Section I and illustrated by Fig. 1. It is such that turbulence tends to be created in the mixture as admitted, on increasing the rate of supply. A "stilling" length of tube was not provided and initial turbulence would persist as the gaseous mixture passed upwardly through combustion tubes of the length and diameter used for the experiments of this Part. Thus, turbulence, after being initiated by increasing rate of mixture supply to the requisite value, would increase as rate continued to be increased although the Reynolds Number, even at the highest rate used for experiments, was far below the critical value. The effect on flow configuration would be that circulating convection currents would tend to be replaced by turbulence when rate of mixture supply exceeded a value which can be determined by experiment only. Experiments carried out accordingly are described in this Section.

Stainless Steel Tube with Clean Surface

The changes in the relation between A.I.T. and hydrogen concentration that occurred as the mixture supply was increased from 60 to 2000 cc./min. are shown by the family of graphs, Fig. 10. It will be seen that they fall into two groups of plainly different characteristics.

The first group comprises the graphs for values of A.I.T. obtained when mixtures were supplied at 60 to 400 cc./min. Definite minimum values for A.I.T. differing little from 608°C. were then obtained when the mixture was approximately correct. Values of A.I.T. increased rapidly with increasing concentrations of hydrogen. The rate of increase diminished as rate of supply was increased to 400 cc./min. Thus for example when the concentration of hydrogen in the mixture was 50%, the A.I.T. was 755°C. with a rate of supply of 60 cc./min. and 630°C. with a rate of 400 cc./min. It is indicated by the experimental results and those described earlier in this Part that circulating convection currents persisted in the mixture passing through the tube until rate of supply was increased to at least 400 cc./min.

The second group comprises the graphs for values of A.I.T. observed when mixtures were supplied at rates of from 700 to 2000 cc./min. It will be seen that the increase in rate of supply of from 400 to 700 cc./min. was accompanied by an increase in the minimum value of A.I.T. from 608° to 622°C. Moreover, the higher value instead of increasing with an increase in hydrogen concentration, remained substantially constant over the hydrogen concentration range of 30 to 50%. The minimum value for A.I.T. continued to increase with increases in the rate of mixture supply and as this occurred it extended over an increasing range of hydrogen concentration. Finally when rate of supply had been increased to 2000 cc./min., a minimum value for A.I.T. of 650±2°C. was obtained for hydrogen concentrations ranging from 30 to 80%.

As the concentration of hydrogen was decreased from 30 to 10%, values of A.I.T. increased at nearly similar rates as the rate of mixture supply was increased from 700 to 2000 cc./min. The total increase was 15°C. with mixtures supplied at 700 or 1000 cc./min. and 20°C. at a rate of 1500 or 2000 cc./min.

The radical change in ignition characteristics that occurred on increasing rate of mixture supply from 400 to 700 cc./min. is attributed to circulating convection currents having been displaced by turbulence.

Experiments with Correct Hydrogen–Air Mixtures Supplied at 50 to 2500 cc./Min. to Silica and Clean Stainless Steel Tubes

The values obtained for apparent ignition temperatures as rate of supply of a correct mixture was increased from 50 to 2500 cc./min. are given by the graphs of Fig. 11. It is shown by Graph B of the figure that when the combustion tube was of clean stainless steel, the relation between A.I.T. and rate of mixture supply follows closely that obtained in the earlier experiments with a similar tube as shown by the graphs of Fig. 10.

Experiments were not carried out earlier with a silica tube and rates of mixture supply greater than 200 cc./min. The A.I.T. at this rate as shown by

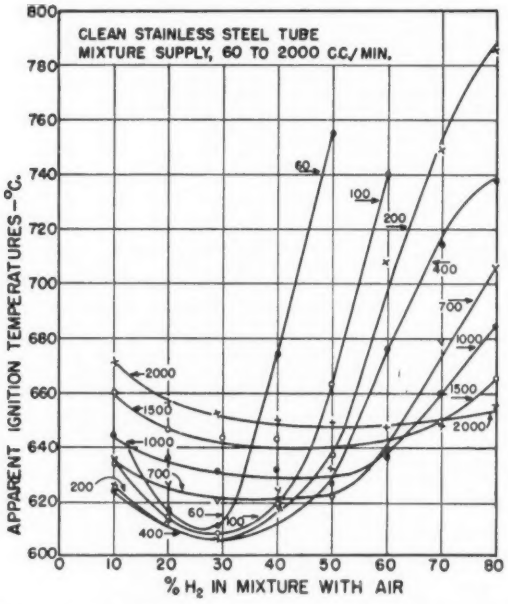

FIG. 10. The change in the characteristics of apparent ignition temperature obtained when, by increasing rate of mixture supply, the flow configuration due to heat convection is replaced by turbulence. Hydrogen concentrations ranging from 10 to 80% in mixtures with air supplied to a stainless steel combustion tube at 50 to 2000 cc./min.

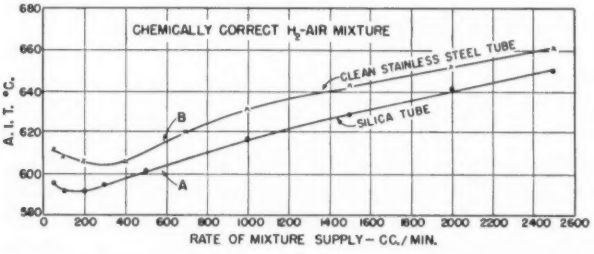

FIG. 11. The effects on apparent ignition temperatures obtained on replacing flow configuration due to heat convection by that due to turbulence, correct hydrogen–air mixtures supplied to silica and stainless steel combustion tubes at 50 to 2500 cc./min.

Graph A of Fig. 11 was 590°C. It was 604°C. with the clean stainless steel tube, Graph B of the figure. The respective values obtained earlier, as shown by Fig. 9, were 596° and 607°C. The consistency is as good as would be expected in view of small changes in surface state which cannot be avoided. The significant feature of the experiments is that when a *correct* mixture was supplied to the combustion tubes, the difference between values obtained for A.I.T. varied little as circulating convection currents were replaced by turbulence.

Experiments with Mixtures Containing 50% of Hydrogen Supplied at 50 to 2500 cc./Min. to Silica and to Stainless Steel Tubes, Clean, and Aged

It was shown by the experimental results, Fig. 10, obtained when a clean stainless steel tube was used, that circulating convection currents tended to be replaced by turbulence as the rate of mixture supply exceeded 400 cc./min. and that the transition had been completed when the rate was 700 cc./min. These results, obtained with one variety of surface, do not illustrate the corresponding effect on rate of reaction, and the consequent value of A.I.T., of other more or less active surfaces when hydrogen concentration is greater than required for a correct mixture. Surfaces in order of increasing activity are provided by combustion tubes of silica, stainless steel with a clean and with an aged surface. Values obtained for A.I.T. when using these tubes and a mixture with air containing 50% of hydrogen are given by the graphs of Fig. 12. They show that when flow configuration was due to heat convection, the

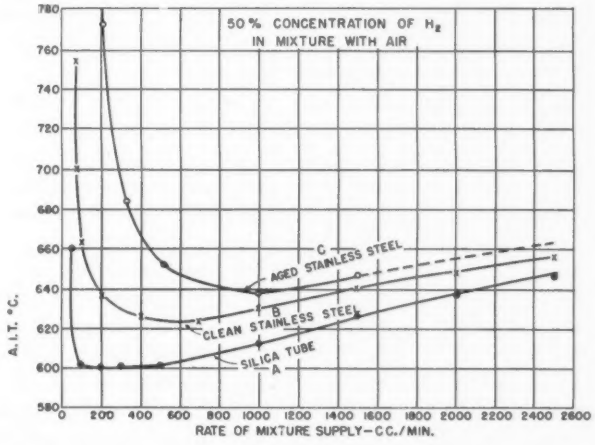

FIG. 12. The effects on apparent ignition temperature obtained on replacing flow configuration due to heat convection by that due to turbulence. 50% of hydrogen in mixtures with air supplied at 50 to 2500 cc./min. to a silica tube and to a stainless steel tube with a clean and with an aged surface.

values of A.I.T. and the extreme difference between them, which was dependent on the degree of surface activity, decreased rapidly as mixture supply was increased and time of residence diminished, and that after turbulence had been established, the values *increased* slowly and differences due to the degree of surface activity tended to disappear. Thus values of A.I.T. began to rise at rates of mixture supply of 400, 600, and 1000 cc./min. when the tubes used were of silica, and of stainless steel with a clean and with an aged surface, respectively. The over-all difference in the values of A.I.T. of nearly 180°C., which was obtained with a mixture supply of 200 cc./min., diminished to 37°C. on increasing the rate to 700 cc./min. and to 18°C. as it was further increased to 2500 cc./min. Thus surface activity, which was a predominant factor in

respect of the values obtained for A.I.T. when mixtures containing excess hydrogen were supplied at relatively low rates, became of very secondary importance when convection circulations were replaced by turbulence.

Apparent Ignition Temperatures were, as explained earlier, measured by thermocouples on the outer surface of a combustion tube at the position of maximum temperature. The effective temperature is that on the inner surface at the same position. This temperature has been found to be the lower by 10° or 12°C., at small rates of mixture supply. The difference would be expected to increase as rate of supply of turbulent mixture increased. This effect and the drop in temperature of the gas passing through a combustion tube when the area of heated surface remains nearly constant while the velocity of the gas flow increases may account for the rise in values of A.I.T. that occurred after turbulence became established.

VI. PEROXIDES

Numerous attempts were made to detect hydrogen peroxide by titration of an aliquot of the liquid reaction product as trapped in condensers cooled with a dry ice – acetone mixture. Peroxide was not detected in the product from either the silica or the steel combustion tube when a 0.02 *N* potassium permanganate solution in water was used for the titration. It may be concluded that peroxide was not formed when reaction occurred in the flow configuration conditions of the experiments or, if formed, decomposition must have occurred before the mixture left the combustion tube.

DISCUSSION

Many attempts have been made to show that mixtures of hydrogen with air or oxygen can be ignited apart from surfaces, by the application of heat. A comprehensive description of the methods tried and the results obtained is given by Jost (4, pp. 3–46). It appears accordingly that flow configuration has not been regarded as a determining factor in respect of the temperatures required for ignition. Dixon (2), for example, when using his concentric tube method, sought to avoid the wall effect by increasing the diameter of the outer tube which was heated electrically. He does not seem to have realized that by injecting the hydrogen through a small orifice in the end of the inner tube which projected halfway up the length of the outer one, a contra flow was set up which would bring reacting mixture into contact with its surface. It appears therefore that ignition occurred when the surface of the inner tube attained the necessary temperature and that the observed delay periods represented merely the times required.

Alyea and Haber (1) used the crossed streams method of determining the ignition temperature of mixtures of hydrogen and oxygen. The tubes carrying the heated gases to orifices in their ends were apparently far enough apart to prevent recirculation around them of a mixture of the gases. In these conditions no ignition occurred at reduced pressures of from 10 to 200 mm. Hg at temperatures up to 540°C. if pressure were gradually reduced so that what is generally regarded as the normal explosion region was entered. When however a surface

of quartz, porcelain, or glass was placed at the junction of the crossing streams, an ignition always occurred when the explosion region was approached or entered.

Goldmann (3) using normal pressure and higher temperatures found that ignition occurred when one or other of the streams of hydrogen and oxygen was heated to 560°C. or higher. It was concluded that formation of active atoms or radicals producing a chain reaction leading to ignition was possible in the gas phase at temperatures above 560°C. but that at lower temperatures and pressures a surface was necessary for their production. The streams of gases issued from orifice tubes only a few millimeters apart and, in the light of the flow configuration experiments described in this Part, it is probable that a mixture of the reacting gases circulated about the tube carrying the heated gas. Thus it is possible that ignition as observed by Goldmann was a surface effect instead of one occurring in the gas phase.

Flow Configuration Due to Heat Convection in a Vertical Combustion Tube

The mixture supplied to the lower end of the tube forms a convection circulation over the lower temperature gradient and is separated from the wall by the boundary layer. When however reaction occurs on the surface the reacted mixture containing steam diffuses through the boundary layer to join the ascending stream of the convection circulation and is replaced by less reacted mixture diffusing through the boundary layer in the opposite direction. The normally laminar flow in the boundary layer is disturbed accordingly. The rate of surface reaction at a particular position on the tube surface will be governed in the circumstances by its temperature, the nature of the surface, and the rates of diffusion which would in turn depend on the thickness of the boundary layer, its density, and the density of the mixtures diffusing through it. The densities would diminish on increasing the concentration of hydrogen in the mixture with air. The concentration of steam in the mixture at the position of maximum temperature would then depend on the factors mentioned and rate of supply of unreacted mixture to the tube.

If the oppositely moving streams of the lower circulation form toroidal vortices instead of remaining intact, all of the effects mentioned would increase in magnitude; rates of diffusion especially would increase because of the tendency of the vortices to expand and thereby reduce the thickness of the boundary layer. Its thickness has been shown by Fig. 1 as uniform but in reality it would increase or diminish as the vortices contracted or expanded according to temperature difference between the oppositely moving streams of the convection circulation.

The consequent effect of the factors described above on rates of reaction is shown by experiments described in Section II. For example, when a mixture containing hydrogen in a concentration of 45% was supplied to a stainless steel tube with an aged surface at 100 cc./min. while the midsection was maintained at 775°C., all of the electrolytic gas in it was reacted to steam in the length of tube below the midsection. The effect of excess hydrogen is again illustrated by a comparison of the rates of reaction obtained when mixtures

containing 19 and 52% of hydrogen were supplied to the tube at 200 cc./min. while the midsection temperature was maintained at 585°C. Both mixtures contained 30% of electrolytic gas but, as shown by the graphs of Fig. 6, 11% was reacted when the mixture contained excess oxygen and 42% when the mixture contained excess hydrogen. Conditions were similar in both cases except that, as supplied to the tube, the density of the mixture containing excess oxygen was 60% the greater. Secondary effects which are difficult to evaluate were the more rapid formation of steam in the mixture containing excess hydrogen and the smaller effect of the vortices in the less dense mixture to penetrate the boundary layer.

The relative rates of reaction in further experiments were taken to be indicated by the corresponding values of the A.I.T. It is of interest accordingly that when correct mixtures were used, the A.I.T. observed with a clean stainless steel tube to which the mixture was supplied at 200 cc./min. was approximately 10°C. only higher than when a similar mixture was supplied to a silica tube at either 100 or 200 cc./min., Fig. 9. The A.I.T. observed when the silica tube was used, if it had been measured on the inner wall, would differ little from the value of 585°C. assumed by Dixon to have been obtained apart from a surface (2). The rise in the values of A.I.T. as the concentration of hydrogen in mixtures supplied to the silica tube was increased is attributed to the decreasing density of the boundary layer and it will be noted that the rate of rise of A.I.T. increased on reducing the rate of mixture supply from 200 to 100 cc./min. as might be expected accordingly.

Turbulence in the Combustion Tube and in the Combustion Chamber of an Engine

The establishment of turbulence in the combustion tube was accompanied by a decrease in the thickness of the boundary layer and in the time of residence of the hydrogen–air mixture in the tube. There was therefore an increase in the rate of abstraction of heat from the inner surface of the tube and it became necessary to compensate for this effect by raising the temperature on the outer surface. Then because of the decrease in time of residence there was a diminution in the surface reaction of electrolytic gas to steam in the length of tube below the midsection; the variation in the amount of reaction due to differences in the nature of the tube surface also diminished. There was in consequence an increase in temperature required for ignition, as measured on the outer wall at the midsection, and a decrease in the effect of changes in the nature of the surface, on that temperature. There was then a corresponding decrease in the rise of the apparent ignition temperature that was observed in earlier experiments carried out at relatively low rates of supply of mixtures containing hydrogen in excess of the concentration required for a correct mixture. The combined effect of the factors mentioned increased as turbulence was increased on increasing rate of mixture supply, and thereby decreasing the time of residence in the tube. The result was that with a mixture supply of 2000 cc./min., the surface temperature required for ignition remained substantially constant while hydrogen concentration was increased from 30 to 80% and varied little with changes in the nature of the surface. The total difference due to changing

from a silica to an aged stainless steel surface was approximately 20°C. It was more than 200°C. when a mixture containing 50% of hydrogen was supplied at 200 cc./min. and flow configuration depended on heat convection.

Experiments with hydrogen–air mixtures supplied to an Otto cycle engine were carried on in association with the combustion tube experiments. Turbulence in both cases was increased by increasing the rate of mixture supply. This tended to reduce the temperature of the wall of the combustion tube but to *raise* the temperature of the wall of the combustion chamber of the engine, if it was operated at full throttle. The increase occurred because the increase in rate of mixture supply to the engine was obtained by increasing speed and consequently the heat load. The indirectly cooled surfaces of the exhaust valve and the ceramic core of the spark plug then tended to attain an igniting temperature in respect of the mixture as speed was raised in an attempt to develop maximum horsepower. The occurrence of premature ignition, in the circumstances, was avoided by a reduction in the exposed area of the ceramic core of the spark plug and by a reduction of the temperature of the exhaust valve, mainly by sodium cooling. The experiments will be described in the next of the present series of papers.

ACKNOWLEDGMENTS

The experiments described in this Part were carried out in the Department of Chemical Engineering, University of Toronto, with the co-operation of Professor R. R. McLaughlin, Head of the Department and with technical assistance by Mrs. S. M. Burrows and Miss G. H. Whittemore. The authors are indebted to the Chairman of the Defence Research Board (Canada) for permission to publish.

REFERENCES

1. ALYEA, H. N. and HABER, F. Z. physik. Chem. B, 10: 193–204. 1930.
2. DIXON, H. B. and COWARD, H. F. J. Chem. Soc. 95: 514–543. 1909.
3. GOLDMANN, F. Z. physik. Chem. B, 5: 316–326. 1929.
4. JOST, W. Explosion and combustion processes in gases. 1st ed. McGraw-Hill Book Company, Inc., New York and London. 1946.
5. KING, R. O. and ALLAN, A. B. Can. J. Technol. 30: 44–60. 1952.
6. KING, R. O. and ALLAN, A. B. Can. J. Technol. 32: 220–241. 1954.
7. KING, R. O., DURAND, E. J., ALLAN, A. B., and HANSEN, E. J. T. Can. J. Technol. 30: 29–43. 1952.
8. KING, R. O., DURAND, E. J., ALLAN, A. B., HANSEN, E. J. T., and BOWEN, V. E. Can. J. Technol. 30: 222–257. 1952.
9. KING, R. O., SANDLER, S., and STROM, R. Can. J. Technol. 32: 102–126. 1954.